

Understanding the Dynamics of Ion Locking in Doubly-Polymerized Ionic Liquids

by

Swati Arora

Bachelor of Science in Chemistry, St. Stephen's College, Delhi University, India, 2009

Master of Science, Purdue University, 2017

Submitted to the Graduate Faculty of the
Dietrich School of Arts and Sciences in partial fulfillment
of the requirements for the degree of
Doctor of Philosophy

University of Pittsburgh

2022

UNIVERSITY OF PITTSBURGH

DIETRICH SCHOOL OF ARTS AND SCIENCES

This dissertation was presented

by

Swati Arora

It was defended on

August 2, 2022

and approved by

Peng Liu, Associate Professor, Department of Chemistry

Yiming Wang, Assistant Professor, Department of Chemistry

Sachin Velankar, Associate Professor, Swanson School of Engineering

Thesis Advisor/Dissertation Director: Haitao Liu, Professor and Director of Graduate Studies,
Department of Chemistry

Copyright © by Swati Arora

2022

Understanding the Dynamics of Ion Locking in Doubly-Polymerized Ionic Liquids

Swati Arora, PhD

University of Pittsburgh, 2022

Controlling the dynamics of ion motion in polymerized ionic liquids remains enticing for the development of advanced organic electronics.^{1,2} Previous studies have extensively reported ion dynamics in singly polymerized ionic liquids (SPILs).³⁻⁷ However, a lot needs to be uncovered with regards to a molecular-level understanding of dynamics in “doubly polymerized” ionic liquids, or DPILs, in which both ionic species are covalently linked to polymer chains.⁸⁻¹¹ Polymerizing both the ionic species in an ionic liquid drastically decreases the ionic conductivity and lock the ions in place. While intentionally restricting the ion motion may be counterintuitive, given that a large focus of the polymerized ionic liquid community has so far been optimizing ion transport without sacrificing mechanical properties, it has been recently shown that “locking” ions in place in polymeric materials can actually enable new classes of organic electronics, which has been an important motivation for our work.^{12,13}

Significantly deeper fundamental understanding, however is needed to examine the factors that influence the time duration until which the ions can be locked in place called as the “electric double layer” (EDL) retention time. To investigate these questions, we characterized these materials using Broadband dielectric spectroscopy (BDS) over a broad frequency and temperature range.

The dielectric studies demonstrate that the polymerization of both the ionic species in DPIL not only radically reduces the bulk conductivities of the material significantly, but also slows the

relaxation timescales corresponding to ionic rearrangement by more than four orders of magnitude relative to SPILs which we attributed to ionic interactions effectively forming physical crosslinks between the polymer chains.

Understanding the fundamental mechanisms of ion locking in these materials, and using this knowledge to inform design rules for tunable functional device, will be critical in moving these applications forward. Thus, this study will stimulate advances for investigating the fundamental properties of ion-containing polymers and developing DPIL as promising materials in novel device applications.

Table of Contents

Acknowledgements	xviii
1.0 Introduction and Motivation	1
2.0 Thermally-Triggered Ionic Liquids: A New Platform for On-Command Release	
of Ions.....	9
2.1 Introduction	9
2.2 Experimental.....	15
2.2.1 Materials	15
2.2.2 Characterization of Synthetic Products	16
2.2.3 Synthesis of Triggerable Singly-Polymerizable Ionic Liquid.....	16
2.2.3.1 Synthesis of (2)	17
2.2.3.2 Synthesis of (3)	18
2.2.3.3 Synthesis of (4)	20
2.2.3.4 Synthesis of (5)	21
2.2.4 Synthesis of Non-Triggerable Singly-Polymerizable Ionic Liquid	23
2.2.4.1 Synthesis of (7)	23
2.2.4.2 Synthesis of (8)	24
2.2.4.3 Synthesis of (9)	25
2.2.5 Synthesis of Doubly Polymerizable Ionic Liquid	26
2.2.5.1 Synthesis of (11)	28
2.2.5.2 Synthesis of (12)	29
2.2.5.3 Synthesis of (13)	30

2.2.5.4 Synthesis of (14)	31
2.2.5.5 Synthesis of (15)	33
2.2.6 Polymerization of Ionic Liquid Monomers.....	34
2.2.6.1 Photopolymerization.....	34
2.2.6.2 Thermal Polymerization	35
2.2.7 Characterization.....	36
2.2.7.1 Differential Scanning Calorimetry.....	36
2.2.7.2 Cyclic Voltammetry.....	36
2.2.8 Capacitor Measurements of Ion Release.....	37
2.2.8.1 Capacitor Fabrication	37
2.2.8.2 Deposition and UV Polymerization of Polymerizable Ionic Liquids	38
2.2.8.3 Electrical Characterization.....	38
2.3 Results and Discussion	39
2.3.1 Synthesis of the IL monomers.....	39
2.3.2 Differential Scanning Calorimetry (DSC)	42
2.3.3 Polymerization of the PIL monomers	43
2.3.3.1 Thermal Polymerization	43
2.3.3.2 Photopolymerization.....	46
2.3.4 Cyclic Voltammetry (CV).....	47
2.3.5 Capacitor Studies on Designed PILs	50
2.4 Conclusion	56
3.0 Dynamics of Ion Locking in Doubly-Polymerized Ionic Liquids	57
3.1 Introduction	57

3.2 Experimental	62
3.2.1 Materials	62
3.2.2 Synthetic Methods	63
3.2.2.1 Synthesis of Singly-and Doubly-Polymerizable Monomers	63
3.2.2.2 Polymerization of sPIL and dPIL Monomers	64
3.2.3 Characterization of Polymerizable Ionic Liquids	64
3.2.3.1 NMR Analysis	64
3.2.3.2 Differential Scanning Calorimetry (DSC)	65
3.2.3.3 FTIR Analysis of DPIL samples	65
3.2.3.4 Broadband Dielectric Spectroscopy	65
3.3 Results	66
3.3.1 Monomer and Polymer Synthesis	66
3.3.2 NMR analysis	70
3.3.3 FTIR Analysis	72
3.3.4 Thermal Analysis	72
3.3.5 Ionic Conductivity	78
3.3.6 Analysis of dielectric T_g	85
3.3.7 The Dielectric Function ϵ'	88
3.3.8 Dielectric Relaxations	90
3.3.9 Static Dielectric Constant	97
3.3.10 Barton-Nakajima-Namikawa (BNN) Function	99
3.4 Discussion	102
3.5 Conclusion and Future Work	106

Appendix A NMR Characterization for synthetic intermediates in Chapter 2 and 3.....	110
Appendix B Supporting Data for Chapter 3	128
Appendix B.1 Conductivity of SPIL and DPIL samples.....	128
Appendix B.2 Electrical Modulus of SPIL and DPIL samples	130
Appendix B.3 Permittivity of SPIL and DPIL samples	132
Bibliography	134

List of Tables

Table 1 Glass transition temperature of photopolymerized ionic liquids	47
Table 2 Electrochemical stability windows of commercial, non-polymerizable [EMIM][TFSI] and all four PILs used in this work	50
Table 3 Glass-Transition temperatures of polymerized Ionic Liquids from DSC and BDS Measurements	73
Table 4 Room-Temperature DC conductivities of monomers and polymers investigated in this work	81
Table 5 Fit parameters for the DC conductivity of polymerized ionic liquids above and below their glass transition temperatures.....	83
Table 6 Fit Parameters for the Conductivity Relaxation Frequencies of Polymerized Ionic Liquids above and below Their Glass-Transition Temperatures.....	87
Table 7 Fitting Parameters for the Arrhenius ($T < T_g$) and VFT ($T > T_g$) temperature dependence of the ion rearrangement frequencies obtained from fits to ϵ_{der}.....	95
Table 8 Parameters for BNN fit for investigated PILs	101

List of Figures

Figure 1 Representation of Different Types of Ionic Liquids	2
Figure 2 Polymerization-based electric double layer locking under an applied voltage.....	3
Figure 3 Incorporation of thermally-sensitive linkages for designing triggerable ionic liquids.	4
Figure 4 Potential Mechanisms of EDL dissipation	5
Figure 5 DPIL modeled to commercially available ionic liquid [EMIM][TFSI]	5
Figure 6 Monomeric (sPIL) and polymerized (SPIL)	6
Figure 7 Characterization by Dielectric Relaxation Spectroscopy	7
Figure 8 Ion locking to create a stable p-n junction in a two-dimensional semiconductor..	11
Figure 9 Incorporation of thermally-labile linkers for designing triggerable ionic liquids.	13
Figure 10 Chemical structure of doubly-polymerizable ionic liquid with only thermally- triggerable cation	14
Figure 11 Reaction Scheme: Synthesis of triggerable singly-polymerizable ionic liquid 5..	17
Figure 12 Reaction Scheme: Synthesis of non-triggerable singly polymerizable ionic liquid 9	23
Figure 13 Reaction Scheme: Synthesis of non-triggerable doubly polymerizable ionic liquid 14.....	27
Figure 14 Reaction Scheme: Synthesis of triggerable doubly polymerizable ionic liquid 15.	28

Figure 15 Differential scanning calorimetry thermograms of (a) all four polymers used in this work and (b) polymerized T-SPIL at two different scan rates. Arrows in panels (a) and (b) indicate the glass transition temperatures (midpoints) of each material 43

Figure 16 DSC thermograms of (a) NT-SPIL and (b) NT-DPIL after polymerization with AIBN..... 45

Figure 17 DSC thermograms of T-SPIL (a) before and (b, c) after polymerization with (b) AIBN at 65 °C and (c) DMPA under UV light at room temperature 45

Figure 18 Cyclic voltammograms all of materials used in this work (b-d). Scans of the supporting electrolyte (a) and commercial [EMIM][TFSI] (b) are included for reference..... 49

Figure 19 Schematic representation for interpretation of electrical measurements on polymerized ionic liquids..... 51

Figure 20 Capacitor response of (a) non-triggerable and (b) triggerable singly-polymerized ionic liquids at 298 K, measured before polymerization, immediately after polymerization, and after a full thermal cycle in which the temperature of the sample was increased to 400 K before being returned to room temperature. Each trace depicts the response of the material to a step potential applied across a capacitor with 10 μm electrode spacing. 52

Figure 21 Temperature-dependent current amplitudes for capacitors with (a) non-triggerable and (b) triggerable singly-polymerized ionic liquids deposited and polymerized across the electrodes. Arrows labeled T_g and rDA indicate the glass transition temperature and retro Diels-Alder temperatures of the samples, respectively. 54

Figure 22 Capacitor response of (a) non-triggerable and (b) triggerable doubly-polymerized ionic liquids at 298 K, measured right before polymerization, immediately after polymerization, and after a full thermal cycle in which the temperature of the sample was increased to 400 K before being returned to room temperature.	55
Figure 23 Scheme: Chemical structures of polymerizable ionic liquid monomers (a, b, and c) and their corresponding polymers (d, e, and f) investigated in the present work: (a) sPIL(+), (b) sPIL(-), (c) dPIL, (d) SPIL(+), (e) SPIL(-), and (f) DPIL	67
Figure 24 FTIR spectra of polymerized DPIL at room temperature	69
Figure 25 ATR-FTIR spectra of the dPIL monomer and DPIL polymer, illustrating disappearance of the C=C bond peak at 1636 cm⁻¹ upon polymerization. Spectra are normalized to the carbonyl stretch at 1710 cm⁻¹.....	70
Figure 26 ¹³C solid-state NMR of DPIL	71
Figure 27 DSC thermograms of PILs obtained during the cooling cycle of the DSC run. Arrows indicate the glass transition temperatures of each material.	73
Figure 28 Complete DSC profiles of all the PILs; (a) SPIL(+), (b) SPIL(-), and (c) DPIL investigated in the present study.	75
Figure 29 DSC profiles of all (a) SPIL(+), (b) SPIL(-), and (c) DPIL, illustrating batch-to-batch variation between the samples. Black traces correspond to Batch 1 and red traces correspond to Batch 2 for each material.	77
Figure 30 Plot of the real part of the conductivity (σ') of (a) SPIL(+), (b) SPIL(-), and (c) DPIL as a function of angular frequency across the range of temperatures investigated in this work.....	78

Figure 31 DC conductivity of PILs as a function of (a) $1000/T$ and (b) T_g/T . Solid lines show VFT fits above T_g , while dashed lines show the Arrhenius fits below T_g . T_g values were obtained from analysis of the electrical modulus, as described below..... 80

Figure 32 Conductivity relaxation frequencies obtained from M'' . Solid lines show VFT fits above T_g , while dashed lines show the Arrhenius fits below T_g 86

Figure 33 Frequency dependence of (a-c) the dielectric permittivity and (d-f) the dielectric loss derivative function ϵ_{der} for (a, d) SPIL(+), (b, e) SPIL(-), and (c, f) DPIL across the range of temperatures investigated in this work. 89

Figure 34 Dielectric loss derivative spectra at T_g fit to the sum of a power law for EP and derivative form of HN function for ion rearrangement of (a) SPIL(+), (b) SPIL(-), and (c) DPIL. The solid curves are three-parameter fits to eq 7 with following values of s , a , and b for (a) SPIL (+): $s = 1.45$, $a = 0.9$, $b = 0.34$ (b) SPIL (-): $s = 1.7$, $a = 0.74$, $b = 0.45$ (c) DPIL: $s = \text{Varied}$, $a = 0.76$, $b = 1.0$ 92

Figure 35 Temperature dependence of relaxation frequency maxima, ω_{max} , obtained from fits to ϵ_{der} . Overlaid curves indicate fits to an Arrhenius model (dashed lines) below T_g and a VFT model (solid curves) above T_g 94

Figure 36 Temperature dependence of relaxation strengths $\Delta\epsilon$ corresponding to ion-rearrangements process for all investigated PILs..... 96

Figure 37 Temperature dependence of static dielectric constant for all PILs in the current study 98

Figure 38 BNN plot for all three polymerized ionic liquids investigated in this work. 100

Figure 39 Mechanism of ion transport in SPILs vs. DPIL..... 105

Figure 40 $^1\text{H-NMR}$ for synthetic intermediate 7 in Figure 12 110

Figure 41 ^{13}C -NMR for synthetic intermediate 7 in Figure 12.....	111
Figure 42 ^1H -NMR for synthetic intermediate 8 in Figure 12.....	111
Figure 43 ^{13}C -NMR for synthetic intermediate 8 in Figure 12.....	112
Figure 44 ^1H -NMR for synthetic intermediate 9 in Figure 12.....	112
Figure 45 ^{13}C -NMR for synthetic intermediate 9 in Figure 12.....	113
Figure 46 ^{19}F -NMR for synthetic intermediate 9 in Figure 12.....	114
Figure 47 ^1H -NMR for synthetic intermediate 11 in Figure 13.....	114
Figure 48 ^{13}C -NMR for synthetic intermediate 11 in Figure 13.....	115
Figure 49 ^1H -NMR for synthetic intermediate 12 in Figure 13.....	115
Figure 50 ^{13}C -NMR for synthetic intermediate 12 in Figure 13.....	116
Figure 51 ^{19}F -NMR for synthetic intermediate 12 in Figure 13.....	117
Figure 52 ^1H -NMR for synthetic intermediate 13 in Figure 13.....	118
Figure 53 ^{13}C -NMR for synthetic intermediate 13 in Figure 13.....	118
Figure 54 ^{19}F -NMR for synthetic intermediate 13 in Figure 13.....	119
Figure 55 ^1H -NMR for synthetic intermediate 14 in Figure 13.....	120
Figure 56 ^{13}C -NMR for synthetic intermediate 14 in Figure 13.....	120
Figure 57 ^{19}F -NMR for synthetic intermediate 14 in Figure 13.....	121
Figure 58 ^1H -NMR for synthetic intermediate 2 in Figure 11.....	121
Figure 59 ^{13}C -NMR for synthetic intermediate 2 in Figure 11.....	122
Figure 60 ^1H -NMR for synthetic intermediate 3 in Figure 11.....	123
Figure 61 ^{13}C -NMR for synthetic intermediate 3 in Figure 11.....	124
Figure 62 ^1H -NMR for synthetic intermediate 5 in Figure 11.....	124
Figure 63 ^{19}F -NMR for synthetic intermediate 5 in Figure 11.....	125

Figure 64	^{13}C-NMR for synthetic intermediate 5 in Figure 11	125
Figure 65	^1H-NMR for synthetic intermediate 15 in Figure 14	126
Figure 66	^{19}F-NMR for synthetic intermediate 15 in Figure 14	126
Figure 67	^{13}C-NMR for synthetic intermediate 15 in Figure 14.....	127
Figure 68	Real part of the conductivity (σ') for SPIL(+) as a function of angular frequency across the range of temperatures investigated in this work.....	128
Figure 69	Real part of the conductivity (σ') for SPIL(-) as a function of angular frequency across the range of temperatures investigated in this work.....	129
Figure 70	Real part of the conductivity (σ') for DPIL as a function of angular frequency across the range of temperatures investigated in this work.....	129
Figure 71	Imaginary part of the electrical modulus (M'') for SPIL(+) as a function of angular frequency across the range of temperatures investigated in this work. Each trace is offset by a factor of $(10)^{1/2}$ from the preceding trace to minimize overlap and make it easier to see the peaks in each plot.	130
Figure 72	Imaginary part of the electrical modulus (M'') for SPIL(-) as a function of angular frequency across the range of temperatures investigated in this work. Each trace is offset by a factor of $(10)^{1/2}$ from the preceding trace to minimize overlap and make it easier to see the peaks in each plot.	131
Figure 73	Imaginary part of the electrical modulus (M'') for DPIL as a function of angular frequency across the range of temperatures investigated in this work. Each trace is offset by a factor of $(10)^{1/2}$ from the preceding trace to minimize overlap and make it easier to see the peaks in each plot.	131

Figure 74 Real part of the permittivity (ϵ') and its derivative spectrum (ϵ_{der}) for SPIL(+) as a function of angular frequency across the range of temperatures investigated in this work..... 132

Figure 75 Real part of the permittivity (ϵ') and its derivative spectrum (ϵ_{der}) for SPIL(-) as a function of angular frequency across the range of temperatures investigated in this work..... 132

Figure 76 Real part of the permittivity (ϵ') and its derivative spectrum (ϵ_{der}) for DPIL as a function of angular frequency across the range of temperatures investigated in this work..... 133

Acknowledgements

I would like to extend my profound gratitude towards Prof. Haitao Liu, Prof. Jennifer Laaser, and Prof. Raul Hernández Sánchez for their constant support and guidance through my graduate research career at the University of Pittsburgh. I am incredibly grateful to them for letting me take my own decisions and consequently I have turned into an independent researcher. Today I have been able to fruitfully accomplish my research projects only because of their creativity, scientific knowledge, and expertise that had constantly motivated me to keep going and never give up on any scientific problem that has been presented before me. Thank you all for not losing faith in me.

I had also like to thank my committee members, Prof. Peng Liu, Prof. Yiming Wang, and Prof. Sachin Velankar for their advice, feedback and being a valuable part of my graduate career throughout the years.

I wish to acknowledge all my group members past and present for constantly motivating me and engaging me in amazing scientific discussions that not only helped me in troubleshooting my scientific problems but also taught me the art of scientific communications. I particularly want to thank Zijian Huo and Julisa Rozon for teaching me MATLAB, Inkscape and helping me developing my computational skills. I also like to thank Jun Huang for being my lab mate buddy so that I can work safely in the lab during night. I am grateful to Frances.J. Morin and Victoria Kong for placing all my order request for chemicals and the laboratory scientific tools ASAP. Specifically, I would like to thank Saber Mirzaei, Victor Espinoza Castro, Brett Lucht and Manasseh Osei. Hats off to you guys for making me a great scientist and really helping me to survive through weekly sub-group meeting and research meetings.

Finally, I wish to thank my parents, friends, and teachers for holding my hand and walking with me throughout my graduate journey from Purdue University to University of Pittsburgh that had many turns and twists.

1.0 Introduction and Motivation

Although advances in electronics over the last 60 years have changed the landscape of the technological world, security threats inherent to electronic devices like hardware counterfeiting and piracy of intellectual property still pose a daunting challenge at the forefront of U.S. economy.¹⁴ In particular, in military and defense applications, it is critical to ensure that enemy combatants cannot uncover sensitive information by reverse-engineering the devices. The protection of electronic components requires new security primitives in the area of hardware and authentication, despite some of these needs being handled by software advances. We aim to solve this problem by fine tuning the molecular properties of the polymers, developing innovative chemistries for these polymer-based platform, control ion content in these polymeric materials and further understand the dynamics of ion motion in these materials.

Ionic liquids are salts containing weakly-bound charged ions that are liquid at room temperature and are typically composed of bulky organic species (Figure 1a).^{16,17} Because of their high ionic conductivities at application-relevant temperatures and low volatilities, they are attractive platforms for applications such as electrolytes in fuel cells, and flexible electronics.¹⁸⁻²³ A related class of materials, called singly-polymerized ionic liquids also called as SPILs, have gained increasing attention (Figure 1b). In these materials, one of the two ionic species is covalently attached to a polymer backbone, while the other remains mobile, enabling ion transport in mechanically-robust materials. These materials have high charge mobility, but with improved mechanical properties.²⁴⁻²⁶

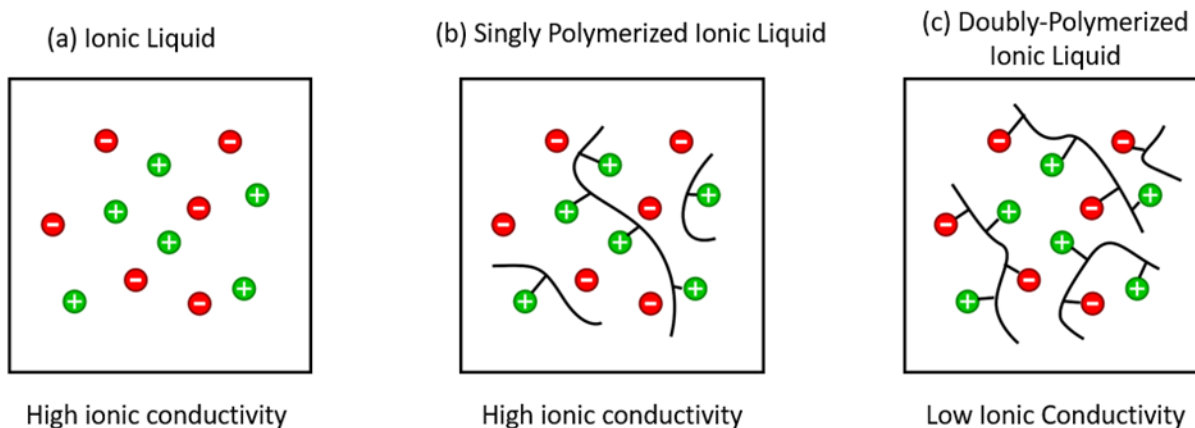


Figure 1 Representation of Different Types of Ionic Liquids

We had begun to study a third related class of materials that we refer to as “doubly polymerized” ionic liquids, or DPILs, in which both the cationic and the anionic species are covalently linked to polymer chains (Figure 1c).⁸⁻¹¹ This dramatically decreases the ionic conductivity of the polymers. Aside from being fundamentally interesting, it turns out that being able to “lock” ions in place actually have the potential to enable some new and exciting classes of organic electronics, which has been an important motivation for our work.

Recently with Fullerton’s group, in the Swanson School of Engineering at the University of Pittsburgh, we demonstrated that “ion locking” in a DPIL can be used to create functional electronic devices.¹³ This is exciting, because ‘locking’ the ions in place by chemically linking them through a process called polymerization can be exploited to store information about the voltage that was applied. We refer to this approach as the electric double layer (EDL) locking. The period over which the ions remain locked, or the lifetime over which the stored information is still readable, is called the retention time of the EDL. This would enable us to control the timescale of the programming of the device. Thus, it can actually be advantageous to lock all of the ions in a

polymer in place, rather than just trying to engineer polymerized ionic liquids for maximum conductivity (Figure 2).

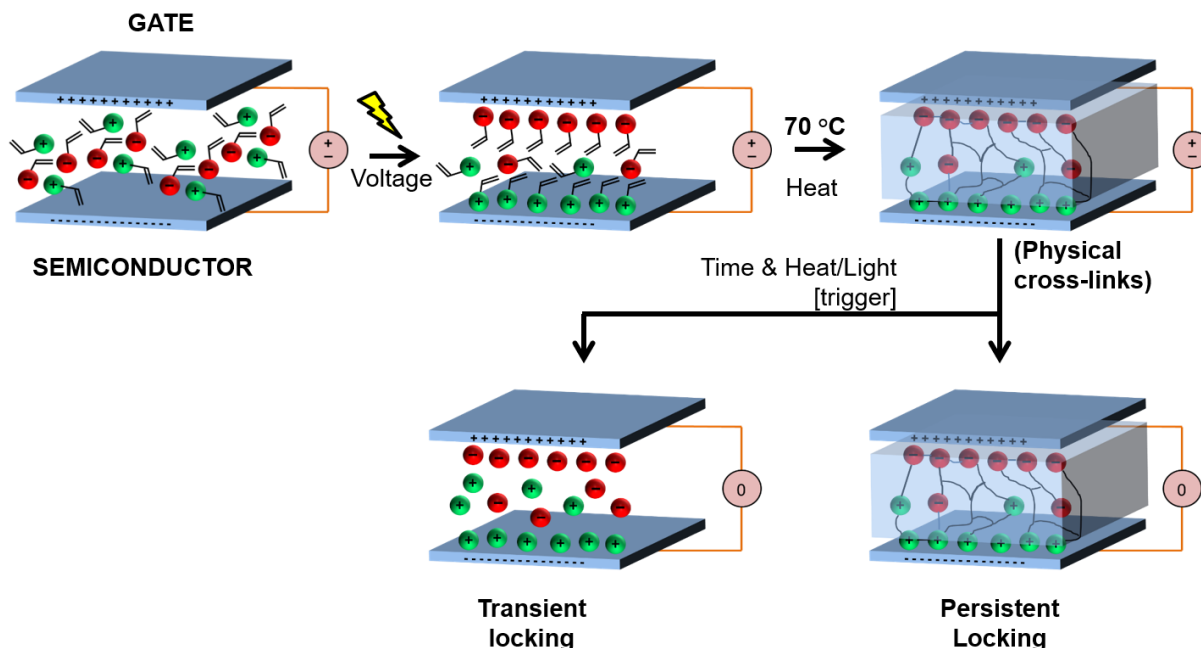


Figure 2 Polymerization-based electric double layer locking under an applied voltage . The EDL might be degraded over time, depending on the chemical constitution of the polymerized ionic liquid (PIL), or degradation may be triggered by an external stimulus.

Ideally, it would also be possible to deprogram the device on command, by using a trigger to degrade the EDL. We recently showed that the inclusion of heat-sensitive linkages also known as the Diels-Alder linkages between the polymer and the charged pendant allows ions to be released from the “locked” DPIL in response to a thermal trigger and thus deletion of the stored information on command (Figure 3).¹² This capability represents a novel approach of controlling the mobile ion content in polymeric materials.

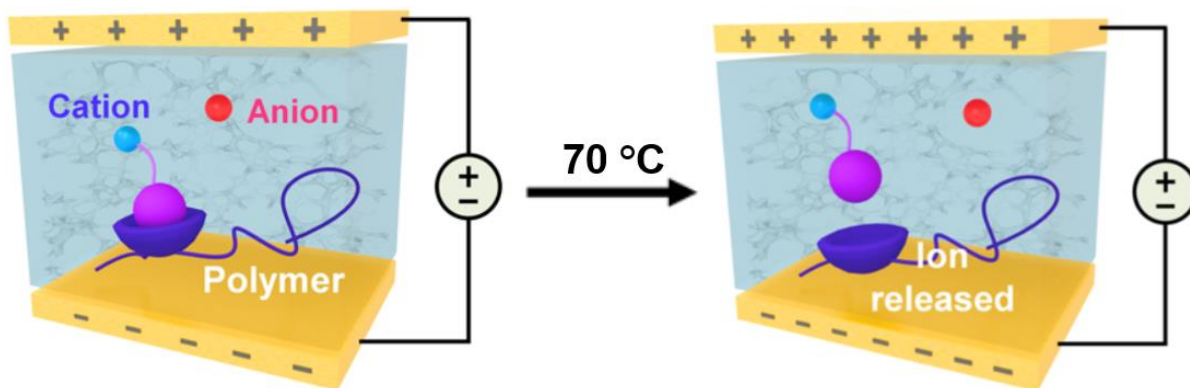


Figure 3 Incorporation of thermally-sensitive linkages for designing triggerable ionic liquids.

Significantly deeper fundamental understanding, however, is needed to examine the factors that influence the EDL retention time. In particular, in the applications, in which the device function depends on “locking” an electric double layer might in place at interface, there are potentially different mechanisms by which the EDL might dissipate, in turn degrading the function of the device. First, bulk ionic conductivity – for example, of any remaining un-polymerized ions – could allow ions to migrate to or from the interface, dissipating the EDL in the process (Figure 4a). Second, however, even local rearrangements of the charges near the interface – for example, rotation around the polymer backbone – could disrupt the electrical double layer enough to change the transfer characteristics of the device (Figure 4b). Thus, understanding both the bulk ionic conductivity of these materials and the local motions available to the charged groups is critical for developing DPIL-based devices that respond in well-defined and tunable ways.

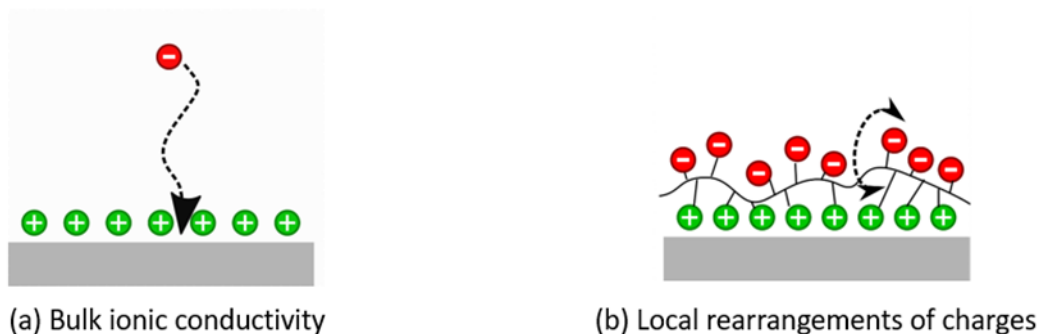


Figure 4 Potential Mechanisms of EDL dissipation

To investigate these questions, we designed a model DPIL system. We chose to focus on the dPIL in Figure 5b. This dPIL has very similar charged groups to the commonly used [EMIM][TFSI] ionic liquid Figure 5a, with an imidazolium cation and a trifluorosulfonylimide anion, but it has polymerizable methacrylate groups on both of the ionic species.²⁷⁻³² When this material is polymerized, it yields what is effectively a statistical copolymer with both cationic and anionic functional groups attached to each polymer chain Figure 5c. Importantly, if the reaction goes to full conversion, there should be no free ions in this system.

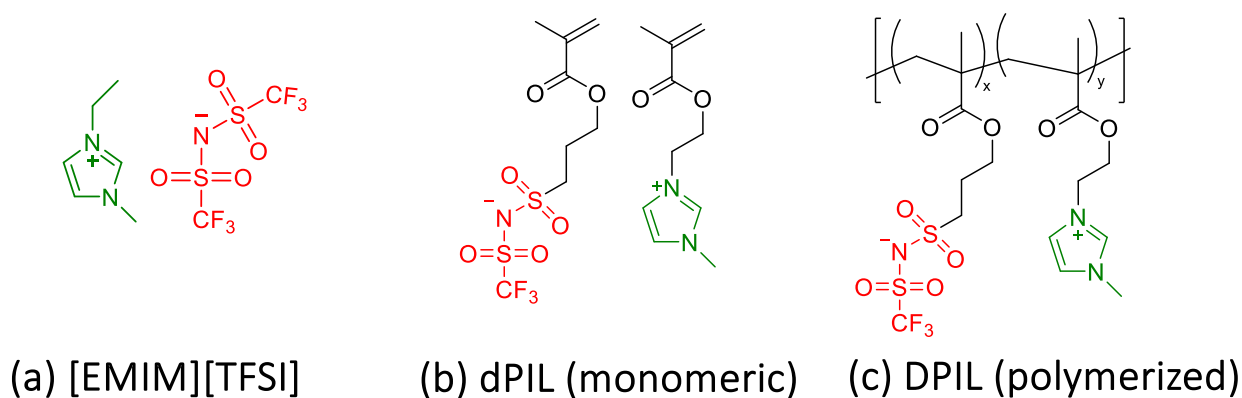


Figure 5 DPIL modeled to commercially available ionic liquid [EMIM][TFSI]

Because we want to understand how these materials are similar to and different from “conventional” polymerized ionic liquids, we also prepared and characterized both of the singly-polymerizable ionic liquids shown in Figure 6a and 6b. When these materials are polymerized, they will – in contrast to the DPIL - form polymers in which only one of the ionic species is covalently bound to the polymer chain while the other is free to move throughout the material as shown in Figure 6c and 6d.

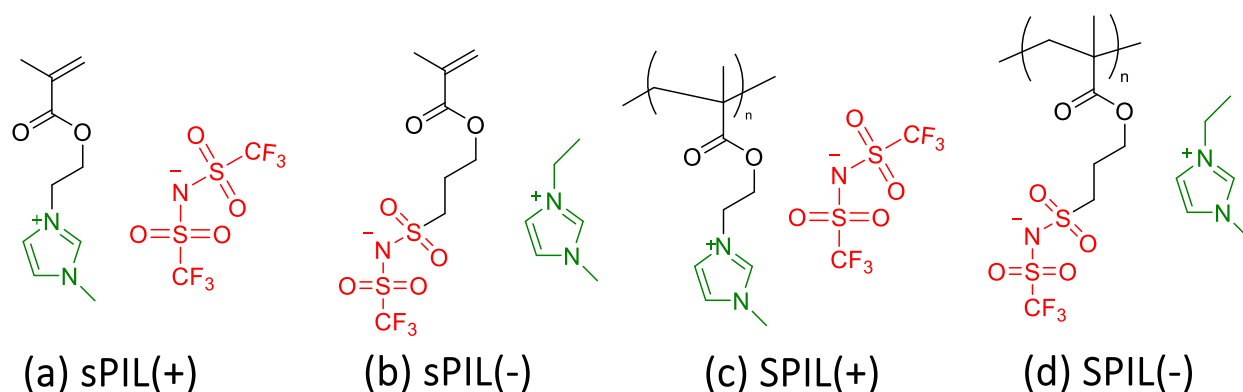


Figure 6 Monomeric (sPIL) and polymerized (SPIL)

We characterized these materials using dielectric relaxation spectroscopy, or DRS. In a DRS measurement, the sample is placed between two electrodes which effectively forms a parallel plate capacitor.³³ For the DPIL samples we deposited the materials into the sample cell in their liquid, monomeric form, and then polymerize the materials directly in the cell by heating them under vacuum with a small amount of added thermal initiator. Once the sample is prepared, an oscillating voltage is applied across the electrodes of the sample cell, and the resulting current response is measured (Figure 7). To a first approximation, the in-phase part of the response tells us about the resistance of the sample, from which we can calculate conductivity, while the out-of-phase part of the response tells us about the capacitance of the sample, which we can use to

calculate the material's dielectric permittivity (Figure 7). Carrying this measurement out at different frequencies allows us to build up a complete picture of how the material responds over a wide range of timescales.

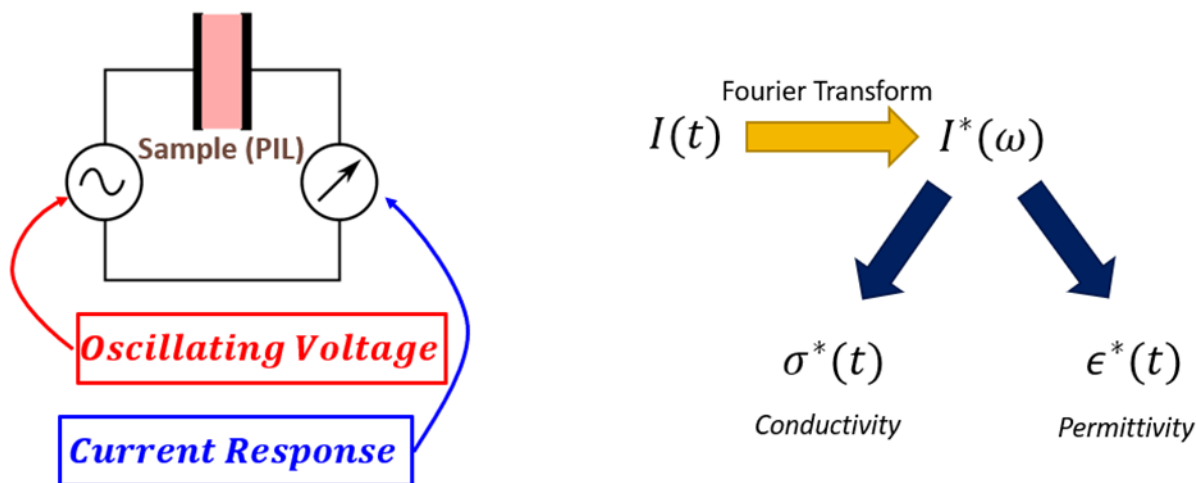


Figure 7 Characterization by Dielectric Relaxation Spectroscopy

DRS was used to elucidate the mechanism of ion transport in these materials, and the extent of ion immobilization critical to achieving effective EDL locking. To understand how DPILs are similar to and different from “conventional” polymerized ionic liquids, we also characterized SPILs shown in Figure 6. Although our main focus in this work was to understand the behavior of the DPIL systems, inclusion of both the positively- and negatively-charged SPILs as control samples provided an interesting opportunity to investigate whether there are any important differences in the ion conduction depending on which charged group is mobile and which is linked to the polymer backbone. When these materials are polymerized, they will – in contrast to the DPIL - form polymers in which only one of the ionic species is covalently bound to the polymer chain while the other is free to move throughout the material.

Taken together our comprehensive BDS analysis lets us draw some useful conclusion about how bulk ion transport is likely occurring in these materials. In the SPIL systems, above the glass transition temperature, there is sufficient free volume for the mobile ions to move throughout the material; although we don't investigate the mechanism of this motion here, it is likely an intra-chain ion hopping mechanism, as has been seen in experimental and computational work on similar polymerized ionic liquid systems.^{4,7}

In the DPIL, however, even above the glass transition temperature, the ionic conductivity is significantly restricted, although it is not zero, either. One possible origin of this residual ionic conductivity is motion of a small number of free ions that were not successfully reacted during the polymerization step. In this case, the residual free ions may require rearrangement of multiple ion pairs to hop to their next position, significantly restricting ion transport. Alternatively, the measured conductivity may not actually reflect bulk conductivity at all, and may instead be a signature of slow rearrangements of the polymer at the interface which lead to slow changes in the apparent amount of charge build-up. Either way, it is clear that copolymerizing both ionic species in an ionic liquid significantly restricts bulk ion transport in these materials.

Our results point a clear path towards the design of DPIL materials where achievement of ion motion shutdown is desirable. Because, DPILs are comparatively new and generally unexplored ionic polymeric material, we envision that the fundamental insight gained through this work will provide comprehensive information regarding the factors controlling ion motion in these materials and facilitate the advancement of new applications beyond ion-motion shutdown.

2.0 Thermally-Triggered Ionic Liquids: A New Platform for On-Command Release of Ions

2.1 Introduction

Ion-containing polymers, or synthetic organic polymers bearing charge-carrying ionic species, offer an exciting platform for the development of lightweight, flexible, easily processable electronic materials and devices.^{2,34} In the past, organic and organic/inorganic hybrid materials have been designed for sensing, energy collection and storage and information storage. However, data security is still a challenging problem.³⁵⁻⁴³

Transient electronics present an enticing solution to this problem.⁴⁴⁻⁴⁶ In these electronic devices, the physical properties of the material govern the degradation of the material and thus erasure of the stored information on the pre-determined timescales. Such platforms have been based on substrates and active components that have prolonged degradation timescales.⁴⁴⁻⁴⁶ They are ideal for applications in biomedical devices such as implantable sensors where the material particularly degrades into non-toxic components.⁴⁸ However, in environments that does not allow for dissolution-based degradation, alternative solution for transience of device is needed.⁴⁸⁻⁵⁰

Recent advances in the chemistry and physics of ion-containing polymers have enabled the semiconductor community to study the properties of two-dimensional semiconductors and interfaces by “locking” non-equilibrium ions distributions in place near a semiconductor surface.⁵¹⁻⁵⁸ Electrical double-layer locking in ionic materials may also provide an attractive route to transient information storage. Recently, it was demonstrated that the use of a polymer/salt system such as polyvinyl alcohol (PVA) mixed with LiClO₄ could achieve ion-locking for approximately 4 h.⁵⁹ This EDL retention time is six orders of magnitude longer than the one achieved using PEO-based

electrolytes at the same temperature.^{60,61} However, significant further improvements are still needed for practical applications and achieving both ‘on-command’ locking and unlocking of these types of ion distributions.

Polymerized ionic liquids (PILs) have emerged as promising materials for applications in electrochemical devices ranging from fuel cells to capacitors and batteries.²⁴⁻²⁶ In polymerized ionic liquids, one or both of the ionic species are tethered to the polymer backbone which restricts the mobility of the charged species. For advanced organic electronic applications, controlling the ion mobilities in these types of materials is central.

Previously, it has been shown that copolymerizing both ionic species in an ionic liquid composed of vinylimidazole and vinylsulfonic acid, dropped the overall ionic mobility of the material significantly.^{8,11} The resulting conductivity of the material was on the order of 10^{-9} Siemens·cm⁻¹. The addition of a small amount of non-polymerizable ionic liquid increased the conductivity by 4-5 orders of magnitude highlighting the critical role of free ions in the overall ion mobility in these materials. These studies clearly indicate that polymerizing both the cation and the anions in an ionic liquid will drastically reduce the ion mobility, thus making them attractive for ion-locking applications.

Inspired by this work, we investigated a doubly-polymerizable ionic liquid as a viable platform for EDL locking on application-relevant timescales in collaboration with Susan Fullerton’s group in the Department of Chemical and Petroleum Engineering at the University of Pittsburgh.¹³ In this work we demonstrated that “ion locking” in DPIL can be used to create functional electronic devices. To achieve this, DPIL was deposited in graphene, which is a 2-D semiconductor. Applying the right set of voltages across the electrodes drove ions to the interface, in turn inducing a p-n junction doping pattern in the underlying semiconducting material. By

polymerizing the ionic liquid while in this state, we were able to “lock” the ions in place, producing a stable p-n junction that persisted even after the “programming” voltages were turned off (Figure 8). The resulting transfer characteristics of a representative device are shown in Figure 8; the presence of two current minima with variation in the back gate voltage are the tell-tale signature of successful formation of a p-n junction. This is exciting, because two-dimensional semiconductors are very difficult to dope by conventional methods such as substitutional doping.

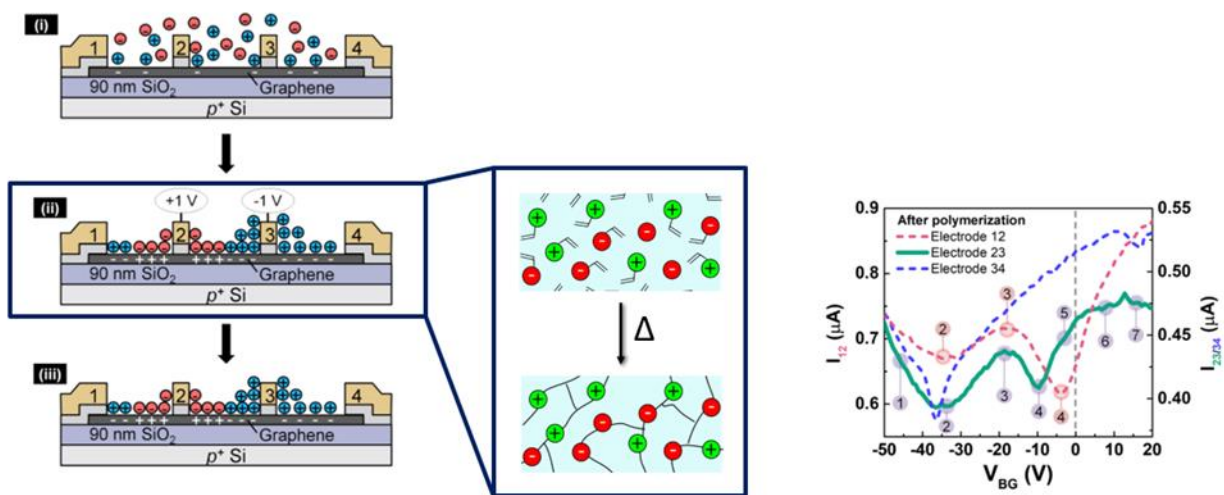


Figure 8 Ion locking to create a stable p-n junction in a two-dimensional semiconductor

On the other hand, many applications require the mobile ion content to be increased rather than decreased. To this end, researchers have pursued a number of strategies to improve the ionic conductivity of PILs.⁶² For example, the coulombic interactions among the ions in PILs can be manipulated to achieve lower glass transition temperatures and enhanced ionic conductivity at room temperature. In general, sulfonated polymeric materials exhibit low ionic conductivity due to stronger Coulombic interactions between the “hard” sulfonate ion and the cation. Thus, to increase conductivity, the $-\text{SO}_3$ group has been modified into “softer”

bis(trifluoromethylsulfonyl)imide, tricyanomethanide and dicyanamide anions, imparting three orders of magnitude improvement in conductivity in sulfonated polymeric materials.⁶³

The chemical nature of the mobile ion also has a profound influence on the ionic conductivity of these materials because it affects the segmental mobility of the polymer chains.⁶⁴ Wang et al. demonstrated that imidazolium-containing hyperbranched PILs with bromide counter-ion exhibit significantly higher T_g (79 °C) than PILs containing bis(trifluoromethylsulfonyl)imide counter-ions ($T_g = -6$ °C).⁶⁵ Lee and coworkers also incorporated a glycol linker between the polymer backbone and imidazolium moiety to extend that separation distance for achieving PILs with even lower T_g s and higher ion conductivity. This improvement in conductivity was attributed to enhanced mobility of imidazolium cation with increasing length of the flexible spacer.⁴

Thus, changing the chemical nature of the ionic groups,⁶³ their spacing along the polymer chains,⁶⁶ and their separation from the polymer backbone^{66,67} can enhance the ionic conductivity in PILs. However, none of these approaches enables changing the mobile ion content of PILs under a given set of experimental conditions. Although the ionic conductivity of a PIL can be increased by heating it above its glass transition temperature, it eventually returns to the baseline once the PIL is cooled.⁶⁶ Thus, the ionic conductivity of the PILs is effectively fixed at a given temperature as the parameters that can change the conductivity of the PIL are set when the sample is prepared. However, new classes of electronic devices, such as information storage systems that can be erased with heat, might be realized if a strategy for changing the mobile ion content of PILs under a given set of fixed experimental conditions can be developed.

Here, we propose a novel way of addressing this challenge by incorporating thermally labile linkages between the polymer backbone and charged functional group. Careful control of the chemistry of these materials will allow us to achieve ‘on-command’ release of ions and enable

the development of new classes of triggerable electronic devices. The thermally labile linkage used in this work is a furan-maleimide Diels-Alder adduct (Figure 9).⁶⁸

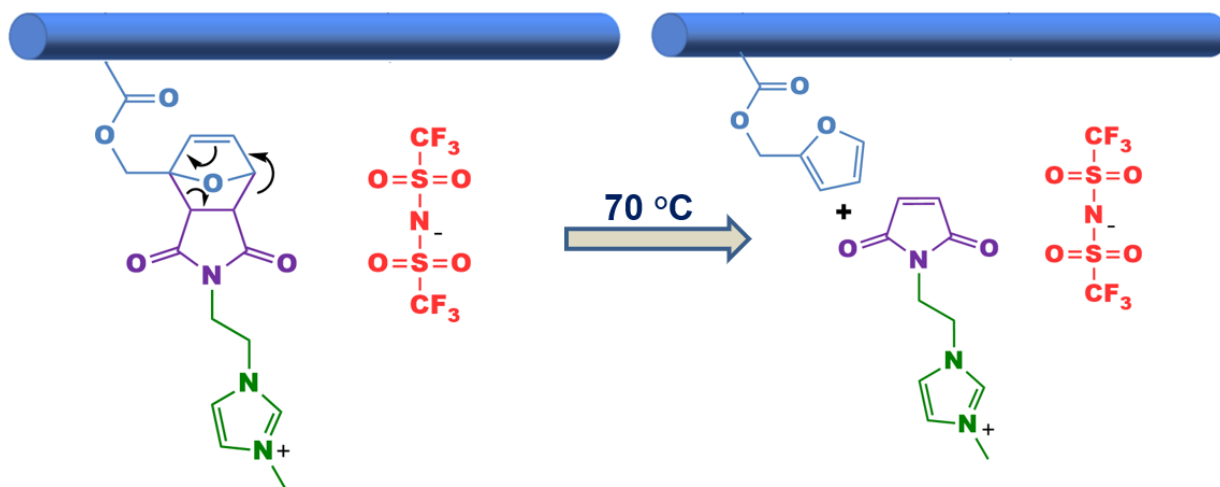


Figure 9 Incorporation of thermally-labile linkers for designing triggerable ionic liquids

The Diels-Alder reaction has emerged as an attractive way to incorporate thermally-reversible bonds into polymeric materials. Previously, Diels-Alder linkages have been successfully incorporated to yield thermally degradable and self-healing materials.⁶⁹⁻⁷¹ The furan/maleimide couple is one of the most widely used diene/dienophile pairs for the development of well-defined life cycle materials. The low-temperature requirement and the high yield for the furan/maleimide Diels-Alder and retro Diels-Alder reactions make it an ideal platform for thermally triggered ion release in polymerized ionic liquid systems.⁶⁸

We anticipate cleavage of the thermally-labile bond at elevated temperatures will separate the ionic groups from the polymer chain, allowing them to move throughout the material and thus contributing to ionic motion. This capability-releasing ions “on command” in response to a simple physical trigger-is not feasible in current generations of polymerizable ionic liquids, and represents

a fundamentally new way of controlling the mobile ion content in polymeric materials. This approach will stimulate advances across polymer chemistry and organic electronics.

Here we describe the synthesis and characterization of polymerizable ionic liquids with thermally reversible Diels-Alder linkages between the charged group and the polymer backbone. We first targeted thermally labile singly polymerized ionic liquids (T-SPIs) that released ions in response to temperature increases (Figure 9). We then extended this approach to doubly polymerized ionic liquids in which only the cationic sidechains are thermally labile (Figure 10).

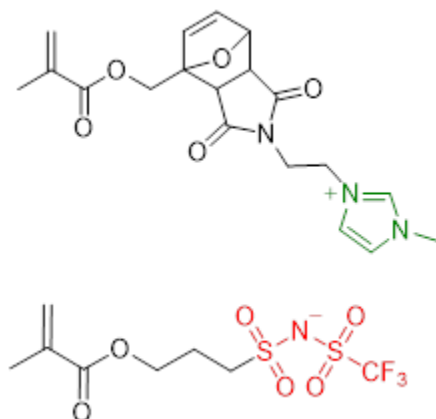


Figure 10 Chemical structure of doubly-polymerizable ionic liquid with only thermally-triggerable cation

The materials were characterized by cyclic voltammetry, differential scanning calorimetry, and charging/discharging measurements in capacitors. We find clear evidence of ion release in the triggerable materials (T-SPIs) in response to temperature increase, which is not observed in non-triggerable polymerized ionic liquids (NT-SPIs). This result demonstrates the promise of these materials for the development of polymerizable ionic liquids with thermally-controllable conductivities that are responsive to a wide range of physical and chemical triggers.

2.2 Experimental

2.2.1 Materials

For monomer and polymer synthesis, 1-methylimidazole (99%), methacryloyl chloride (97%), 2-bromoethanol (95%), maleimide (99%), 2,2-dimethoxy-2-phenylacetophenone (99%), anhydrous N,N-dimethylformamide (99.8%), and 2,2'-azobisisobutyronitrile (AIBN, 98%) were purchased from Sigma Aldrich. 4-methoxyphenol (98%), phosphorus pentoxide (98%), thionyl chloride (99%), and calcium hydride (90-95%) were purchased from Alfa Aesar. Lithium hydride (97%), anhydrous potassium carbonate (99%), anhydrous diethyl ether, and triethylamine (99%) were purchased from ACROS Organics. Magnesium sulfate, methanol (ACS), hexanes (ACS), and ethyl acetate (ACS) were purchased from Fisher Scientific. Trifluoromethanesulfonamide (98%), furfuryl methacrylate (95%), lithium bis(trifluoromethanesulfonyl)imide (98%), and 3-sulfopropyl methacrylate potassium salt (97%) were purchased from TCI America.

Anhydrous THF was obtained from a SOLV-TEK solvent system. Triethylamine was dried over CaH₂ and distilled under inert atmosphere. 3-sulfopropyl methacrylate potassium salt was dried at 25 °C for 2 hours under vacuum, and AIBN was recrystallized from methanol before use. Deionized water (18.2 MΩ · cm) was obtained from a Synergy water purification system (Millipore Sigma). All other reagents were used as received.

For electrochemistry experiments, tetrabutylammonium hexafluorophosphate (99%), anhydrous acetonitrile (99.8%), and silver nitrate (99%) were purchased from Sigma Aldrich and used as received. Ferrocene (99%) was purchased from Alfa Aesar. Glassy carbon, Pt wire, and the Ag⁺/Ag reference electrode were purchased from CH Instruments (Austin, TX). For capacitor measurements, Si substrates with 90 nm SiO₂ (resistivity 0.001-0.005 ohm·cm) were purchased

from Graphene Supermarket. Photoresist (Lor5B) and remover were purchased from MicroChem, and additional photoresist (S1805) and developer (Microposit 351) were purchased from Microposit and Microchemical (AS 400K).

2.2.2 Characterization of Synthetic Products

Nuclear magnetic resonance (NMR) spectra were obtained on a Bruker AMV-500 spectrometer at 25 °C in deuterated solvent. Fourier-transform infrared (FTIR) spectra were recorded in the attenuated total reflectance geometry on a UATR Spectrum 2 spectrometer (Perkin-Elmer) equipped with a diamond ATR cell. High-resolution mass spectra (HRMS) were obtained on a Micromass Ultima Q-TOF instrument using electrospray ionization. Because their thermal instability precluded elemental analysis, HRMS and NMR were used to confirm the composition and purity of the newly-reported Diels-Alder adducts used in this work (See Appendix).

2.2.3 Synthesis of Triggerable Singly-Polymerizable Ionic Liquid

Triggerable polymerizable ionic liquid **5** (**T-SPIL**) was synthesized as shown in Figure 11. Briefly, furfuryl methacrylate (**1**) was treated with maleimide at room temperature to yield Diels-Alder adduct **2** as a mixture of *endo* and *exo* products (*endo/exo* ratio: 70/30).⁷² This adduct was then modified by nucleophilic substitution with 1,2-dibromoethane followed by treatment with 1-methylimidazole to yield imidazolium salt **4**. Finally, salt metathesis with lithium bis(trifluoromethanesulfonyl)imide yielded the desired thermally triggerable polymerizable ionic liquid **5**. Throughout this synthetic pathway, the reaction temperatures were kept below 50 °C to

avoid side reactions such as cycloreversion of the furan-maleimide Diels-Alder adduct and polymerization of the methacrylate group.

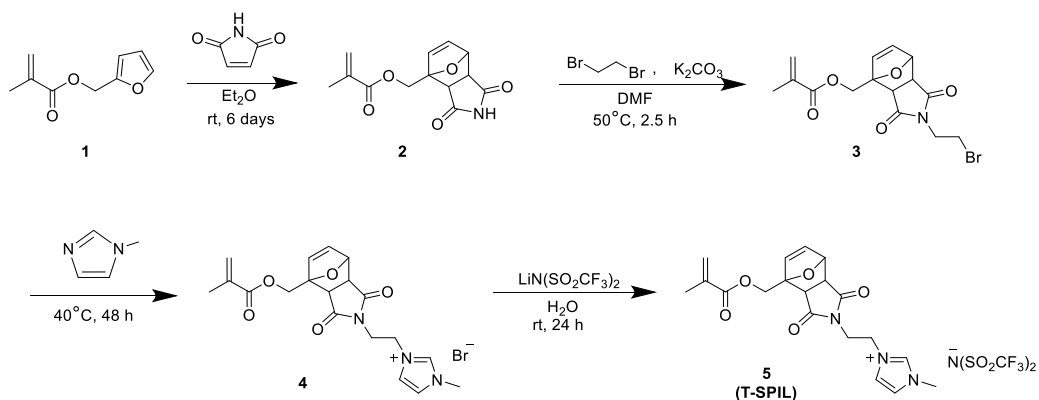
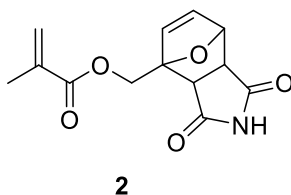


Figure 11 Reaction Scheme: Synthesis of triggerable singly-polymerizable ionic liquid 5

Full synthetic details and characterization data for isolated compounds are given below.

2.2.3.1 Synthesis of (2)



The synthesis of Diels-Alder adduct **2** was adapted from the literature.⁷² Maleimide (3.4 g, 0.035 mol) was suspended in 28 mL anhydrous diethyl ether in an oven-dried flask. Furfuryl methacrylate (8.8 g, 0.053) was then added dropwise at room temperature under inert atmosphere. The reaction mixture was protected from light and allowed to stir at room temperature for six days. Diethyl ether was then evaporated at reduced pressure at 30 °C. Residual furfuryl methacrylate was removed by drying the product under vacuum (<1 mmHg), yielding **2** as a white solid (7.8 g, 85%, *endo/exo* ratio: 70/30 (NMR)).

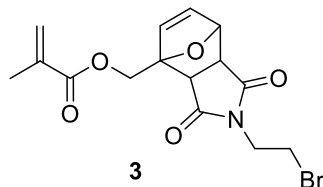
^1H NMR (500 MHz, DMSO): δ 11.28 (endo, s, 1H, -CO-NH-CO), 10.95 (exo, s, 1H, -CO-NH-CO), 6.56-6.55 (m, 1H, -O-CH-CH=CH), 6.47 (t, 1H, J= 5.5 Hz, -CH=CH-C-O-), 6.06 (endo, m, 1H, CH₂=C(CH₃)-), 6.00 (exo, m, 1H, CH₂=C(CH₃)-), 5.72-5.69 (endo, m, 1H, CH₂=C(CH₃)-), 5.69-5.65 (exo, m, 1H, CH₂=C(CH₃)-), 5.25 (endo, dd, 1H, J= 5.6 Hz, J= 1.8 Hz, -CH-O-), 5.12 (exo, m, 1H, -CH-O-), 4.78 (endo, d, 1H, J=12.6 Hz, -O-C-CH₂-O-), 4.75 (exo, d, 1H, J=12.6 Hz, -O-C-CH₂-O-), 4.57 (endo, d, 1H, J=12.6 Hz, -O-C-CH₂-O-), 4.48 (exo, d, 1H, J=12.2 Hz, -O-C-CH₂-O-), 3.63 (endo, dd, 1H, J=7.6 Hz, J=5.6Hz, -CH-CH-CO-), 3.43 (endo, d, 1H, J=7.6 Hz, -C-CH-CO-), 3.03 (exo, d, 1H, J=6.5 Hz, -C-CH-CO-), 2.95 (exo, d, 1H, J= 6.5 Hz, -CH-CH-CO-), 1.88 (endo, s, 3H, CH₂=C(CH₃)-), 1.86 (exo, s, 3H, CH₂=C-CH₃).

^{13}C NMR (126 MHz, DMSO) δ 177.49, 176.17, 166.14, 137.38, 136.82, 135.84, 135.49, 134.45, 126.45, 126.28, 89.14, 88.94, 80.52, 78.78, 62.14, 61.70, 51.13, 49.53, 48.94, 47.93, 17.91.

HRMS: m/z [M]⁺ calculated for C₁₃H₁₄O₅N: 264.08665; found 264.08739.

IR (cm⁻¹): 3233, 3072, 2942, 1774, 1706, 1686, 1560, 1444, 1318, 1350, 1178, 1142, 1081, 1016, 964, 904, 855, 799, 746, 683, 632, 527.

2.2.3.2 Synthesis of (3)



Product 2 (1.1 g, 0.004 mol), 4-methoxyphenol (800 ppm), and potassium carbonate (2.9 g, 0.021 mol) were suspended in 30 mL of anhydrous DMF in an oven-dried flask. Dibromoethane (1.5 g, 0.008 mol) was added dropwise at room temperature under an inert atmosphere. The reaction mixture was heated to 50 °C and stirred for 2.5 h. When the reaction was completed, as monitored by thin-layer chromatography, the reaction mixture was cooled to room temperature

and DMF was removed under vacuum. The crude residue was dissolved in ethyl acetate and filtered to remove suspended solids. The remaining solution was washed three times with water. The organic layer was then washed with brine, dried over anhydrous magnesium sulfate, filtered and then concentrated under reduced pressure at 30 °C. The crude product was then purified by silica gel column chromatography using hexanes/ethyl acetate (7/3, v/v) as the eluent ($R_f = 0.3$). Removal of the mobile phase and vacuum drying yielded **3** as a colorless viscous liquid (1.0 g, 70%, *endo/exo* ratio: 73/27 (NMR)).

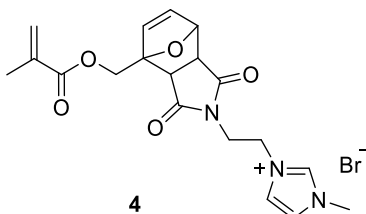
^1H NMR (500 MHz, CD_2Cl_2): δ 6.6 (endo, m, 1H, -O-CH-CH=CH), 6.53 (exo, dd, 1H, $J=5.5$ Hz, $J=1.5$ Hz, -O-CH-CH=CH), 6.50 (endo, d, 1H, $J=5.5$ Hz, -CH=CH-C-O-), 6.41 (exo, d, 1H, $J=6$ Hz, -CH=CH-C-O-), 6.17 (endo, m, 1H, CH₂=C(CH₃)-), 6.12 (exo, m, 1H, CH₂=C(CH₃)-), 5.67-5.65 (endo, m, 1H, CH₂=C(CH₃)-), 5.64-5.62 (exo, m, 1H, CH₂=C(CH₃)-), 5.35 (endo, dd, 1H, $J=5.5$ Hz, $J=1.5$ Hz, -CH-O-), 5.29 (exo, d, 1H, $J=2$ Hz, -CH-O-), 4.95 (endo, d, 1H, $J=13$ Hz, -O-C-CH₂-O-), 4.90 (exo, d, 1H, $J=12.5$ Hz, -O-C-CH₂-O-), 4.69 (endo, d, 1H, $J=13$ Hz, -O-C-CH₂-O-), 4.53 (exo, d, 1H, $J=12.5$ Hz, -O-C-CH₂-O-), 3.92 (endo, td, 1H, $J=7$ Hz, $J=2.5$ Hz, -N-CH₂-), 3.80-3.77 (endo, exo, m, 2H, -N-CH₂), 3.74-3.71 (endo, m, 1H, -CH-CH-CO-), 3.56-3.52 (endo, m, 1H, -CH₂-Br), 3.48-3.43 (endo, exo, m, 2H, -CH-CH-CO-, -CH₂-Br), 3.08 (exo, d, 1H, $J=6.5$ Hz, -CH-CH-CO-), 3.01 (exo, d, 1H, $J=6.5$ Hz, -C-CH-CO-), 1.98 (endo, m, 3H, CH₂=C(CH₃)-), 1.97 (exo, m, 3H, CH₂=C-CH₃).

^{13}C NMR (126 MHz, CD_2Cl_2) δ 175.63, 174.36, 166.95, 137.75, 137.45, 136.24, 135.01, 126.37, 126.20, 90.18, 89.94, 81.51, 79.96, 62.51, 61.94, 50.34, 48.82, 48.18, 47.18, 40.51, 40.32, 27.77, 27.63, 18.39.

HRMS: m/z $[\text{M}]^+$ calculated for $\text{C}_{15}\text{H}_{17}\text{O}_5\text{NBr}$: 370.02846; found 370.02945.

IR (cm⁻¹): 3364, 2970, 2926, 2886, 1775, 1703, 1643, 1556, 1399, 1303, 1156, 949, 857, 814, 723, 645, 592, 487.

2.2.3.3 Synthesis of (4)



3 (1.2 g, 0.003 mol) was combined with a small amount (800 ppm) of 4-methoxyphenol to inhibit polymerization. 1-methylimidazole (0.5 g, 0.006 mol) was added dropwise under inert atmosphere, and the reaction mixture was stirred for 48 h at 40 °C. The reaction mixture was then cooled to room temperature, dissolved in methanol and precipitated three times in diethyl ether. The precipitate was filtered off and the product dried under vacuum (<1 mmHg), yielding **4** as dark red, needle-like crystals (0.75 g, 55%, *endo/exo* ratio: 52/48 (NMR)).

¹H NMR (500 MHz, CDCl₃): δ 10.50 (*endo*, s, 1H, -N-CH-N-), 10.28 (*exo*, s, 1H, -N-CH-N-), 7.65 (*endo*, t, 1H, J= 1.8 Hz, -N-CH=CH-N-Me), 7.53 (*exo*, t, 1H, J= 1.8 Hz, -N-CH=CH-N-Me), 7.31 (*endo*, t, 1H, J= 1.8 Hz, -N-CH=CH-N-Me), 7.29 (*exo*, t, 1H, J= 1.8 Hz, -N-CH=CH-N-Me), 6.56 (*endo*, dd, 1H, J= 5.8 Hz, J= 1.8 Hz, -O-CH-CH=CH), 6.45 (*endo*, d, 1H, J=5.8 Hz, -CH=CH-C-O), 6.43 (*exo*, dd, 1H, J= 5.8 Hz, J= 1.6 Hz, O-CH-CH=CH-), 6.28 (*exo*, d, 1H, J= 5.8 Hz, -CH=CH-C-O-), 6.15 (*endo*, bs, 1H, CH₂=C(CH₃)-), 6.10 (*exo*, bs, 1H, CH₂=C(CH₃)-), 5.62-5.58 (m, 1H, CH₂=C(CH₃)-), 5.25-5.21 (m, 1H, -CH-O-), 4.84 (*endo*, d, 1H, J=12.8 Hz, -O-C-CH₂-O-), 4.76-4.70 (*exo*, m, 1H, -O-C-CH₂-O-), 4.67-4.57 (m, 3H, -O-C-CH₂-O-, N-CH₂-CH₂-N-Im), 4.07-4.00 (m, 4H, -N-CH₃, N-CH₂-CH₂-N-Im), 3.99-3.96 (*endo*, m, 1H, -CH-CH-CO-), 3.85 (t, 1H, J= 5 Hz, N-CH₂-CH₂-Im), 3.69 (*endo*, d, 1H, J= 7.7 Hz, -C-CH-CO), 3.21 (*exo*, d, 1H,

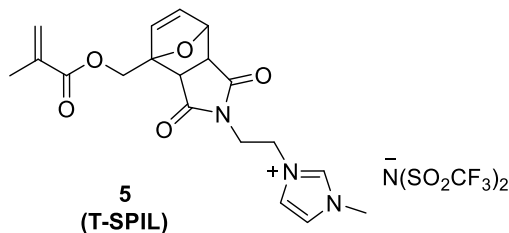
J= 6.4 Hz, -C-CH-CO-), 3.12 (exo, d, 1H, J=6.5 Hz, -CH-CH-CO-), 1.94 (endo, bs, 3H, CH₂=C(CH₃)-), 1.92 (exo, bs, 3H, CH₂=C-CH₃).

¹³C NMR (126 MHz, CDCl₃) δ 175.75, 174.98, 174.87, 174.42, 167.01, 138.68, 138.57, 137.59, 136.87, 136.15, 135.70, 134.77, 126.86, 126.79, 123.33, 123.13, 122.83, 89.78, 81.34, 79.45, 62.36, 61.40, 50.48, 48.97, 48.59, 48.20, 47.87, 47.71, 39.51, 38.81, 36.75, 18.39.

HRMS: *m/z* [M]⁺ calculated for C₁₉H₂₃O₅N₃Br: 452.08156; found 452.08154.

IR (cm⁻¹): 3377, 3154, 3099, 2969, 1778, 1702, 1629, 1581, 1394, 1322, 1162, 1024, 987, 949, 883, 816, 753, 621.

2.2.3.4 Synthesis of (5)



To synthesize triggerable polymerizable ionic liquid **5**, **4** (0.104 g, 0.230 mmol) was dissolved in 2.5 mL water at room temperature. A solution of lithium bis(trifluoromethanesulfonyl)imide (0.099 g, 0.345 mmol) in 1 mL water was then added dropwise, upon which formation of oily droplets was immediately observed in the reaction mixture. The reaction was allowed to stir for 24 h at room temperature, during which the reaction mixture separated into two layers. The top layer was decanted, and the bottom layer was dissolved in dichloromethane and washed with distilled water. The dichloromethane layer was dried over magnesium sulfate. Magnesium sulfate was then removed by vacuum filtration and the dichloromethane was evaporated under reduced pressure at 25 °C. The obtained product was dried under vacuum (<1 mmHg) at room temperature for 12 h with a drying tube filled with P₂O₅ inserted

between the vacuum chamber and the vacuum line, yielding **5** as a pale pink viscous liquid (0.112 g, 50%, *endo/exo* ratio: 46/54 (NMR)).

^1H NMR (500 MHz, CD_2Cl_2): δ 8.71 (endo, s, 1H, -N-CH-N-), 8.62 (exo, s, 1H, -N-CH-N-), 7.38 (endo, t, 1H, $J=2$ Hz, -N-CH=CH-N-Me), 7.36 (exo, t, 1H, $J=2$ Hz, -N-CH=CH-N-Me), 7.30-7.27 (m, 1H, -N-CH=CH-N-Me), 6.57 (endo, dd, 1H, $J=5.5$ Hz, $J=0.5$ Hz, -O-CH-CH=CH), 6.49 (endo, d, 1H, $J=6$ Hz, -CH=CH-C-O-), 6.41 (exo, dd, 1H, $J=5.5$ Hz, $J=1.7$ Hz, O-CH-CH=CH-), 6.27 (exo, d, 1H, $J=5.5$ Hz, -CH=CH-C-O-), 6.12 (d, 1H, $J=6$ Hz, CH₂=C(CH₃)-), 5.66-5.61 (m, 1H, CH₂=C(CH₃)-), 5.27 (endo, dd, 1H, $J=5.5$ Hz, $J=1.5$ Hz, -CH-O-), 5.10 (exo, d, 1H, $J=1.5$ Hz, -CH-O-), 4.82 (endo, d, 1H, $J=13$ Hz, -O-C-CH₂-O-), 4.71 (exo, d, 1H, $J=13$ Hz, -O-C-CH₂-O-), 4.62 (endo, d, 1H, $J=13$ Hz, -O-C-CH₂-O-), 4.61 (exo, d, 1H, $J=13$ Hz, -O-C-CH₂-O-), 4.46-4.42 (m, 1H, -N-CH₂-CH₂-N-Im), 4.30 (t, 1H, $J=5.5$ Hz, -N-CH₂-CH₂-N-Im), 4.01-3.95 (m, 1H, N-CH₂-CH₂-N-Im), 3.93 (endo, s, 3H, -N-CH₃), 3.85 (exo, s, 3H, -N-CH₃), 3.83-3.79 (m, 1H, -N-CH₂-CH₂-Im), 3.75-3.71 (endo, m, 1H, -CH-CH-CO), 3.47 (endo, d, 1H, $J=7.5$ Hz, -C-CH-CO-), 3.06 (exo, d, 1H, $J=6$ Hz, -C-CH-CO-), 2.99 (exo, d, 1H, $J=6.5$ Hz, -CH-CH-CO-), 1.93 (d, 3H, $J=1.5$ Hz, CH₂=C(CH₃)-).

^{13}C NMR (126 MHz, CD_2Cl_2) δ 175.38, 174.73, 167.37, 137.76, 137.11, 137.01, 136.23, 136.15, 134.90, 126.92, 126.56, 124.31, 124.13, 123.36, 123.15, 121.44, 118.89, 116.34, 90.15, 81.77, 79.84, 62.37, 61.48, 50.39, 48.80, 48.25, 47.80, 47.20, 38.79, 38.25, 36.94, 18.35. $J_{\text{CF}} = 322$ Hz, N-SO₂-CF₃.

HRMS: m/z [M]⁺ calculated for C₁₉H₂₂O₅N₃ (cation): 372.15540; found 372.15622; calculated for C₂F₆NO₄S₂ (anion): 279.91784; found: 279.91483.

IR (cm⁻¹): 3543, 3159, 3107, 2972, 1778, 1704, 1640, 1564, 1399, 1346, 1181, 1137, 1055, 987, 948, 884, 850, 791, 736, 650, 611, 570, 510.

2.2.4 Synthesis of Non-Triggerable Singly-Polymerizable Ionic Liquid

The non-triggerable singly-polymerizable ionic liquid (**NT-SPIL**) was synthesized following a procedure adapted from the literature and summarized in Figure 12.^{73,74} Briefly, N-methylimidazole (**6**) was quaternized with 2-bromoethanol in the absence of solvent to yield imidazolium salt **7**. **7** was then treated with methacryloyl chloride at room temperature to yield polymerizable imidazolium salt **8**. Monomer **8** was finally ion-exchanged with [Li][TFSI] to yield the desired singly-polymerizable ionic liquid **9** (**NT-SPIL**).

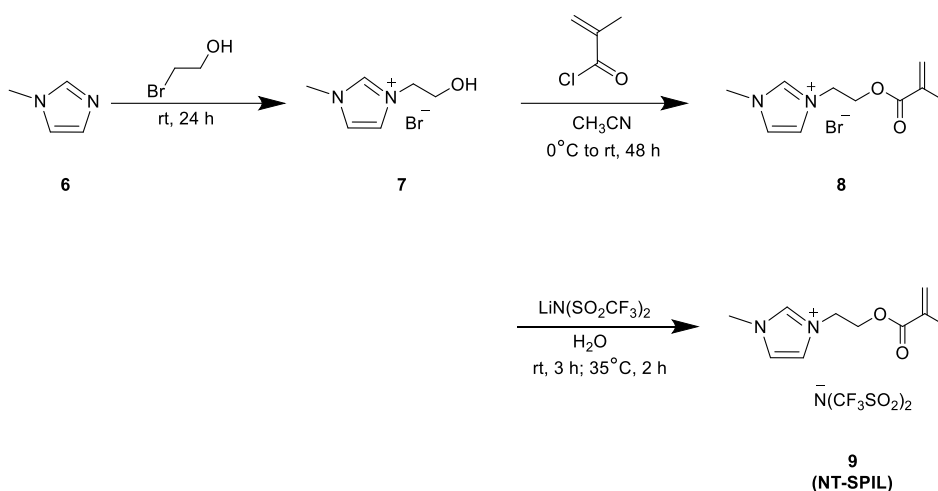
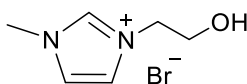


Figure 12 Reaction Scheme: Synthesis of non-triggerable singly polymerizable ionic liquid **9**

Full synthetic details and characterization data for isolated compounds are given below.

2.2.4.1 Synthesis of (7)



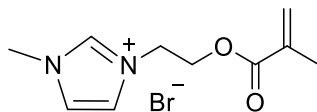
7

1-(2-hydroxyethyl)-3-methylimidazolium bromide (**7**) was synthesized according to a previously reported procedure.⁷⁴ To an oven dried round-bottom flask containing 1-methylimidazole (4.15 g, 0.0505 mol), 2-bromoethanol (6.25 g, 0.05 mol) was added dropwise at room temperature under an argon atmosphere. The reaction mixture was protected from light and stirred for 24 h at room temperature. A highly viscous product was obtained that solidified when dried under vacuum (<1 mmHg) at room temperature for 12 h, yielding **7** as a white solid (10.16 g, 98%).

¹H NMR (500MHz, DMSO): δ 9.20 (s, 1H, -N-CH-N-), 7.77 (t, 1H, J=1.8 Hz, -N-CH=CH-N-Me), 7.74 (t, 1H, J=1.8 Hz, -N-CH=CH-N-Me), 5.16 (t, 1H, J=5.3 Hz, -OH), 4.23 (t, 2H, J=4.9 Hz, -N-CH₂-), 3.87 (s, 3H, -N-CH₃), 3.70 (q, 2H, J=5.3 Hz, -CH₂-OH).

¹³C NMR (126 MHz, DMSO): δ 136.78, 123.29, 122.62, 59.26, 51.54, 35.69.

2.2.4.2 Synthesis of (**8**)



8

1-(2-methacryloyloxyethyl)-3-methylimidazolium bromide (**8**) was synthesized according to a previously reported procedure.⁷⁴ In an oven-dried round bottom flask, **7** (6.02 g, 0.029 mol) was gently crushed and suspended in 60 mL of anhydrous acetonitrile under an argon atmosphere. The suspension was cooled on an ice-bath to 0 °C. Methacryloyl chloride (6.07 g, 0.06 mol) was then diluted in 8 mL of anhydrous acetonitrile under argon and added dropwise to the suspension, upon which the reaction mixture turned milky white. The reaction mixture was allowed to

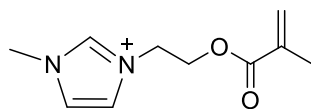
gradually warm to room temperature and was stirred for a further 48 h under inert atmosphere, after which acetonitrile was evaporated under reduced pressure at 30 °C.

The crude reaction mixture was then dissolved in 5 mL dichloromethane and precipitated two times in 20 mL diethyl ether to remove unreacted methacryloyl chloride. The residual ether was evaporated under reduced pressure at 25 °C and the remaining solution of product in dichloromethane was dried over magnesium sulfate. Magnesium sulfate was then removed by vacuum filtration and the dichloromethane was removed under reduced pressure at 25 °C. The final product was dried under vacuum (<1 mmHg) at room temperature for 12 h with a drying tube filled with P₂O₅ inserted between the vacuum chamber and the vacuum line, yielding **8** as a pale yellow viscous liquid (7.58 g, 95%).

¹H NMR (500 MHz, CDCl₃): δ 10.19 (s, 1H, -N-CH-N-), 7.64 (t, 1H, J= 1.5 Hz, -N-CH=CH-N-Me), 7.62 (t, 1H, J=1.5 Hz, -N-CH=CH-N-Me), 6.03 (s, 1H, CH₂=C-), 5.54 (s, 1H, CH₂=C-), 4.76 (t, 2H, J=5Hz, -CH₂-O-), 4.50 (t, 2H, J=5 Hz, N-CH₂-), 4.03 (s, 3H, -N-CH₃), 1.82 (s, 3H, CH₂=C-CH₃).

¹³C NMR (126 MHz, CDCl₃): δ 166.45, 137.55, 135.09, 127.14, 123.68, 122.95, 62.81, 48.81, 36.81, 18.27.

2.2.4.3 Synthesis of (9)



$\bar{\text{N}}(\text{CF}_3\text{SO}_2)_2$

9
(NT-SPIL)

A solution of lithium bis(trifluoromethanesulfonyl)imide (6.29 g, 0.022 mol) in 4 mL water was added dropwise to a solution of **8** (3.96 g, 0.0145) in 4 mL water at room temperature, upon which oily droplets formed in the reaction mixture. The reaction was stirred for 24 h at room temperature, during which the mixture separated into two layers. The top layer was decanted and the bottom layer was dissolved in dichloromethane and washed with water. The dichloromethane layer was dried over magnesium sulfate. Magnesium sulfate was then removed by vacuum filtration and the dichloromethane was evaporated under reduced pressure at 25 °C. The resulting product was dried under vacuum (<1 mmHg) at room temperature for 12 h with a drying tube filled with P₂O₅ inserted between the vacuum chamber and the vacuum line, yielding **9** as a colorless viscous liquid (5.17 g, 75%).

¹H NMR (500 MHz, CD₂Cl₂): δ 8.78 (s, 1H, -N-CH-N-), 7.34 (t, 1H, J= 1 Hz, -N-CH=CH-N-Me), 7.28 (t, 1H, J=1 Hz, -N-CH=CH-N-Me), 6.1 (t, 1H, J=1 Hz, CH₂=C-), 5.67 (m, 1H, CH₂=C-), 4.55-4.53 (m, 2H, -CH₂-O-), 4.51-4.49 (m, 2H, N-CH₂-), 3.95 (s, 3H, -N-CH₃), 1.92 (t, 3H, J=1.5 Hz, CH₂=C-CH₃).

¹³C NMR (126 MHz, CD₂Cl₂): δ 166.70, 137.05, 135.74, 127.18, 125.15, 124.05, 123.36, 121.50, 118.95, 116.39, 62.61, 49.61, 37.06, 18.34. J_{CF} = 322 Hz, N-SO₂-CF₃.

¹⁹F NMR (471 MHz, CD₂Cl₂) δ -79.54 (s, CF₃).

2.2.5 Synthesis of Doubly Polymerizable Ionic Liquid

The polymerizable anionic monomer used in in preparation of the doubly-polymerizable ionic liquids was prepared according to the literature procedure.^{63,75} Briefly, as shown in Figure 13, potassium 3-(methacryloyloxy)propane-1-sulfonate (**10**) was activated with thionyl chloride to yield 3-(chlorosulfonyl)propyl methacrylate (**11**). Compound **11** was then converted into the

triethylammonium salt of a polymerizable TFSI analog (**12**) using trifluoromethanesulfonamide in the presence of triethylamine. The triethylammonium cation was then exchanged with Li^+ using LiH in anhydrous THF, yielding lithium salt **13**. Non-triggerable doubly-polymerizable ionic liquid **14** (**NT-DPIL**) was obtained by ion-exchange of **13** with cationic monomer **8**. Finally, triggerable polymerizable ionic liquid **15** (**T-DPIL**) was similarly obtained by ion-exchange of **13** with triggerable cationic monomer **4** as shown in Figure 14. Full synthetic details and characterization data for all isolated compounds are given below.

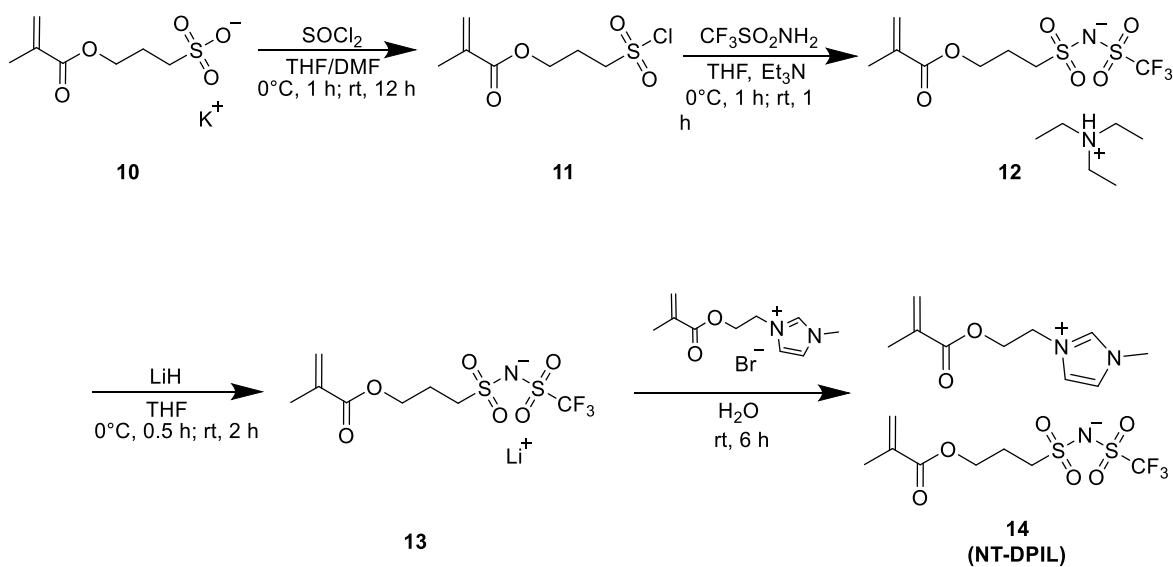


Figure 13 Reaction Scheme: Synthesis of non-triggerable doubly polymerizable ionic liquid 14.

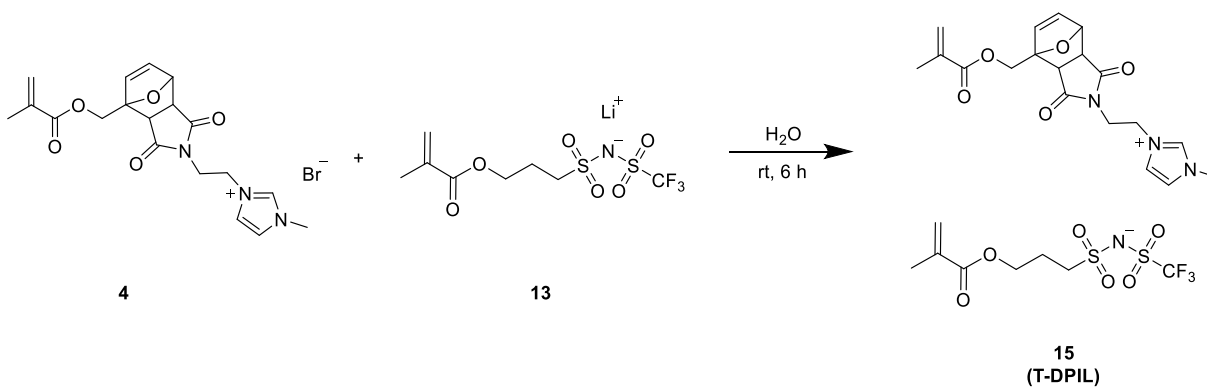
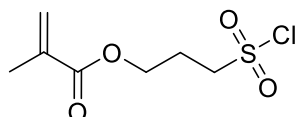


Figure 14 Reaction Scheme: Synthesis of triggerable doubly polymerizable ionic liquid 15.

2.2.5.1 Synthesis of (11)



11

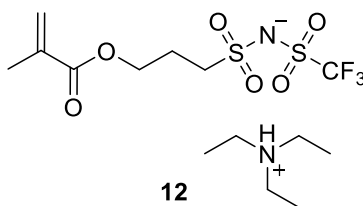
3-(Chlorosulfonyl)propyl methacrylate (**11**) was synthesized according to a previously reported procedure.⁶³ 3-(methacryloyloxy)propane-1-sulfonate (5.0 g, 0.020 mol) was suspended in 8 mL of anhydrous THF in an oven-dried flask. DMF (0.6 mL) was injected under an inert atmosphere. The reaction flask was cooled to 0 °C and thionyl chloride (13.3 g, 0.112 mol) was injected dropwise while stirring. The reaction was stirred at 0 °C for 1 h, and was then allowed to proceed at room temperature for a further 12 h. After 12 h, the crude suspension was added dropwise into ice-cold water. Oily droplets were formed immediately upon addition, and the mixture gradually separated into two layers. The top aqueous layer was decanted; the oily bottom layer was dissolved in dichloromethane washed with distilled water and dried over magnesium sulfate. Magnesium sulfate was then removed by vacuum filtration, and dichloromethane was evaporated under reduced pressure at 25 °C. The resulting product was dried under vacuum (<1

mmHg) at room temperature for 12 h with a drying tube filled with P₂O₅ inserted between the vacuum chamber and the vacuum line, yielding **11** as a colorless viscous liquid (3.6 g, 80%).

¹H NMR (500 MHz, CDCl₃): δ 6.10 (s, 1H, CH₂=C(CH₃)–), 5.60 (m, 1H, CH₂=C(CH₃)–), 4.31 (t, 2H, J= 5.9 Hz, CO–O–CH₂–), 3.77 (m, 2H, –CH₂–SO₂Cl), 2.41 (m, 2H, CO–O–CH₂–CH₂–), 1.92 (s, 3H, CH₂=C(CH₃)–).

¹³C NMR (126 MHz, CDCl₃): δ 166.95, 135.75, 126.43, 62.29, 61.33, 24.24, 17.93.

2.2.5.2 Synthesis of (**12**)



Triethylammonium salt **12** was synthesized according to a previously reported procedure.⁶³ To an oven-dried round bottom flask loaded with trifluoromethanesulfonamide (2.4 g, 0.016 mol), freshly distilled anhydrous triethylamine (3.6 g, 0.036 mol) was added dropwise under inert atmosphere. Anhydrous THF (13 mL) was added to dissolve the reaction mixture, and the resulting colorless solution was cooled to 0 °C. A solution of **11** (3.7 g, 0.016 mol) in 5 mL anhydrous THF was then added dropwise while stirring. The reaction was stirred at 0 °C for 1 h, and was then allowed to proceed for a further 1 h at room temperature. The white precipitate produced during the reaction was filtered off under inert atmosphere and the filtrate was concentrated under reduced pressure at 25 °C. The resulting yellow oil was dissolved in dichloromethane and washed with distilled water. The dichloromethane solution was dried over magnesium sulfate; magnesium sulfate was filtered off, a small amount of 4-methoxyphenol (800 ppm) was added to inhibit polymerization, and the dichloromethane solution was removed under reduced pressure at 25 °C.

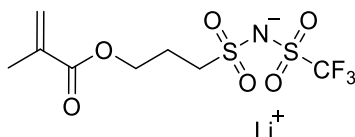
The obtained product was dried under vacuum (<1 mmHg) at room temperature for 12 h with a drying tube filled with P₂O₅ inserted between the vacuum chamber and the vacuum line, yielding **12** as a dark yellow viscous liquid (5.4 g, 76%).

¹H NMR (500 MHz, CDCl₃): δ 8.1 (bs, 1H, H-N(C₂H₅)₃), 6.07 (s, 1H, CH₂=C(CH₃)–), 5.55 (t, 1H, J=1.6 Hz, CH₂=C(CH₃)–), 4.24 (t, 2H, J= 6.2 Hz, CO–O–CH₂–), 3.27-3.22 (m, 2H, –CH₂–SO₂–N–), 3.18 (q, 6H, J= 7.3 Hz, H-N(CH₂CH₃)₃), 2.25-2.18 (m, 2H, O–CH₂–CH₂–CH₂–), 1.90 (s, 3H, CH₂=C(CH₃)–), 1.33 (t, 9H, J=7.3 Hz, H- N(CH₂CH₃)).

¹³C NMR (126 MHz, CDCl₃): δ 167.27, 136.13, 125.89, 124.09, 121.52, 118.96, 116.39, 62.73, 51.93, 46.72, 23.78, 18.33, 8.62. J_{CF} = 323 Hz, N-SO₂–CF₃

¹⁹F NMR (471 MHz, CDCl₃) δ -78.03(s, CF₃).

2.2.5.3 Synthesis of (13)



13

Lithium salt **13** was synthesized according to a literature procedure.⁶³ A solution of **12** (3.3 g, 0.007 mol) in 10 mL anhydrous THF was loaded into an oven-dried round-bottom flask and cooled to 0 °C. A suspension of lithium hydride (0.086 g, 0.011 mol) in 5 mL anhydrous THF was injected dropwise under inert atmosphere. The reaction preceded for 30 minutes at 0 °C, and was then allowed to proceed for a further 2 h at room temperature. After 2 h, the excess LiH was filtered off under inert atmosphere and the filtrate was concentrated under reduced pressure at 25 °C. The resulting oil was washed three times with hexanes. The hexane layers were decanted and the

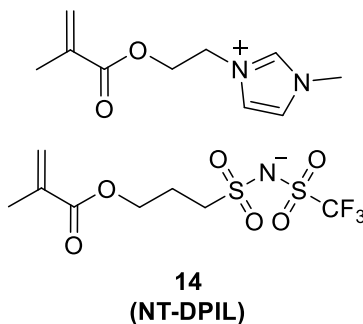
obtained product was dried under vacuum at 1 mmHg at room temperature for 2 h, yielding **13** as a pale yellow viscous liquid (2.4 g, 99%).

^1H NMR (500 MHz, MeOD): δ 6.08 (s, 1H, $\text{CH}_2=\text{C}(\text{CH}_3)-$), 5.59 (t, 1H, $J=1.7$ Hz, $\text{CH}_2=\text{C}(\text{CH}_3)-$), 4.24 (t, 2H, $J=6.2$ Hz, $\text{CO}-\text{O}-\text{CH}_2-$), 3.24-3.20 (m, 2H, $-\text{CH}_2-\text{SO}_2-\text{N}-$), 2.20-2.13 (m, 2H, $\text{O}-\text{CH}_2-\text{CH}_2-\text{CH}_2-$), 1.90 (s, 3H, $\text{CH}_2=\text{C}(\text{CH}_3)-$).

^{13}C NMR (126 MHz, MeOD) δ 167.34, 136.22, 125.03, 124.02, 121.46, 118.91, 116.35, 62.63, 51.73, 23.55, 17.01. $J_{\text{CF}} = 323$ Hz, $\text{N}-\text{SO}_2-\text{CF}_3$

^{19}F NMR (471 MHz, MeOD) δ -79.74 (s, CF_3).

2.2.5.4 Synthesis of (14)



A solution of **13** (1.6 g, 0.004 mol) in 6 mL water was added dropwise to a solution of **8** (1.6 g, 0.006 mol) in 3 mL water at room temperature while stirring, upon which oily droplets were immediately observed in the reaction mixture. The reaction was allowed to stir for 6 h at room temperature, during which the mixture gradually separated into two layers. The top (aqueous) layer was decanted and the oily bottom layer was dissolved in dichloromethane and washed with water. The dichloromethane layer was dried over magnesium sulfate. Magnesium sulfate was then removed by vacuum filtration, 4-methoxyphenol (800 ppm) was added to inhibit polymerization, and the dichloromethane was removed under a reduced pressure at 25 °C. The resulting product

was dried under vacuum at 1 mmHg at room temperature for 6 h, yielding **14** as a pale yellow viscous liquid (0.96 g, 45%).

^1H NMR (500 MHz, CDCl_3): δ 9.10 (s, 1H, -N-CH-N-), 7.41 (s, 1H, -N-CH=CH-N-Me), 7.38 (s, 1H, -N-CH=CH-N-Me), 6.05 (cation, anion, s, 2H, CH₂=C-, CH₂=C-), 5.59 (cation, s, 1H, CH₂=C-), 5.53 (anion, s, 1H, CH₂=C(CH₃)-), 4.57 (cation, t, 2H, J=5 Hz, -CH₂-O-), 4.46 (anion, t, 2H, J= 4.5 Hz, CO-O-CH₂-), 4.22 (t, 2H, J=6.4 Hz, N-CH₂-), 3.95 (s, 3H, -N-CH₃), 3.21-3.16 (m, 2H, -CH₂-SO₂-N-), 2.23-2.13 (m, 2H, O-CH₂-CH₂-CH₂-), 1.88 (cation, s, 3H, CH₂=C(CH₃)-), 1.86 (anion, s, 3H, CH₂=C-CH₃).

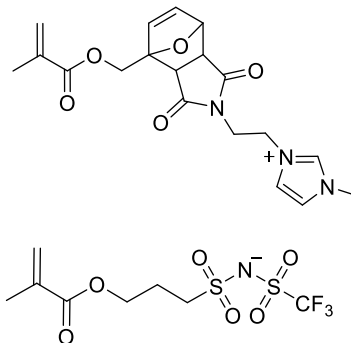
^{13}C NMR (126 MHz, CDCl_3) δ 167.31, 166.50, 137.25, 136.12, 135.27, 127.03, 125.84, 124.16, 123.76, 123.04, 121.59, 119.02, 116.46, 62.87, 62.71, 52.01, 48.88, 36.52, 23.83, 18.29, 18.21. $J_{\text{CF}} = 323$ Hz, N-SO₂-CF₃

^{19}F NMR (471 MHz, CDCl_3) δ -78.39 (s, CF₃).

HRMS: m/z [M]⁺ calculated for C₁₀H₁₅O₂N₂ (cation): 195.11280; found 195.11348; calculated for C₈H₁₁F₃NO₆S₂ (anion): 337.99853; found 337.99125.

IR (cm⁻¹): 3025, 2963, 2950, 1718, 1637, 1555, 1453, 1409, 1381, 1314, 1178, 1121, 1056, 950, 816, 753, 620, 596, 514.

2.2.5.5 Synthesis of (15)



15
(T-DPIL)

A solution of **13** (0.69 g, 0.002 mol) in 3 mL water was added dropwise to a solution of **4** (0.45 g, 0.001 mol) in 5 mL water at room temperature while stirring, upon which oily droplets were immediately observed in the reaction mixture. The reaction was allowed to stir for 6 h at room temperature, during which the reaction mixture gradually separated into two layers. The top (aqueous) layer was decanted and the oily bottom layer was dissolved in dichloromethane then washed with water. The dichloromethane layer was dried over magnesium sulfate. Magnesium sulfate was then removed by vacuum filtration, 4-methoxyphenol (800 ppm) was added to inhibit polymerization, and the dichloromethane was removed under reduced pressure at 25 °C. The resulting product was dried under vacuum at 1 mmHg at room temperature for 6 h, yielding **15** as a pale yellow viscous liquid (0.30 g, 42%).

$^1\text{H NMR}$ (500 MHz, CDCl_3): δ 9.17 (endo, s, 1H, -N-CH-N-), 9.11 (exo, s, 1H, -N-CH-N-), 7.40 (endo, t, 1H, $J = 1.75$ Hz, -N-CH=CH-N-Me), 7.34 (exo, t, 1H, $J = 1.75$ Hz, -N-CH=CH-N-Me), 7.25 (m, 1H, -N-CH=CH-N-Me), 6.55 (endo, dd, 1H, $J = 5.8$ Hz, $J = 2$ Hz, -O-CH-CH=CH), 6.45 (endo, d, 1H, $J = 5.8$ Hz, -CH=CH=C-O), 6.39 (exo, dd, 1H, $J = 5.6$ Hz, $J = 1.7$ Hz, O-CH-CH=CH-), 6.26 (exo, d, 1H, $J = 5.8$ Hz, -CH=CH-C-O-), 6.15 (endo, cation, t, 1H, $J = 1.35$ Hz,

$\underline{\text{CH}_2}=\text{C}(\text{CH}_3)-$), 6.10 (exo, cation, t, 1H, $J= 1.25$ Hz, $\underline{\text{CH}_2}=\text{C}(\text{CH}_3)-$), 6.09 (anion, t, 1H, $J= 1.3$ Hz, $\underline{\text{CH}_2}=\text{C}(\text{CH}_3)-$), 5.62-5.58 (cation, m, 1H, $\underline{\text{CH}_2}=\text{C}(\text{CH}_3)-$), 5.57-5.54 (anion, m, 1H, $\underline{\text{CH}_2}=\text{C}(\text{CH}_3)-$), 5.24 (endo, dd, 1H, $J= 5.5$ Hz, $J= 1.6$ Hz, $-\underline{\text{CH}}-\text{O}-$), 5.17 (exo, d, 1H, $J= 1.7$ Hz, $-\underline{\text{CH}}-\text{O}-$), 4.84 (endo, d, 1H, $J=12.8$ Hz, $-\text{O}-\text{C}-\underline{\text{CH}_2}-\text{O}-$), 4.62 (endo, d, 1H, $J= 13$ Hz, $-\text{O}-\text{C}-\underline{\text{CH}_2}-\text{O}-$), 4.60 (exo, d, 1H, $J= 12.5$ Hz, $-\text{O}-\text{C}-\underline{\text{CH}_2}-\text{O}-$), 4.59 (exo, d, 1H, $J=13$ Hz, $-\text{O}-\text{C}-\underline{\text{CH}_2}-\text{O}-$), 4.40-4.36 (m, 1H, $\text{N}-\underline{\text{CH}_2}-\text{CH}_2-\text{N}-\text{Im}$), 4.25 (t, 2H, $J= 6.4$ Hz, $-\text{O}-\underline{\text{CH}_2}-\text{CH}_2-$), 4.03-3.91 (m, 5H, $-\text{N}-\underline{\text{CH}_3}$, $\text{N}-\text{CH}_2-\underline{\text{CH}_2}-\text{N}-\text{Im}$), 3.81-3.76 (exo, m, 2H, $-\text{CH}-\underline{\text{CH}}-\text{CO}-$, $\text{N}-\underline{\text{CH}_2}-\text{CH}_2-\text{N}-\text{Im}$), 3.52 (endo, d, 1H, $J= 7.65$ Hz, $-\text{C}-\underline{\text{CH}}-\text{CO}$), 3.25-3.20 (m, 2H, $-\underline{\text{CH}_2}-\text{SO}_2-\text{N}-$), 3.09 (exo, d, 1H, $J= 6.5$ Hz, $-\text{C}-\underline{\text{CH}}-\text{CO}-$), 3.00 (exo, d, 1H, $J=6.6$ Hz, $-\text{CH}-\underline{\text{CH}}-\text{CO}-$), 2.26-2.19 (m, 2H, $\text{O}-\text{CH}_2-\underline{\text{CH}_2}-\text{CH}_2-$), 1.94-1.91 (cation, anion, m, 6H, $\text{CH}_2=\text{C}(\underline{\text{CH}_3})-$).

^{13}C NMR (126 MHz, CDCl_3) δ 175.59, 174.63, 174.24, 167.40, 166.96, 138.00, 137.56, 136.89, 136.25, 135.97, 135.71, 134.66, 126.86, 126.74, 125.88, 123.58, 123.45, 123.10, 122.70, 121.60, 118.97, 89.87, 81.36, 79.49, 76.77, 63.01, 62.19, 61.31, 51.88, 50.13, 48.63, 48.08, 47.77, 47.06, 39.09, 38.30, 36.70, 25.43, 23.89, 18.41. $J_{\text{CF}} = 323$ Hz, $\text{N}-\text{SO}_2-\underline{\text{CF}_3}$

HRMS: m/z $[\text{M}]^+$ calculated for $\text{C}_{19}\text{H}_{22}\text{O}_5\text{N}_3$ (cation): 372.15540; found 372.15607; calculated for $\text{C}_8\text{H}_{11}\text{F}_3\text{NO}_6\text{S}_2$ (anion): 337.99853; found 337.99405.

IR (cm^{-1}): 3464, 3161, 3113, 2970, 1779, 1705, 1623, 1582, 1399, 1318, 1164, 1120, 1052, 947, 887, 852, 814, 730, 617, 512.

2.2.6 Polymerization of Ionic Liquid Monomers

2.2.6.1 Photopolymerization

For DSC measurements, the IL monomers were directly polymerized on the aluminum DSC pans. Briefly, a 40 mM stock solution of the photoinitiator (2,2-dimethoxy-2-

phenylacetophenone, DMPA) was prepared in dichloromethane.⁷⁶ 10 mg of polymerizable ionic liquid **5** was then deposited on the DSC pan. DMPA stock solution was added to achieve different target concentrations of DMPA (0.125 wt%, 0.25 wt%, and 0.50 wt%) in the IL monomer. The pan was protected from light and dichloromethane was allowed to evaporate. The DSC pan was then placed in a 20 mL scintillation vial and covered with a septum. The vial containing the DSC pan was degassed by flushing with argon, and the sample was then exposed to UV radiation for 30 minutes using a UV nail lamp (MelodySuzy, 36 W at 365 nm) before DSC measurement. The other IL monomers were polymerized using the same method with a DMPA concentration of 0.25 wt%. A slightly longer UV exposure of 45 minutes was required to polymerize doubly-polymerizable ionic liquids **14** and **15**. A control experiment was also performed in which polymerizable ionic liquid **5** was exposed to UV in the absence of DMPA.

2.2.6.2 Thermal Polymerization

Non-triggerable polymerizable ionic liquids **9** and **14** were also polymerized using thermal initiator azobisisobutyronitrile (AIBN).^{77,78} Briefly, a stock solution of AIBN (6.1 mM) was prepared in dichloromethane. 10 mg of the polymerizable monomer was then deposited on the DSC pan. The AIBN stock solution was then added to the DSC pans containing the ILs monomers to target a monomer: initiator of 500:1. The pan was protected from light and dichloromethane was allowed to evaporate. The DSC pan was then carefully placed in a vacuum oven, and samples were heated under vacuum at 70-80 °C for 12 h. The samples were allowed to cool to room temperature prior to DSC measurements.

A similar method was used to attempt thermal polymerization of triggerable ionic liquid monomers **5** and **15**. For better temperature control, however, the samples were polymerized by placing them in a 20 mL scintillation vial, flushing the vial with argon, and then heating the sample

in an oil bath at 65 °C for 12 h. Samples were allowed to cool to room temperature before DSC measurements. Control experiments were performed by heating the triggerable ionic liquid under the same conditions in the absence of AIBN.

2.2.7 Characterization

2.2.7.1 Differential Scanning Calorimetry

The glass transition temperature (T_g) of the polymerized ionic liquids was analyzed via differential scanning calorimetry (DSC, TA Instruments). Measurements were performed under a constant flow rate of nitrogen (50 ml/min). Samples were prepared in hermetically-sealed aluminum pans, with an empty pan used as the reference. Two sets of conditions were used for DSC measurements. For tests of the polymerization conditions, samples were heated from 0 °C or 20 °C to 160 °C, then cooled from 160 °C back to the starting temperature, and finally heated back to 160 °C, at a constant rate of 2 °C/min throughout the thermal cycle. Because the temperature at which the retro Diels-Alder reaction is observed depends on heating rate, samples prepared under the optimized polymerization conditions were also analyzed in measurements carried out between -60 °C and 170 °C with a constant heating or cooling rate of 10 °C/min throughout the thermal cycle.

2.2.7.2 Cyclic Voltammetry

Electrochemical experiments were conducted using an EC EpsilonTM Potentiostat (BASi, West Lafayette, IN). A conventional three-electrode set up, comprised of a 3.00 mm-diameter glassy carbon working electrode,⁷⁹ 0.5 mm Pt wire counter electrode,⁸⁰ and Ag⁺/Ag reference electrode, was used. The Ag wire was immersed in a solution of 10 mM AgNO₃ and 100 mM

NBu₄PF₆ in acetonitrile.⁸¹ The glassy carbon was mechanically polished in a figure-8 polishing motion with 1.0 μm α alumina powder followed by 0.05 μm γ alumina powder mixed with water on a clean MicroCloth polishing pad (Buehler, Lake Bluff, IL). After polishing, the electrode was thoroughly rinsed with deionized water and then sonicated sequentially in deionized water and absolute ethanol to remove any remaining particles. The electrode was then dried under nitrogen flow.

To prepare the reference electrode, a solution of 10.0 mM AgNO₃ and 100 mM NBu₄PF₆ in acetonitrile was injected into glass tubing with a porous Teflon tip sealed to the glass. The tubing was tapped to ensure no air bubbles were trapped in the bottom of the tubing. An Ag wire with a Teflon cap was slowly inserted into the glass tubing. After filling the reference electrode compartment, the reference electrode was immediately immersed in a solution of identical composition to prevent the exposure of the porous tip to air. The reference electrode was left undisturbed for a minimum of 24 h before use. Sample solutions were then prepared at a concentration of 10 mM analyte and were rigorously purged with argon for 10 minutes to remove dissolved oxygen. Anodic and cathodic behavior were recorded separately. Voltammograms were recorded at a scan rate of 50 mV/s at room temperature and the potentials were calibrated to the ferrocene (Fc)/ferricenium (Fc⁺) redox couple in each sample.

2.2.8 Capacitor Measurements of Ion Release

2.2.8.1 Capacitor Fabrication

1×1 cm² Si substrates with 90 nm SiO₂ (Graphene Supermarket, resistivity 0.001 - 0.005 ohm·cm) were pre-cleaned with acetone, isopropanol (IPA), deionized (DI) water and dried with N₂. LOR5B (MicroChem) photoresist was spin-coated on the substrate at 4000 rpm for 1 min and

annealed at 195 °C for 9 min. A second photoresist, S1805 (Microposit, 5000 rpm, 1 min), was spincoated on top of the first and annealed at 115 °C for 5 min. Capacitors were patterned by direct write photolithography (Heidelberg MLA100) with 10 μm electrode spacing. Samples were developed for 75 s in Microposit 351, 30 s in DI water, 40 s in AZ 400K (Microchemical), rinsed in DI water for 30 s and dried with N_2 . Ti/Au (3/140 nm) was deposited by e-beam evaporation (Plassys MEB550S) at $< 1 \times 10^{-6}$ Torr. Lift-off was performed in Remover PG (MicroChem) overnight for 9 hours, followed by IPA, DI water rinse and N_2 drying.

2.2.8.2 Deposition and UV Polymerization of Polymerizable Ionic Liquids

The unpolymerized SPILs and DPILs were drop-cast on the capacitors (25 μL over 1 cm^2) in an argon-filled glovebox with H_2O and $\text{O}_2 < 0.1$ ppm. The samples were transferred without air exposure from the glove box to a cryogenic vacuum probe station (Lakeshore, CRX-VF) via a custom load-lock for electrical measurements at $\sim 2 \times 10^{-6}$ Torr and 295 K. After the measurements, the samples were transferred back to the glovebox for UV polymerization. $\sim 5 \mu\text{L}$ of a 0.25 wt% solution of 2,2-dimethoxy-2-phenylacetophenone in dichloromethane was added to the IL by drop-casting and natural drying in the glove box. The samples were UV polymerized using a UVP Compact UV lamp ($\lambda = 365$ nm, $P = 1.3$ mW cm^{-2} at 7.6 cm) at a working distance of ~ 1.5 cm for 30 min. After polymerization, the samples were transferred back to the probe station without exposure to air to complete the electrical characterization over a temperature range of 295 to 400 K.

2.2.8.3 Electrical Characterization

Charging current was monitored with time using a Keysight B1500A semiconductor parameter analyzer. Voltage was applied to terminal 1 (V_1) with terminal 2 (V_2) grounded while

monitoring the current (I_1) for 5 minutes. The current decayed to <50 pA within the measurement time indicating a full charge. $V_1 = +1.5$ V for triggerable and non-triggerable DPIL and triggerable SPIL; V_1 was reduced to $+0.5$ V for non-triggerable SPIL to meet the current sensor range. Similarly, a discharge time of 5 minutes was set to ensure full discharging of the device to avoid hysteresis.

To detect ion mobility as a function of temperature, the charging and discharging measurements were made on the polymerized samples over a temperature range of 295 to 395 K, with 10 K steps and a ramp rate of 2 K/min. Measurements at 400 K were repeated twice with a 4 hour wait time between measurement to monitor stability. Once the setpoint was reached, the sample was held at the set temperature for 5 min prior to measurement to establish thermal equilibrium. Lastly, samples were cooled from 400 to 295 K at 0.3 K/min and measured at 295 K.

2.3 Results and Discussion

2.3.1 Synthesis of the IL monomers

Our synthetic approach for designing the thermally-triggerable polymerizable cation involves a thermally allowed [4+2] cycloaddition Diels-Alder reaction between a diene and a dienophile. It is well known that the Diels-Alder reaction between furan derivatives as the diene and maleimide derivatives as the dienophile is spontaneous at room temperature due to the presence of highly reactive double bonds in furan derivatives.⁶⁸ Previously, it has been reported that the Diels Alder adducts of furfuryl methacrylate and maleimide deadduct easily above their melting point.⁷² Therefore, we decided to introduce the polymerizable residue in the triggerable

cation by choosing furfuryl methacrylate as the diene partner and maleimide as the dienophile. We anticipated that incorporation of thermally labile Diels-Alder linkages between the polymer backbone and ionic species would enable the ionic conductivity of the polymerized ionic liquid under a given set of experimental conditions to be changed, in contrast to typical PILs in which the conductivity is typically fixed at a given temperature.

The adopted synthetic route involved protection of the reactive double bond of maleimide by performing a Diels Alder reaction and then the subsequent functionalization with the imidazolium ion. We began our synthesis by preparing the Diels-Alder adduct between furfuryl methacrylate and maleimide. The reaction was carried out at room temperature in diethyl ether and gave 85% yield. The structure of the Diels Alder adduct was confirmed by ¹H-NMR analysis. The characteristic peaks of the DA adduct were observed at 6.59-6.46 ppm for the endocyclic double bond, 5.25 ppm for the bridgehead proton of the endo adduct and 5.13 ppm for the bridgehead proton of the exo adduct. The protons of the fused rings appear at 3.65-3.44 ppm (endo) and 2.96-3.03 ppm (exo). These assignments are in agreement with previously reported data of similar compounds where the 'endo' adduct has been assigned a higher chemical shift than the 'exo' adduct.^{82,83} To demonstrate our proof-of-concept, we did not target a specific isomer. The endo/exo ratio was found to be 70/30, indicating that the kinetically-favored 'endo' adduct was favored at room temperature, as expected.

The DA adduct with the polymerizable methacrylate was subsequently converted to the thermally-triggerable polymerizable cation by series of reactions that were chosen to avoid side reactions including retro Diels Alder of the DA adduct, hydrolysis of the methacrylate group, and polymerization of the reactive methacrylate group. In the initial stage, the DA adduct was modified by nucleophilic substitution with 1,2-dibromoethane in the presence of K₂CO₃ and DMF at 50 °C.

K_2CO_3 was used to drive the nucleophilic substitution because it is a strong enough base to deprotonate the mildly acidic maleimide proton but is too weak to drive hydrolysis of the methacrylate group under the reaction conditions. The polymerization of the reactive methacrylate group was inhibited with a small amount of 4-methoxyphenol. The reaction progress was monitored by thin layer chromatography and the starting material was consumed within 2.5 h. No cycloreversion of the DA adduct was observed at 50 °C. ^1H NMR revealed that the *endo/exo* ratio did not change significantly and was found to be 73/27.

In the next stage, 1-methylimidazole was quaternized with the bromine functionalized polymerizable DA adduct at 40 °C for two days in the absence of solvent to yield the thermally-triggered polymerizable imidazolium salt. The polymerization of the reactive methacrylate group was inhibited with a small amount of 4-methoxyphenol and no retro Diels-Alder reaction was observed. The desired product was purified by precipitating in diethyl ether. The thermally triggered polymerizable imidazolium salt was characterized by ^1H NMR and the *endo/exo* ratio was found to be 52/48. This might be due to the possible isomerization of *endo*-adduct to *exo*-adduct as the reaction was heated for 48h and thus favoring the thermodynamic *exo* adduct.

The thermally triggered polymerizable imidazolium salt was ion-exchanged in aqueous solution with non-polymerizable $[\text{Li}][\text{TFSI}]$ to yield analogous thermally-triggerable singly polymerizable ionic liquid. Due to its hydrophobic nature, the product crashed out of the aqueous solution as viscous oily droplets. The ion-exchange reaction was confirmed by ^1H NMR analysis as the TFSI counterion caused a dramatic shift of the -N-CH-N- proton on the imidazolium ring to 8.7 ppm compared with a shift of 10.5 ppm for the same cation with a bromide counterion.⁸⁴ The *endo/exo* ratio was found to be 46/54. Although this reaction was performed at room temperature, a slight increase in the *exo* adduct was observed. This might be possible due to isomerization of

endo adduct to *exo* adduct by LiTFSI as it has been previously reported as a promoter of [4+2] cycloaddition reaction favoring *exo* selectivity.⁸⁵

2.3.2 Differential Scanning Calorimetry (DSC)

The thermal transitions of the DA adduct were characterized by differential scanning calorimetry (DSC). DSC was used to locate the temperature at which the retro Diels-Alder reaction begins to occur. It is well reported that the heat required to drive the retro Diels-Alder reaction appears as a broad endotherm in DSC measurements and multiple endotherms are observed for the adducts containing a mixture of *endo* and *exo* isomers.^{68,86} The *endo* isomer is kinetically favored and the *exo* isomer is thermodynamically favored; the rDA of the *endo* stereoisomer was thus assigned to the endothermic peak with the lowest temperature and *exo* to the higher temperature on the DSC curve.⁸⁷ DSC measurements performed at a ramp rate of 2 °C/min showed a broad endothermic peak between 80 °C to 100 °C, corresponding to the *endo* unblocking reaction, and another broad endotherm between 130 °C to 150 °C, corresponding to the *exo* unblocking reaction (Figure 15a).

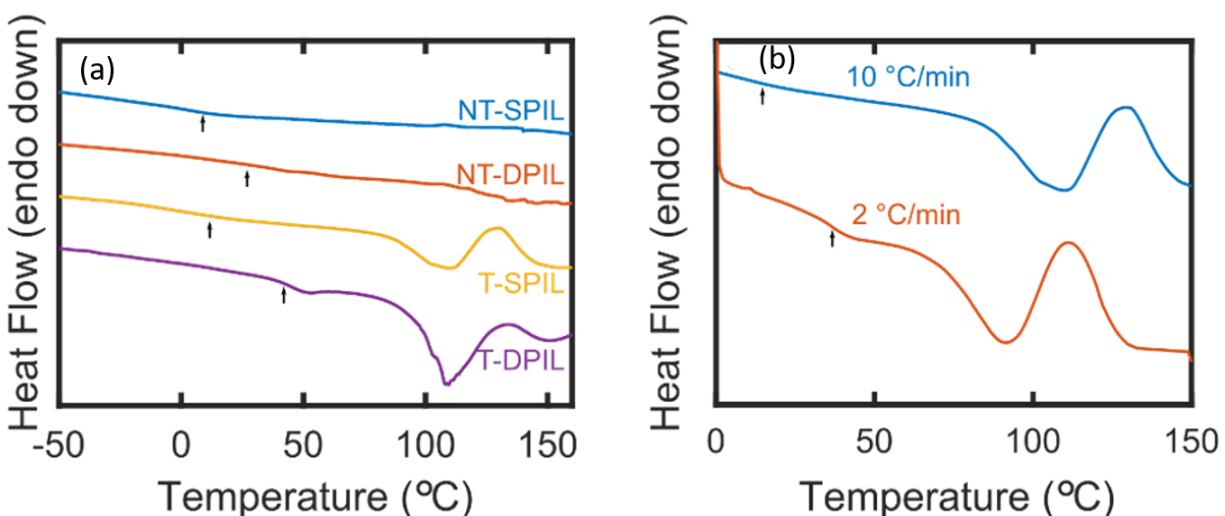


Figure 15 Differential scanning calorimetry thermograms of (a) all four polymers used in this work and (b) polymerized T-SPIL at two different scan rates. Arrows in panels (a) and (b) indicate the glass transition temperatures (midpoints) of each material

An interesting feature observed in the DSC thermogram was that a change in the ramp rate from 2 °C to 10 °C shifted the endothermic peaks corresponding to the thermal transitions of the endo and exo isomers towards higher temperature (Figure 15b). Thermal endo-exo isomerization is a well-known process and has been previously observed by Gandini and co-workers and Jegat et.al but we did not observe this isomerization in the measured DSC traces.^{87,88}

2.3.3 Polymerization of the PIL monomers

2.3.3.1 Thermal Polymerization

Once the synthesis of the thermally-triggered polymerizable cation was successfully achieved, the next challenge to address was the polymerization of the methacrylate group without affecting the thermally-labile Diels-Alder linkages. Azobisisobutyronitrile (AIBN)-induced free radical polymerization of ionic methacrylate monomers has been promising as reported in

literature.⁸⁹ Mikhailov and co-workers have also successfully polymerized the DA adduct of furfuryl methacrylate and maleimide in solution at 70 °C using AIBN without driving the retro-Diels Alder reaction of the adducts at this temperature.⁷² However, Northrop and co-workers have demonstrated the significant influence of substituents on the reversibility of furan-maleimide cycloadditions.⁹⁰ We began by investigating whether the imidazolium substituent on maleimide in the triggerable polymerizable cation would affect the rDA temperature of the DA adduct and thus the polymerization conditions in contrast to Mikhailov's system.

The IL monomers were first polymerized using a thermal initiator, AIBN. Since the half-life of AIBN in toluene is 10 h at 65 °C, the polymerization was performed at 70 °C to 80 °C for 12 h.⁹¹ The non-triggerable PILs (NT-SPIL and NT-DPIL) were successfully polymerized and a distinct T_g was observed in the DSC as seen in Figure 16. For the NT-DPIL, a broad T_g was observed and the value of the T_g obtained during the first heating scan was lower than that obtained during the second heating scan.

For the triggerable PILs, however, DSC indicated that the endo adduct underwent retro DA under the polymerization conditions, as seen in Figure 17. The DSC thermogram showed only the broad endothermic peak corresponding to the (rDA) temperature of the exo adduct, confirming the deadduction of the 'endo' DA adduct during the thermal polymerization. This is in accordance with the previous reports that the *endo* compound is unblocked at a lower temperature than the *exo* compound.⁹² A control experiment was also performed in which the triggerable PIL was heated without AIBN, which confirmed that the cycloreversion of the *endo* adduct was solely due to heat and not AIBN.

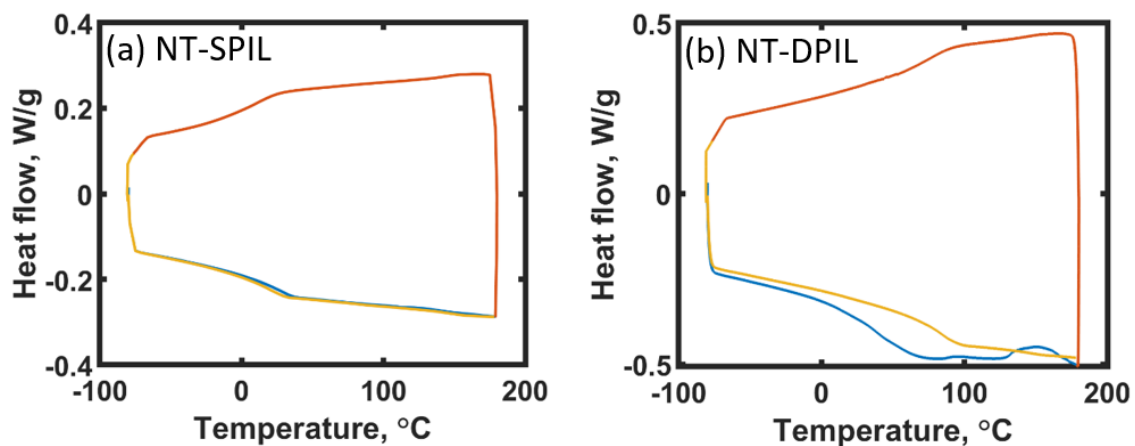


Figure 16 DSC thermograms of (a) NT-SPIL and (b) NT-DPIL after polymerization with AIBN

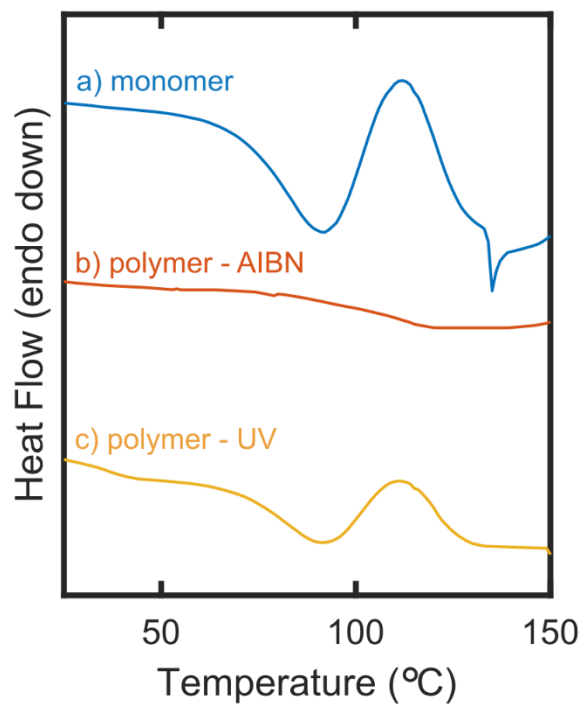


Figure 17 DSC thermograms of T-SPIL (a) before and (b, c) after polymerization with (b) AIBN at 65 °C and (c) DMPA under UV light at room temperature

2.3.3.2 Photopolymerization

To avoid retro Diels-Alder during the polymerization step, photopolymerization was used. 2,2-Dimethoxy-2-phenyl-acetophenone (DMPA) is an attractive photoinitiator for the photopolymerization of methacrylate monomers.⁹³ Facile free radical photopolymerization of methacrylate monomers with high conversions has been achieved with concentrations as low as 0.25 wt.% DMPA at room temperature.⁹⁴ Based on these reports, DMPA was investigated as a photoinitiator for the polymerization of the PILs with and without thermally labile linkages.

Previously, DMPA has been shown to photopolymerize methacrylates efficiently at concentrations between 0.125 wt. % and 0.25 wt. %, while no significant difference was observed in increasing the DMPA content from 0.125 wt. % to 0.5 wt. %.⁹⁴ Keeping the UV irradiation time constant for 30 minutes, we systematically varied the amount of DMPA from 0.125 wt. % to 0.25 wt. %, to 0.50 wt. %. The triggerable PIL (T-SPIL) was polymerized within 30 minutes of UV radiation with each of the DMPA contents as demonstrated in Figure 15. The broad endothermic peaks arising from the thermal transitions of the *endo* and the *exo* adducts were clearly evident from the DSC, and no polymerization exotherm was observed, revealing the successful polymerization of the triggerable SPIL without accompanying the retro-Diels Alder reaction. The glass transition temperature (T_g) of the PILs was obtained by the mid-point method and are been reported in Table 1.

Table 1 Glass transition temperature of photopolymerized ionic liquids

Polymerized Ionic Liquids (PILs)	Glass transition (T_g , °C)
T-SPIL	38.1
NT-SPIL	10.1
T-DPIL	41.5
NT-DPIL	72.2

Due to the insolubility of the resulting triggerable polymerized ionic liquid in any suitable organic solvent the conversion of monomer to polymer could not be quantified. A control experiment was performed in which the triggerable PIL was exposed to UV light in the absence of DMPA which confirmed that the polymerization of the T-SPIL was solely due to DMPA and not an outcome of a side reaction due to UV irradiation. The DSC thermogram showed the thermal transitions from the *endo/exo* adduct but no distinct T_g was observed eliminating the possibility of side reactions due to UV exposure. The non-triggerable PILs (NT-SPIL and NT-DPIL) were photopolymerized in a similar manner using 0.25 wt. % DMPA content and 30 minutes UV irradiation (Figure 15a).

2.3.4 Cyclic Voltammetry (CV)

For applications in organic electronic devices, it is important for PILs to be electrochemically stable. The electrochemical potential windows (EPWs) of PILs depends on the anions and cations of ILs, the water content of the ILs, and the electrode materials including the

working electrode and the reference electrode.⁹⁵ The solvent chosen for the potentiometry experiments also plays an important role and should be such that all the redox reactions of the analyte happen within the ‘solvent window’ of the chosen solvent.⁹⁶ Computational and experimental studies have demonstrated low electrochemical stability of imidazolium-containing ILs due to a presence of a highly acidic proton at C-2 position of the imidazole ring.^{97,98} On the contrary, wider electrochemical windows have been observed for the ILs containing TFSI counterion, contributing to the broad stability of the ILs.⁹⁹

To allow access to a wide electrochemical window, we used acetonitrile as a solvent and glassy carbon (GC) as the working electrode since the potential for oxidation and reduction on GC electrode are very high.⁹⁶ [NBu₄][PF₆] was chosen as the supporting electrolyte due to its high stability and noncoordinating nature.⁹⁶ Figure 18 shows the CVs of different PILs with and without the Diels-Alder linkages and commercial [EMIM][TFSI] salt. The current fluctuations at the higher negative potentials might be due to unstable decomposition of the ionic liquid and the presence of impurities such as oxygen and water.^{32,100} The presence of trace water is evident from the peaks arising at around 1.2 V.³² These peaks were hard to prevent even though the samples were rigorously purged with argon before the potentiometry measurements. Even hydrophobic ionic liquids have a tendency to absorb atmospheric water and thus water is always an impurity along with the ILs.¹⁰¹

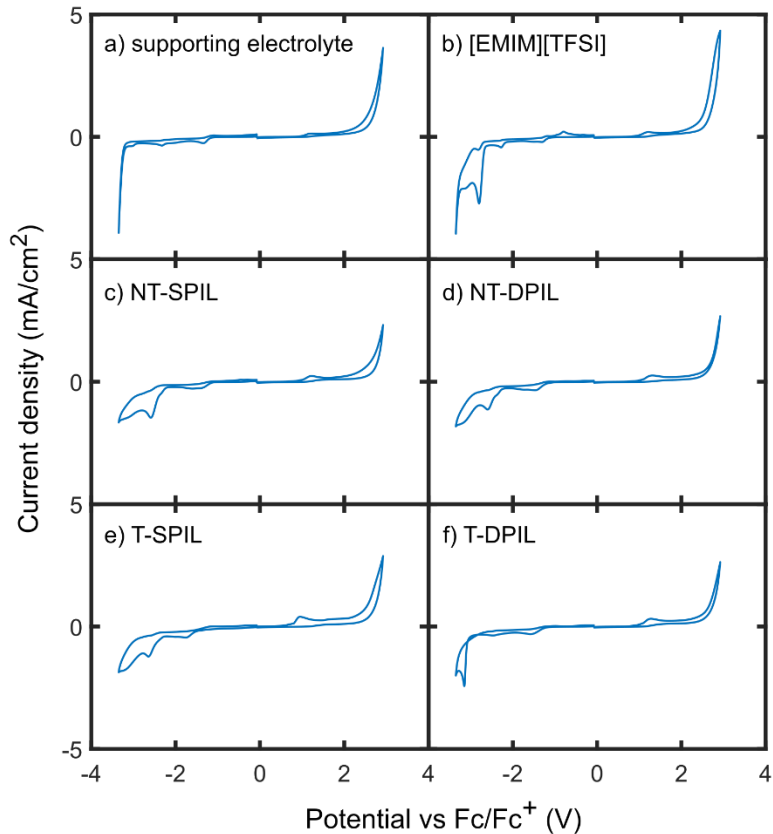


Figure 18 Cyclic voltammograms all of materials used in this work (b-d). Scans of the supporting electrolyte (a) and commercial [EMIM][TFSI] (b) are included for reference.

The potential range in which the limiting current density approached $1.0 \text{ mA}\cdot\text{cm}^{-2}$ is referred to as the electrochemical window of the IL. The EW's reported as the difference between cathodic and anodic potential are given in Table 2.

Table 2 Electrochemical stability windows of commercial, non-polymerizable [EMIM][TFSI] and all four PILs used in this work

Ionic Liquids	Electrochemical Window (EW, V)
[EMIM][TFSI]	4.5
T-SPIL	4.2
NT-SPIL	4.2
T-DPIL	4.3
NT-DPIL	4.1

Taken together, cyclic voltammetry studies demonstrate that the electrochemical window of all the investigated ILs including both triggerable and non-triggerable is similar to non-polymerizable analog [EMIM][TFSI] at approximately 4V, suggesting their viability for application in advanced organic electronics (Figure 18).

2.3.5 Capacitor Studies on Designed PILs

The ion release from the triggerable PILs was investigated using the capacitor measurements performed by our collaborators in the Chemical Engineering Dept. at the University of Pittsburgh. In those measurements, as depicted in Figure 19, the materials were subjected to a step in the applied voltage and the resulting current was measured as function of time. The amplitude of the response indicates the mobile ion content. Ionic conductivity, measured by impedance spectroscopy, is a standard way to access ion mobilities in polymer systems. However,

the present system presents several unique challenges (such as need to access the electrolyte surface to UV cure, and the need to keep the sample in an air-free environment to prevent water adsorption) that make standard impedance measurements difficult. Substrate effects also make it difficult to quantitatively extract mobile ion content from these measurements. Thus, because our primary purpose here is just to monitor relative changes in ion mobility with changes in temperature, we chose to monitor charging current, as it is a simpler measurement to conduct and interpret.

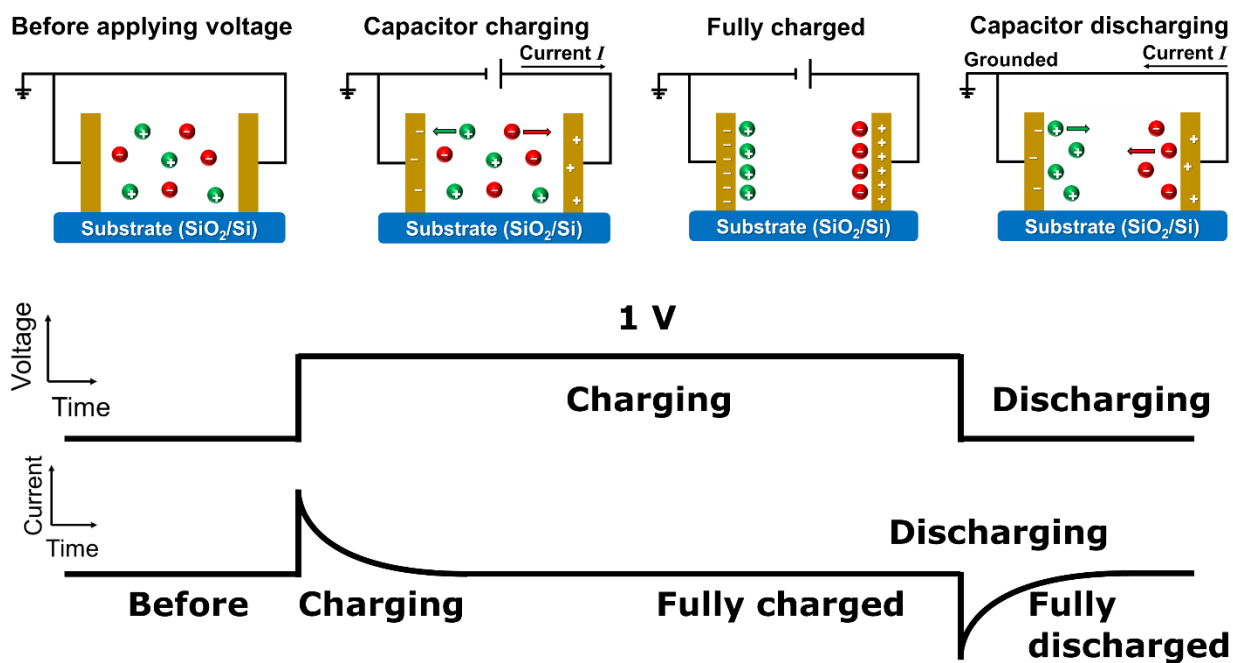


Figure 19 Schematic representation for interpretation of electrical measurements on polymerized ionic liquids.

The ion motion was first examined in the triggerable and non-triggerable singly-polymerized ionic liquids (SPIL). As observed in Figure 20, both the non-triggerable (NT) and triggerable (T) SPIL show evidence of mobile ions before polymerization, with a current spike

followed by a subsequent decay. Once the SPILs were UV polymerized, a significant decrease in the current was observed as the ions were locked in place due to polymerization. When the NT-SPIL was gradually heated to 400 K and then returned to room temperature, the measured capacitor response did not show any change in the mobile ion content and had returned to its post-polymerization baseline. Interestingly, for the T-SPIL the capacitor response returned to its pre-polymerization level, indicating an increase in the mobile ion content due to the thermal cycle. Thus, the capacitor studies indeed confirmed our hypothesis that the incorporation of thermally-labile Diels-Alder linkages between the charged groups and the polymer backbone enables ‘on-command’ release of ions in polymerized ionic liquids.

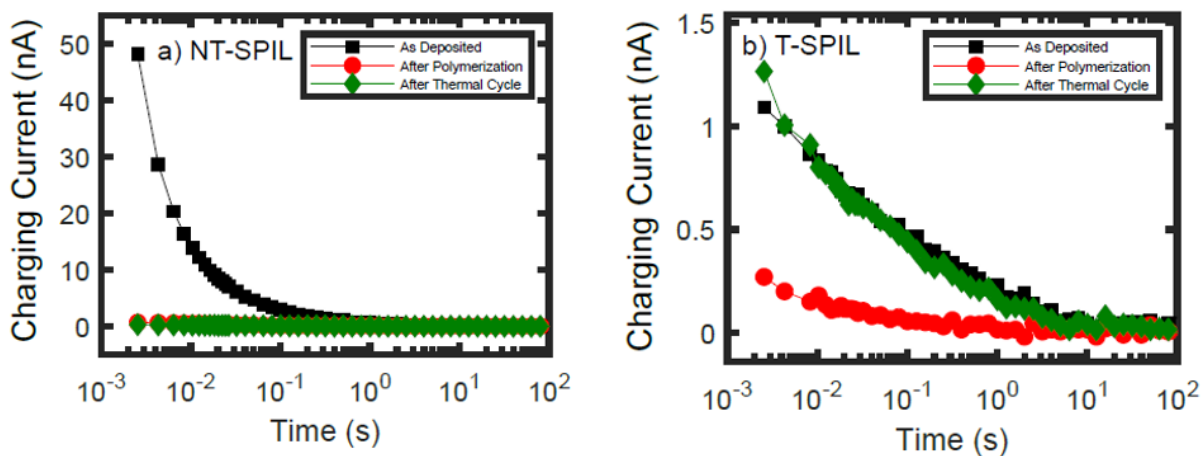


Figure 20 Capacitor response of (a) non-triggerable and (b) triggerable singly-polymerized ionic liquids at 298 K, measured before polymerization, immediately after polymerization, and after a full thermal cycle in which the temperature of the sample was increased to 400 K before being returned to room temperature. Each trace depicts the response of the material to a step potential applied across a capacitor with 10 μm electrode spacing.

As shown in Figure 20, the difference in the initial current for the T-SPIL after polymerization and after thermal cycling is surprisingly small (only 400% more after heating or as the monomer). One reason for the low on/off ratio may be the presence of free anions in the polymerized state. This is almost certainly a factor- in fact, while it is difficult to see due to the different scaling of the axes in the Figure 20 a and 20 b, the response of the polymerized NT-SPILs is almost identical to that of the polymerized T-SPILs before the thermal cycle. This suggests that the response is almost entirely dominated by the mobile anions before release of the cations is triggered. We note that this result does imply that limiting the anion mobility should improve on/off ratios in these materials, which was indeed our motivation for exploring the doubly-polymerized materials as shown in Figure 22.

To gain insight into the observations from the capacitor measurements, it is critical to understand the response of both the materials, T-SPIL and NT-SPIL, during the thermal cycle. In the case of NT-SPIL, a steady increase in the mobile ion content was observed over the entire temperature range (Figure 21a). This behavior is consistent with previous work showing that when a PIL is heated above the glass transition temperature, the conductivity increases. On the contrary, for the T-SPIL (Figure 21b), a distinct “turn-on” behavior is observed around 360 K, which is way higher than the glass transition temperature of the T-SPIL but close to the cycloreversion temperature of the Diels-Alder adduct. Clearly, the increase in the mobile content of the T-SPIL after a full thermal cycle is due to cleavage of the Diels-Alder linkages in the furan-maleimide adduct.

We expected that as the material is cooled, the mobile ion content would decrease due to the reversible nature of the Diels-Alder reaction, which should allow “re-capturing” the ions. However, this behavior was not observed. This might be due to the degradation of the maleimide

or furan derivatives at higher temperatures that might have prevented the recombination of the two, or the kinetics of the forward Diels-Alder reaction may be too slow for this process to occur during the cooling process.

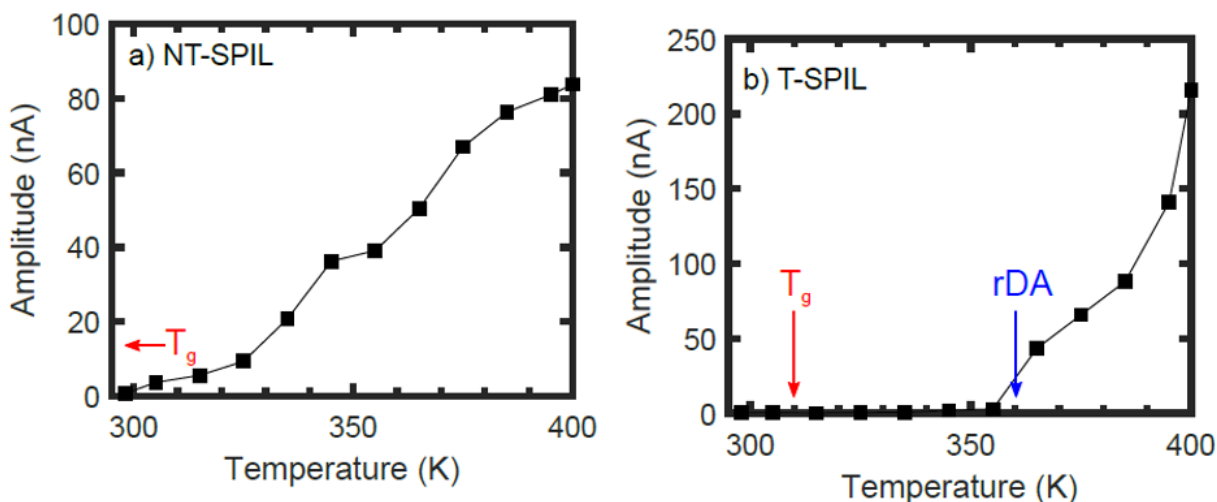


Figure 21 Temperature-dependent current amplitudes for capacitors with (a) non-triggerable and (b) triggerable singly-polymerized ionic liquids deposited and polymerized across the electrodes. Arrows labeled T_g and rDA indicate the glass transition temperature and retro Diels-Alder temperatures of the samples, respectively.

Finally, we emphasize that the on/off ratio before and after the full thermal cycle is only one way to look at the triggering capability of the current material; the abrupt turn-on behavior observed in Figure 21 b is also novel, and suggests that these materials may be useful as thermal “switches”.

We then extended this approach to NT and T-DPILs. As observed in Figure 22, both the non-triggerable (NT) and triggerable (T) DPIL show evidence of mobile ions as-deposited, similar to the SPIL samples. Once the DPILs were UV polymerized, a significant decrease in the current was observed as the ions were locked in place due to polymerization. When the NT-DPIL was

gradually heated to 400 K and then returned to room temperature, the measured capacitor response did not show any change in the mobile ion content. This is in accordance with the previously reported literature that the ionic conductivity drops precipitously on polymerizing the ionic liquid composed of a polymerizable cation and polymerizable anion.⁸

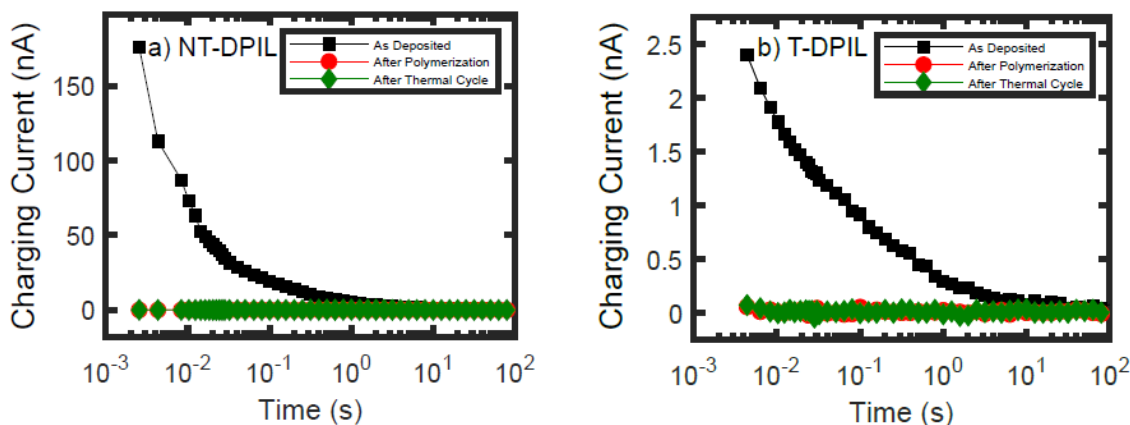


Figure 22 Capacitor response of (a) non-triggerable and (b) triggerable doubly-polymerized ionic liquids at 298 K, measured right before polymerization, immediately after polymerization, and after a full thermal cycle in which the temperature of the sample was increased to 400 K before being returned to room temperature.

Surprisingly, the T-DPIL, unlike the T-SPIL, did not show a distinct ‘turn-on’ behavior near the retro Diels Alder temperature as shown in Figure 22 b. This could be either due to the successful release of only a small fraction of the cations by the deadduction of the Diels-Alder adduct or due to the slow dynamics of the doubly polymerized ionic liquid, which may inhibit transport of the released cations. We hypothesized that designing DPILs with triggerable units on both the cation and the anion may help in changing the mobile ion-content in the DPIL systems considering both the ionic species could be released during the thermal cycle. However, the

triggerable anions turns out to be much more difficult to synthesize and purify than the triggerable cations, in part because trifluoromethanesulfonimide ions catalyze the Diels-Alder reactions (and retro-Diels-Alder reaction) and the anionic sidechain degrades the triggerable linkage during several steps of monomer synthesis.⁸⁵

2.4 Conclusion

In this chapter, we demonstrated a novel strategy for ‘on-command’ release of ions in polymeric materials by incorporating thermal triggers into polymerized ionic liquids. A new type of polymerizable ionic liquid containing a thermally labile Diels-Alder linkage between the polymerizable group and the charged unit was developed. Thermal cleavage of the Diels-Alder linkages between the polymer backbone and charged functional group separates the ionic groups from the polymer chains, allowing them to move throughout the material. This capability-releasing ions “on command” in response to a simple physical trigger-is not feasible in current generations of polymerizable ionic liquids and represents a new way of controlling the mobile ion content in polymeric materials.

This work enables changing the mobile ion content of a polymerized ionic liquid after the sample is prepared, enabling advanced organic electronic applications beyond the potential of existing polymerized ionic liquids. We believe this approach will result in a new class of polymerizable ionic liquids with thermally-controllable conductivities and will pave the way for the future development of polymerized ionic liquids and devices responsive to a variety of physical and chemical triggers like heat, light, and mechanical force.

3.0 Dynamics of Ion Locking in Doubly-Polymerized Ionic Liquids

3.1 Introduction

Polymerized ionic liquids have attracted significant attention in the past decade due to their remarkable physical characteristics such as enhanced chemical stability, broad electrochemical window, and mechanical durability to name only a few.^{3-7, 24-26} With one of the charged species covalently tethered to the polymer backbone, they allow efficient ion transport in mechanically-robust materials.²⁴⁻²⁶ These PIL single-ion conductors have been of considerable interest in applications such as battery separators.^{24-26, 102,103} They have played an integral part in electrolytes for batteries and flexible electronics, and gate dielectrics for field-effect transistors.¹⁷⁻²¹ Nonetheless, controlling ion motion timescales in polymerized ionic liquids remains central for advanced organic electronic applications.

While most work to date has focused on increasing ion mobility without sacrificing mechanical properties, decreasing ion mobility in these materials may also be useful in emerging applications in organic electronics.^{34,66,67,104,105} Electrostatic doping by ions relies on the formation of an electric double layer (EDL) at the electrolyte/channel interface where the image charges induced by the ions serve as dopants in the channel. Electrostatic doping can induce sheet carrier densities in two-dimensional (2D) crystals exceeding 10^{14} cm^{-2} without altering the intrinsic band gap, and the doping is reconfigurable between *p*- and *n*-type or *p-n/n-p* junctions by redistributing ions under the field.¹⁰⁶ However, in conventional electrolytes such as ionic liquids/gels, a gate voltage must be continuously applied to hold the ions in place and therefore set the doping state.^{107,108} What would be useful is a “gateless” electrostatic doping wherein the doping could be

programmed by ions and then locked into position via a trigger until the ions could be unlocked and reconfigured again on demand. Recently we achieved this in collaboration with Fullerton's group using doubly polymerized ionic liquid (DPIL) and consequently demonstrating the first application of DPIL to construct a functional organic electronic device (Figure 8).¹³

In this work, DPIL was dropped on graphene-based two-dimensional transistor, and once voltage was applied across the electrodes, DPIL behaves as a typical electrolyte with mobile ions that can be drifted by an applied field to form EDL. The structure of DPIL is analogous to [EMIM][TFSI], but with additional polymerizable functional groups on both charged species to perform ion ion-locking (Figure 5b). Polymerization of both the ionic species either by UV or heat could effectively lock the non-equilibrium ion distribution and therefore the EDL into place. Once locked, the electric field is removed and EDL does not dissipate. Thus, here ion locking was used to enable well-built lateral p-n junctions that remained intact after the voltages were put off. We attributed this behavior to a sharp drop in mobile ion content after polymerization that is significantly more in contrast to singly-polymerized ionic liquids.

This work has been built on similar phenomena observed in the small number of other doubly-polymerizable ionic liquid systems studied to date. Previously, Yoshizawa *et. al* has shown in doubly-polymerized ionic liquids composed of vinylimidazole and vinylsulfonic acid that copolymerizing both the cations and the anions in an ionic liquid led to a precipitous drop in conductivity to the order of 10^{-9} Siemens cm^{-1} .^{8,11} The addition of a small amount of non-polymerizable LiTFSI increased the conductivity by 4-5 orders of magnitude highlighting the critical role of free ions in the overall ion mobility in these materials. Shaplov *et. al* demonstrated a considerable drop in ionic conductivity via the complete removal of mobile counterions from the

copolymerization of oppositely charged monomers, cationic monomer being based on pyrrolidinium or imidazolium system and the anionic monomer being based on sulfonate system.⁹

Recently Fouillet *et. al.*, showed that polyampholytic copolymers, synthesized by RAFT polymerization of ionic monomers each containing vinyl pendant groups with vinyl-1,2,4-triazole being the common Bronsted base, display overall radically reduced mobility.¹¹ It is well demonstrated that conductivity is significantly affected by polymerization of both the ionic species but very little is understood about the mechanisms of ion relaxation in these materials.^{10,11} Therefore, understanding the dynamics of ion motion in these materials, and their dependence on the chemical structures of the polymerizable ions is crucial for developing these materials as a versatile platform for organic electronics. Our primary goal in the present work is to understand the dynamics of ion motion and to quantify the timescales of ion motion and polymer relaxation in the DPIL system.

Coulombic interactions among the ions strongly influence the properties of ionic liquids. Spectroscopic techniques like NMR, IR, etc. do not have the potential to examine these interactions. On the contrary, dielectric relaxation spectroscopy has proven to be a powerful technique for measuring dynamics of ion motion in ionic liquids covering an expansive spectral range with broadly changing temperature.³³ It has furnished a wealth of information regarding the dynamics and charge transport in polymerized ionic liquids. In this technique, the sample is sandwiched between the two electrodes forming a parallel plate capacitor geometry. Once the oscillating voltage is applied across the two electrodes, the frequency dependent dielectric response is measured. Being receptive to dipolar species, the frequency dependent dielectric function imparts direct access to timescales of dielectric relaxation in the material, which may

originate from processes such as segmental motion of the polymer backbones, side-chain orientation, and ion-transport.^{3,64,109,110}

Previously researchers have used broadband dielectric spectroscopy in conjunction with other techniques to unravel the dynamics of ion motion in ionic liquids and singly-polymerized ionic liquids extensively. Rossler and coworkers investigated the transport mechanisms of charge carriers by measuring the complex dielectric function in BMIM-based RTILs with different anions over a wide temperature range.¹¹¹ They observed that RTIL exhibits an ionic conductor behavior above and a glassy behavior below the T_g. Previously Sokolov and coworkers decoupled the temperature dependence of ionic conductivity from structural relaxation in polymeric materials using broadband dielectric spectroscopy.^{110,112} They demonstrated a strong correlation between the strength of decoupling and fragility of the polymeric material.

Frenzel et.al analyzed the charge transport and molecular dynamics in polymeric polyisobutylene-based ionic liquids by employing broadband dielectric spectroscopy.¹¹³ They attributed the lower conductivity of the PILs relative to the neat IL to a two two-component system generated by microphase separation between the IL-like moieties and the polymeric part. Sangoro and coworkers demonstrated the existence of mesoscale aggregates in imidazolium ILs with alkyl spacer lengths greater than butyl.^{64,114} They elucidated the slow, sub-alpha relaxations corresponding to the dynamics of nanoscale hydrophobic aggregates using broadband dielectric spectroscopy in conjunction to dynamic-mechanical spectroscopy.

Studies by Kremer and coworkers indicated that rapid transport and high ionic conductivities in imidazole based ionic liquids signify the importance of ion hopping in these materials.^{110, 115-118} Recent work on ion transport in singly-polymerized ionic liquids have suggested that the dynamics of ion motion are strongly affected by the nanoscale structure of the

materials, which separate into polar and nonpolar domains on the length scale of single monomers.^{64,114} Colby and coworkers investigated the effect of counterion, spacer length, and the type of spacer between the polymer backbone and the imidazolium cation on the dielectric response of variety of polymerized imidazolium acrylate and methacrylate polymers.³⁻⁶ They demonstrated that the incorporation of diethyleneoxy into the imidazolium cation and presence of shorter alkyl chains impart higher ion mobility and significantly lower the glass transition temperature. They had observed significant ion conduction with TFSI counterion which they attributed to its weak binding with imidazolium ion.

In contrast to extensive studies on the mechanism of ion transport in singly-polymerized ionic liquid, there have been no reports elucidating the comprehensive picture of the dynamics of ion motion in DPIL materials. Understanding the dynamics of ion motion in these materials, and their dependence on the chemical structures of the polymerizable ions will be of specific significance for utilizing them inside field-effect transistors or organic thin-film transistors. Our primary goal in the present work is to understand the dynamics of ion motion and to quantify the timescales of ion motion and polymer relaxation in the DPIL system. Although our main focus in this work was to understand the behavior of the DPIL systems, inclusion of both the positively- and negatively-charged SPILs as control samples provided an interesting opportunity to investigate whether there are any important differences in the ion conduction depending on which charged group is mobile and which is linked to the polymer backbone and further elucidate the mechanism of ion transport in these materials.

Here we used the broadband dielectric relaxation spectroscopy to investigate the dynamics of ion motion in [EMIM][TFSI]- based DPIL and compared its dielectric response to singly polymerizable ionic liquids with the polymerizable cation or the polymerizable anion. The BDS

measurements were made both above and below the material's glass transition temperature, as identified by differential scanning calorimetry, in accordance with the temperature cycle. Interestingly, we found the relaxation dynamics of the cation and the anion are very similar which has not been reported previously. But the dynamics of ion motion are significantly different in DPIL relative to that of singly polymerizable cation and singly polymerizable anion.

The polymerization of the DPIL decreases the ionic conductivity by four orders of magnitude when compared to both SPILs. Similarly, the timescales for local ionic rearrangement are found to be approximately four orders of magnitude slower in the DPILs than in the SPILs, and the DPILs showed a lower static dielectric constant. These results implicate that copolymerization of the charged monomers restrict both the bulk and the local ionic motions in DPIL because of their highly crosslinked state due to strong ionic interactions. Taken together for new classes of organic electronics, these results furnish a rich range of physical, practical, and quantitative information to the energetics and timescales of ion motion in these materials.

3.2 Experimental

3.2.1 Materials

All reagents were purchased from standard commercial suppliers. For monomer and polymer synthesis, 1-methylimidazole (99%), methacryloyl chloride (97%), 2-bromoethanol (95%), anhydrous N,N-dimethylformamide (99.8%), anhydrous acetonitrile (99.8%), and 2,2'-azobisisobutyronitrile (AIBN, 98%) were purchased from Sigma Aldrich. 1-Ethyl-3-methylimidazolium bromide (98%), 4-methoxyphenol (98%), phosphorus pentoxide (98%),

thionyl chloride (99%), and calcium hydride (90-95%) were purchased from Alfa Aesar. Lithium hydride (97%), anhydrous diethyl ether, and triethylamine (99%) were purchased from ACROS Organics. Magnesium sulfate was purchased from Fisher Scientific. Trifluoromethanesulfonamide (98%), lithium bis(trifluoromethanesulfonyl)imide (98%), and 3-sulfopropyl methacrylate potassium salt (97%) were purchased from TCI America.

Anhydrous THF from a SOLV-TEK solvent system was used. A Synergy water purification system from Millipore Sigma was used to obtain deionized water ($18.2 M \Omega \cdot \text{cm}$). Triethylamine was distilled over CaH_2 under an inert atmosphere. 3-Sulfopropyl methacrylate potassium salt was dried under vacuum for 2 h at 25°C . AIBN was purified by recrystallization from methanol below 40°C . All other reagents were used as received.

3.2.2 Synthetic Methods

3.2.2.1 Synthesis of Singly-and Doubly-Polymerizable Monomers

The polymerized ionic liquid monomers were prepared according to previously reported procedures.^{12,32,119,120}

Briefly, the polymerizable cationic monomer, sPIL(+), was prepared by quaternizing *N*-methylimidazole with 2-bromoethanol in the absence of a solvent in quantitative yield. Subsequent acrylation with methacryloyl chloride at room temperature yielded the polymerizable imidazolium salt. The imidazolium salt was then ion-exchanged with [Li][TFSI] to yield singly-polymerizable ionic liquid sPIL(+).^{9,12,119}

The polymerizable anionic monomer, sPIL(-), was prepared by converting potassium 3-(methacryloyloxy)propane-1-sulfonate into its sulfonyl chloride derivative by treatment with thionyl chloride. This product was subsequently converted into a trifluoromethanesulfonamide-

based triethylammonium salt. The triethylammonium cation was then ion-exchanged with Li⁺ to yield a polymerizable trifluoromethanesulfonamide salt that was finally ion-exchanged with 1-ethyl-3-methylimidazolium bromide to yield the desired singly- polymerizable ionic liquid sPIL(-).¹²⁰

Finally, the doubly-polymerizable ionic liquid, dPIL, was prepared by ion-exchanging the polymerizable imidazolium salt with the polymerizable trifluoromethanesulfonamide in a salt-metathesis reaction to yield the doubly-polymerizable ionic liquid dPIL. Successful synthesis of all products was confirmed by ¹H and ¹⁹F NMR. (See Appendix)

3.2.2.2 Polymerization of sPIL and dPIL Monomers

The PIL monomers were polymerized directly onto the appropriate sample cells for each characterization method described below. Briefly, a stock solution of AIBN (6.1 mM) was added to the requisite amount of PIL monomer to achieve a monomer/initiator ratio of 500:1. The reaction mixture was protected from light, and the dichloromethane was allowed to evaporate. The mixture was then transferred to a sample pan (for calorimetric measurements) or electrodes (for BDS), placed in a vacuum oven, and heated to 80 °C overnight. The samples were cooled to room temperature and characterized without any further purification.

3.2.3 Characterization of Polymerizable Ionic Liquids

3.2.3.1 NMR Analysis

¹H and ¹⁹F NMR spectra of the synthesized polymerizable ionic liquid (PIL) monomers were obtained to verify the identity and purity of the synthesized products. Spectra were recorded on a Bruker AMV-500 spectrometer at 25 °C in deuterated solvent and are shown in Appendix.

3.2.3.2 Differential Scanning Calorimetry (DSC)

For DSC measurements, the PIL monomers were polymerized directly onto the DSC pan via thermal initiation with azobisisobutyronitrile (AIBN), with a target mass of 10 mg. The glass-transition temperatures (T_g) of the polymerized ionic liquids were then measured with a DSC 2500 differential scanning calorimeter (TA Instruments) that was calibrated for temperature and heat flow with indium reference samples provided by the manufacturer. Measurements were performed using a heat/cool/heat method under a constant flow rate of nitrogen (50 mL/min). The samples were sealed in a 40 μ L hermetic aluminum pan with a Tzero press. An empty pan sealed with a lid was used as the reference. The PILs were first equilibrated for 5 min at -80 °C. They were then heated to 180 °C at a rate of 10 °C/min and held at this temperature for 5 min. The PILs were then cooled to -80 °C at 10 °C/min and held at this temperature for 5 min. The PILs were finally heated again to 180 °C at 10 °C/min. The T_g was determined by the mid-point method on the cooling cycle thermogram.

3.2.3.3 FTIR Analysis of DPIL samples

The residual ion content of the DPIL samples was characterized by attenuated total reflection-Fourier transform infrared (ATR-FTIR) spectroscopy. Spectra of the dPIL monomer and the DPIL polymer measured on a Perkin Elmer Spectrum Two ATR-FTIR spectrometer are shown in Figure 24 and 25.

3.2.3.4 Broadband Dielectric Spectroscopy

The dielectric response of the polymerized ionic liquids was measured by BDS. Samples were polymerized directly on the sample cell electrodes, as described above. The cell's brass electrodes were mechanically polished and thoroughly cleaned prior to sample deposition by

sequentially sonicating in methanol followed by acetone. The monomer/AIBN mixture was then loaded onto the 30 mm diameter bottom electrode with 50 μm silica fiber spacers. The 15 mm diameter top electrode was then placed onto the sample such that the PIL was sandwiched between two electrodes, forming a parallel plate capacitor.

Following deposition, the PIL was polymerized in the sample cell in a vacuum oven at 80 $^{\circ}\text{C}$ overnight. The top electrode was then pressed down by hand to ensure contact with the silica spacers and a consistent thickness of 50 μm , which was verified using calipers. BDS measurements were carried out using a Concept 40 broad-band dielectric spectrometer (Novocontrol GmbH). The sample was annealed in the instrument at 130 $^{\circ}\text{C}$ for 1 h under a flow of dry nitrogen to ensure complete removal of residual moisture. Frequency sweeps were then carried out at an amplitude of 0.1 V with frequencies ranging from 0.1 to 10^7 Hz for all experiments. Frequency sweeps were carried out between 130 and -150 $^{\circ}\text{C}$ following a cool/ heat/cool cycle. For each cycle, the temperature steps were chosen to be 10 $^{\circ}\text{C}$ near the sample's calorimetric T_g and were gradually increased to 30 $^{\circ}\text{C}$ far from T_g .

3.3 Results

3.3.1 Monomer and Polymer Synthesis

Figure 23 shows the representative structures of the polymerizable ionic liquid monomers each with methacrylate chemical group investigated in this study. The polymerizable ionic liquid monomers include (a) Singly-polymerizable cationic ionic liquid monomer, sPIL (+): It's an imidazolium-based cationic monomer with polymerizable methacrylate group containing free

Tf₂N⁻ counterion (a) Singly-polymerizable anionic liquid monomer sPIL (-): It's a trifluoromethylsulfonimide-based anionic monomer with polymerizable methacrylate group containing free EMIM⁺ and (c) Doubly-polymerizable ionic liquid monomer dPIL (+): It's an imidazolium-based cationic monomer and trifluoromethylsulfonimide-based anionic monomer each containing polymerizable methacrylate group lacking any free counterions. The synthetic route to these sPIL and dPIL monomers has been reported in previous studies.^{12,119,120}

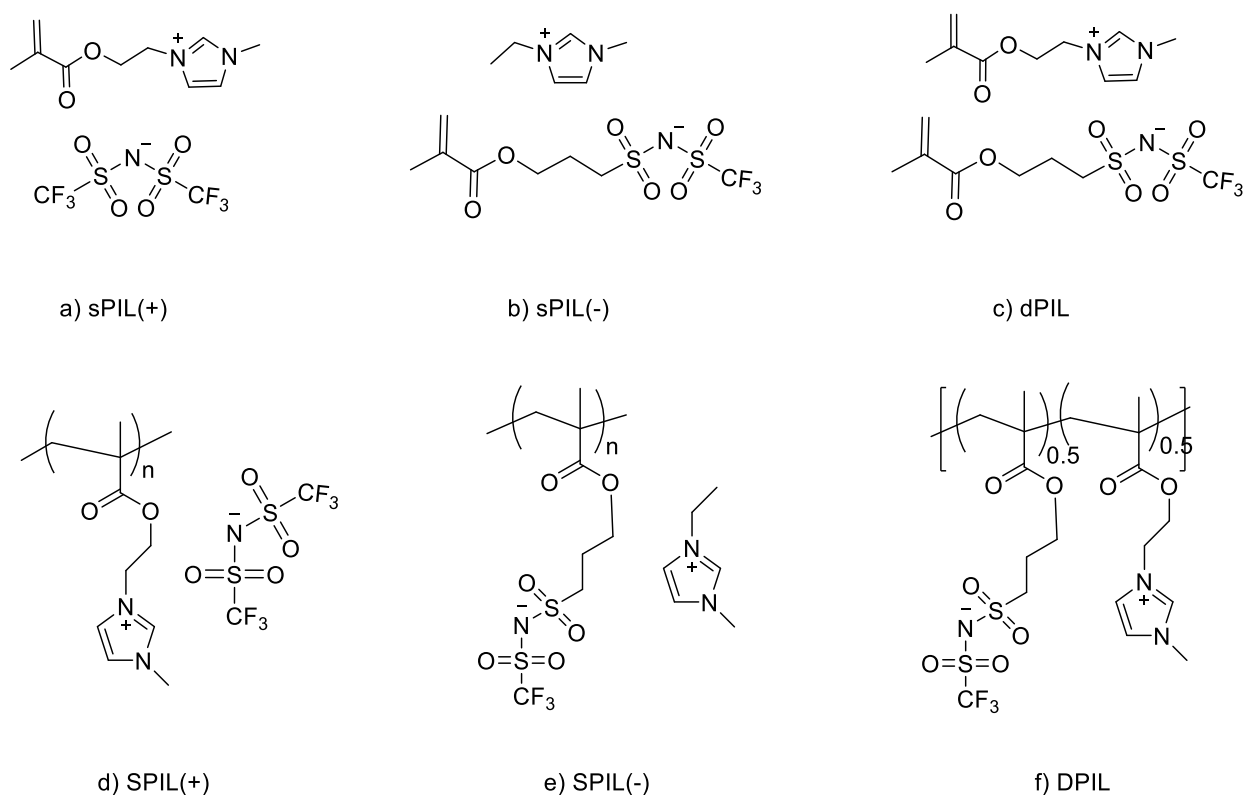


Figure 23 Scheme: Chemical structures of polymerizable ionic liquid monomers (a, b, and c) and their corresponding polymers (d, e, and f) investigated in the present work: (a) sPIL(+), (b) sPIL(-), (c) dPIL, (d) SPIL(+), (e) SPIL(-), and (f) DPIL

Each of these PIL monomers were obtained as viscous liquids at room temperature and stored in a freezer (-20 °C) to prevent polymerization before use. NMR and mass spectrometry

confirmed the purity of the synthesized PILs (see Appendix). The IL monomers were then polymerized overnight via free radical polymerization at 80 °C with 2,2'-azobis(isobutyronitrile) (AIBN) as the initiator. Polymerization of the sPIL monomers gave soft solids. On the contrary, polymerization of the DPIL monomer resulted in a polymer that was insoluble in both polar and nonpolar solvents, likely due to the extensive ionic interactions between the chains.

The insolubility of the polymerized DPIL in standard NMR solvents precluded the quantification of the monomer conversion and thus the residual monomer in the polymerized DPIL samples. However, it is important to know the residual monomer content of the DPIL materials, and thus successfully characterized the residual monomer content by ATR-FTIR. As shown in the IR spectra of polymerized DPIL in Figure 24, it is hard to quantify the conversion of monomer to polymer due to overlapping of the C-C stretching vibration of the polymeric backbone with the C-C stretching vibration of alkyl side chains (around 945 cm^{-1}).

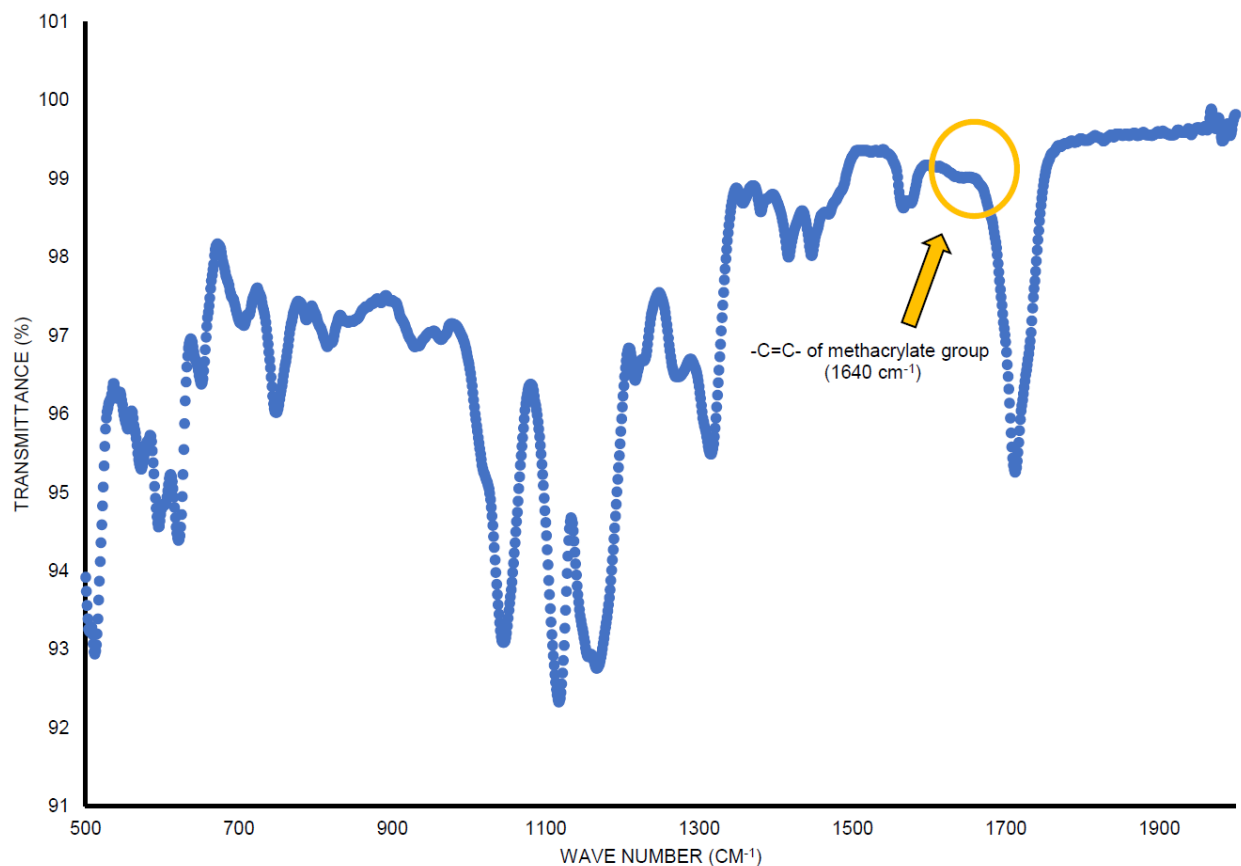


Figure 24 FTIR spectra of polymerized DPIL at room temperature

Notably, the IR spectra of the DPIL copolymer shows a significantly weak C=C stretching of the methacrylate group at 1636 cm^{-1} whereas an intense C=C stretch for the monomeric dPIL sample is observed at 1640 cm^{-1} . This reveals the successful conversion of the monomer to the polymer under the attempted polymerization conditions. As shown in Figure 25, normalization of the absorbance corresponding to the carbonyl stretch at 1710 cm^{-1} and background correction in both the polymeric DPIL and monomeric dPIL yielded 95% conversion of the monomer to the polymer. The presence of a small residual bump in the FTIR spectra of the polymer further confirms the presence of merely 5% residual monomer in the polymeric material.

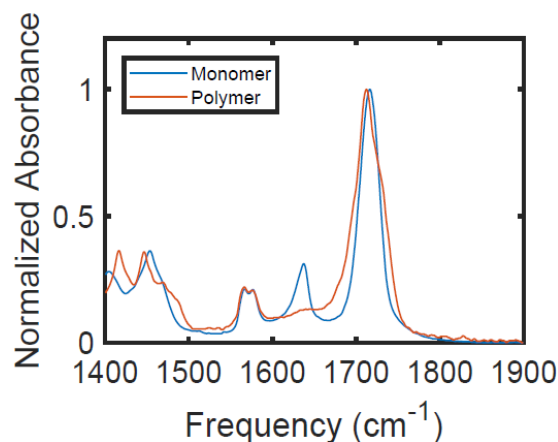


Figure 25 ATR-FTIR spectra of the dPIL monomer and DPIL polymer, illustrating disappearance of the C=C bond peak at 1636 cm^{-1} upon polymerization. Spectra are normalized to the carbonyl stretch at 1710 cm^{-1} .

DPIL samples were prepared directly from a monomeric substance containing a 1:1 ratio of polymerizable cations to polymerizable anions, with no un-polymerizable counterions. FTIR analysis indicates that the vast majority of the monomers (>95%) were polymerized under the described conditions. No washing steps were carried out after polymerization of the samples. As such the composition of the DPL must reflect that of the monomer feed, and the DPIL polymers are, essentially, a 1:1 statistical copolymer of the cationic and the anionic monomers with no free counterions.

3.3.2 NMR analysis

The solution state NMR spectra (^1H , ^{13}C , ^{19}F) of each of the polymerizable ionic liquid monomers were well in accordance with the previously published works and are shown in the Appendix. Residual solvents like DCM and acetone used in the synthesis and purification of these

PILs were observed in trace amount in the NMR. A single peak at the indicated chemical shift was observed (See Appendix).

Due to lack of insolubility of DPIL in NMR solvents the ^1H - ^{13}C CP-MAS solid state NMR of polymerized DPIL was taken (Figure 26). The $-\text{C}=\text{C}-$ of the imidazolium ring displayed a chemical shift exactly identical to that of $-\text{C}=\text{C}-$ of the methacrylate group (around 120-130 ppm), as seen in the attached solid-state 1D NMR. Due to the peaks overlapping it was hard to confirm the presence or absence of any residual monomers.

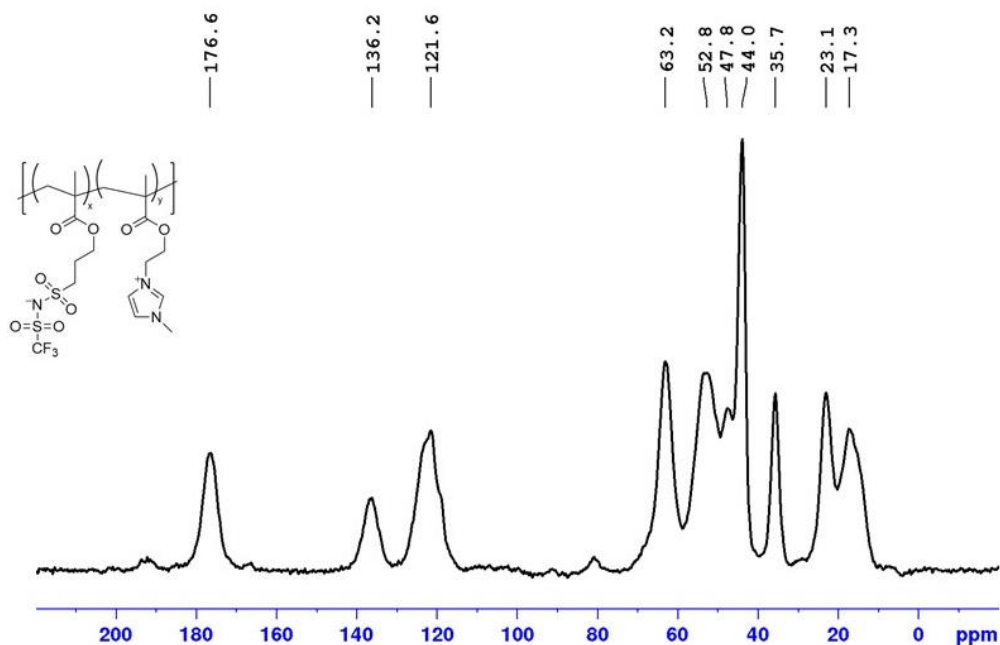


Figure 26 ^{13}C solid-state NMR of DPIL

3.3.3 FTIR Analysis

FTIR analysis of DPIL (Figure 24) showed the overlapping of the C-C stretching vibration of the polymeric backbone with the C-C stretching vibration of alkyl side chains (around 945 cm^{-1}). Further a significantly weak C=C stretching peak at 1640 cm^{-1} (Figure 25) was observed confirming the majority of dPIL monomer has been polymerized successfully under the experimental conditions.

3.3.4 Thermal Analysis

Differential Scanning Calorimetry (DSC) was used to measure the glass transition temperatures (T_g 's) of the polymerized ionic liquids. Figure 27 shows the DSC profiles of the polymerized SPILs and DPIL. Each of the polymerized samples exhibit a broad glass transition temperature in contrast to a sharp T_g within the scanned temperature range. The T_g 's of the polymerized ionic liquids are marked by an arrow in the Figure 27 and also indicated in Table 3.

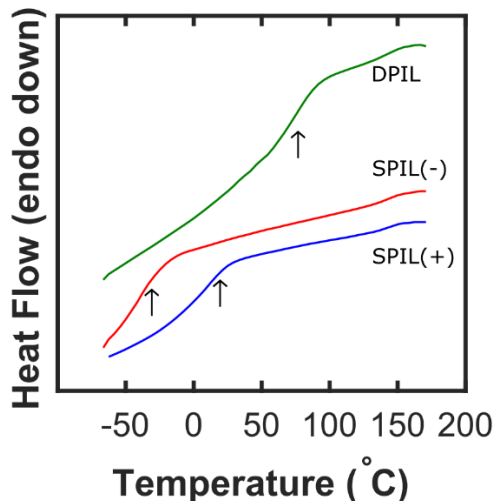


Figure 27 DSC thermograms of PILs obtained during the cooling cycle of the DSC run. Arrows indicate the glass transition temperatures of each material.

Table 3 Glass-Transition temperatures of polymerized Ionic Liquids from DSC and BDS Measurements

PILs	DSC T_g (K)	BDS T_g (K) ^a
SPIL(+)	286	288
SPIL(-)	236	250
DPIL	348	320

^aTemperatures at which conductivity relaxation time scales transitioned from VFT to Arrhenius dynamics; see the Ionic Conductivity section for details

As shown in the table 3, the SPIL(+) displayed a T_g of 286 K which was roughly 50 K higher than that of SPIL(-). As it has been noted in similar systems, the planar structure of the imidazolium monomer makes it considerably less flexible than the anionic monomer, resulting in a higher T_g ⁶. Interestingly, the DPIL had the highest T_g among the investigated PILs. At first glance, the DPIL appears to be a statistical copolymer of SPIL(+) and SPIL(-). In this case, the Fox equation, which is used to estimate the glass transition temperature in polymer blends and

statistical copolymers, cannot be applied to predict the T_g of DPIL.¹²¹ Fox equation is represented as:

$$\frac{1}{T_g} = \frac{w_1}{T_{g1}} + \frac{w_2}{T_{g2}} \quad \text{(Equation 1)}$$

where T_g is the predicted glass transition temperature of the copolymer, w_1 and w_2 are the weight fraction of monomer 1 and 2 in the copolymer, and $T_{g,1}$ and $T_{g,2}$ are the glass transition temperatures of homopolymers 1 and 2.

If applied, it predicts that DPIL's T_g should be approximately 260 K (between the T_g of SPIL(+) and SPIL(-), with the exact value controlled by the weight fraction of each of the components). The observed T_g is 348 K, roughly 60-100 K higher than the predicted value. This disagreement is not surprising, however, since the DPIL is not actually a copolymer of the two SPILs, as it lacks their mobile counterions. In their absence, the strong interactions between the two charged monomers effectively serve as crosslinks, making the structure more rigid and increasing the T_g .^{122,123}

Finally, we note that only the cooling cycle of the DSC run is shown in Figure 27 for consistency with the BDS data whereas complete DSC profiles of all the PILs is shown in Figure 28.

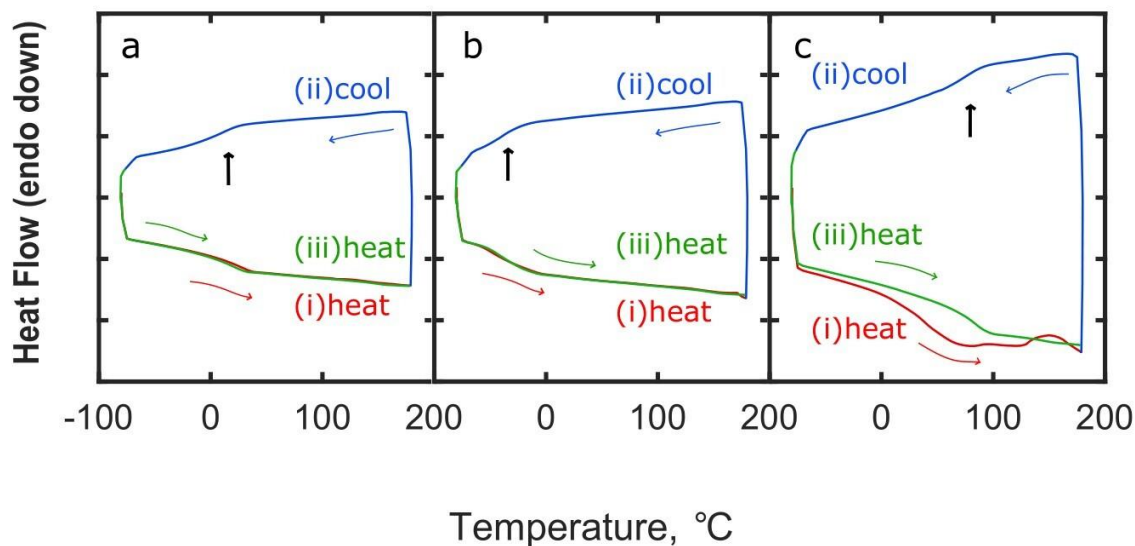


Figure 28 Complete DSC profiles of all the PILs; (a) SPIL(+), (b) SPIL(-), and (c) DPIL investigated in the present study.

Each of the SPILs displayed the same T_g during all the three thermal cycles including the first heating, cooling, and the second heating cycle. However, the DSC profile of DPIL (Figure 28 c) revealed that the T_g of this material shifted 9 K degrees after being cycled to high temperature. The decrease in fractional free volume resulting from strong intermolecular associations near T_g is likely responsible for shifting T_g to a higher temperature. Further this suggests the supercooled glass type character of the as-polymerized sample. Further a presence of the single T_g observed in the DSC data does indeed suggest that the polymerization is relatively random.

While the insolubility of the DPIL in standard NMR solvents prevented direct assessment of the monomer conversion, the absence of a polymerization exotherm in the DSC trace suggested the successful polymerization of the majority of the PIL monomers. The DSC thermograms of the polymers displayed no evidence of crystallization or melting during the thermal cycle. There does indeed appear to be a very small bump at 150 °C in each of the DSC traces, and it appears to be

consistent across all the three types of materials (e.g., it is not unique chemical feature of a specific sample). While this type of feature could result from the presence of a high-boiling solvent while introduced during the synthesis of the materials, no high-boiling solvents are identifiably present in the spectra of the final purified monomers.

While this could be an artifact of the DSC measurement, we acknowledge that it is possible that, despite our best efforts to dry the materials (and keep them dry) before polymerization, the samples absorbed a small amount of atmospheric moisture during sample preparation. While the presence of a trace amount of water in the samples is unlikely to significantly affect the reported results. Notably, each of the polymerized ionic liquids samples exhibited high thermal stability of up to 180 °C, with no signatures of thermal decomposition in the DSC thermogram.

The glass transition temperatures of the polymerized ionic liquids were also measured by BDS analysis as shown in Table 3 and discussed in Section 3.3.6. Some discrepancies were observed between the calorimetric and dielectric T_g 's. This is likely due to batch-to-batch difference arising due to different polymerization method for the samples used both in DSC and BDS as shown in Figure 29.

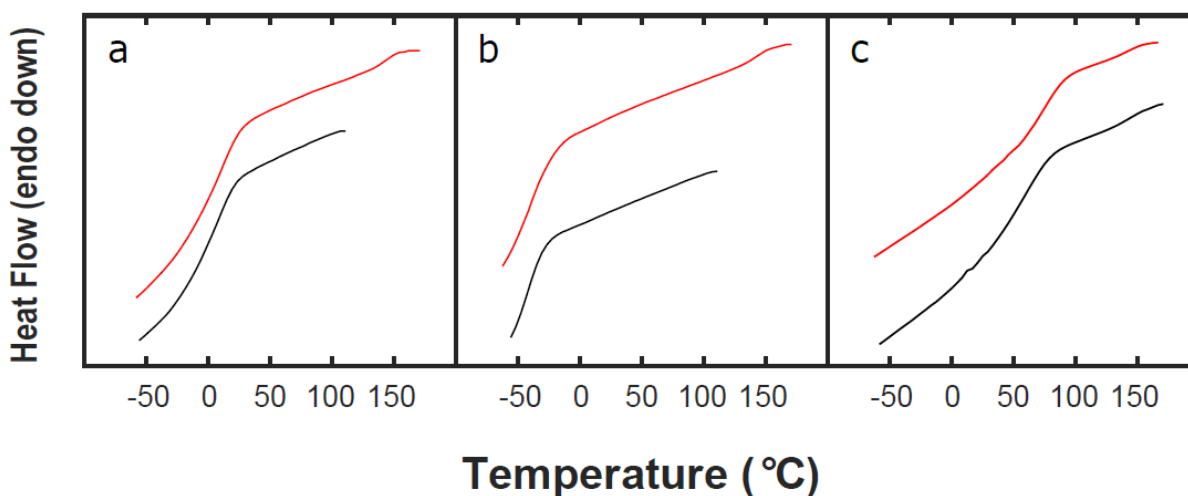


Figure 29 DSC profiles of all (a) SPIL(+), (b) SPIL(-), and (c) DPIL, illustrating batch-to-batch variation between the samples. Black traces correspond to Batch 1 and red traces correspond to Batch 2 for each material.

We did indeed attempt to polymerize the DPIL monomer on a large scale for use in both the DSC and BDS measurements. However, the resulting material could not be successfully hot-pressed to obtain good contact with the BDS electrodes without significant degradation. Thus, the samples for BDS measurements had to be polymerized directly on the BDS electrodes, rather than being obtained from a single larger batch for both BDS and DSC measurements. DSC analysis did suggest that there was some batch-to-batch variation in the glass transition temperatures of the materials, with samples prepared under the same conditions varying by approximately 6 °C for SPILs and up to 16 °C for the DPILs. This is likely a consequence of temperature fluctuations in the vacuum oven used for polymerizing the samples or trapped humidity in the PILs as the site for the preparation of DSC samples was different from the actual site of running DSC experiments.

3.3.5 Ionic Conductivity

The measured ionic conductivity of samples indicates and quantify the changes to the bulk ion transport of the sample when it undergoes polymerization of either one or both the ionic species. The frequency dependence of the in-phase part of the conductivity, σ' , at different temperatures for (a) SPIL(+), (b) SPIL(-), and (c) DPIL is shown in Figure 30. In these plots, the bottom blue curve corresponds to a measurement made at 100 K while the top orange curve corresponds to a measurement at 400 K, with the gradient of colors reflecting progressively increasing temperatures between these limits.

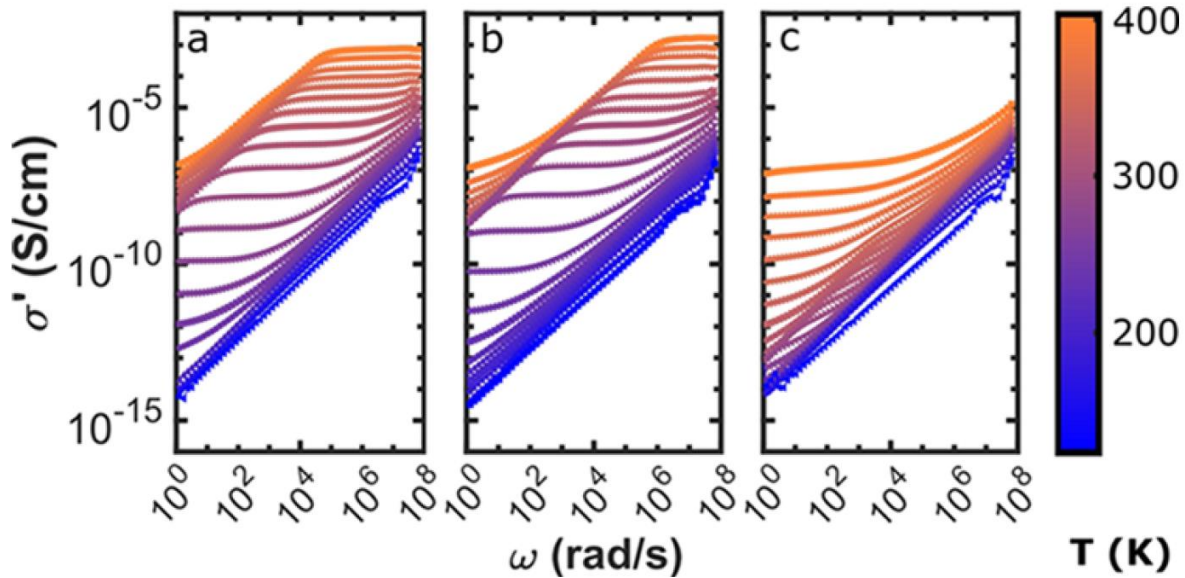


Figure 30 Plot of the real part of the conductivity (σ') of (a) SPIL(+), (b) SPIL(-), and (c) DPIL as a function of angular frequency across the range of temperatures investigated in this work.

As shown in Figure 30, σ' increases with increasing frequency, as is typical of ionic conductor behavior. A distinct plateau corresponding to DC conductivity, as discussed later, is displayed in each trace at higher temperatures. Below this plateau, electrode polarization (EP)

drives a distinct decrease in σ' . Electrode polarization, which is a characteristic response in systems capable of ionic charge transport, arises from build-up of charge at the electrodes, which decreases the field felt by ions in the bulk of the material and consequently decreases the apparent conductivity.^{116,124,125} Interestingly, the electrode polarization signature is distinguished in the SPILs (Figure 30 a, and 30 b), but was not observed in the DPILs even at the lowest frequencies measured (Figure 30 c), qualitatively depicting a precipitous decrease in the mobility of ions towards the electrode interfaces.

The plateau corresponding to DC conductivity is a frequency-independent response caused by the long-range displacements of ionic-conducting species, and the value of σ' across this plateau gives the characteristic DC conductivity of the samples, σ_{DC} .^{111,126} σ_{DC} was extracted by plotting σ' vs. angular frequency, ω and then finding where the derivative of σ' approaches 0 (flattens) and then taking the average of the derivative values that are smaller than a cut-off value. The cut-off value was taken as two times the minimum derivative. Figure 31 a show the extracted DC conductivity of each polymerized ionic liquid across the entire temperature range scanned in this study.

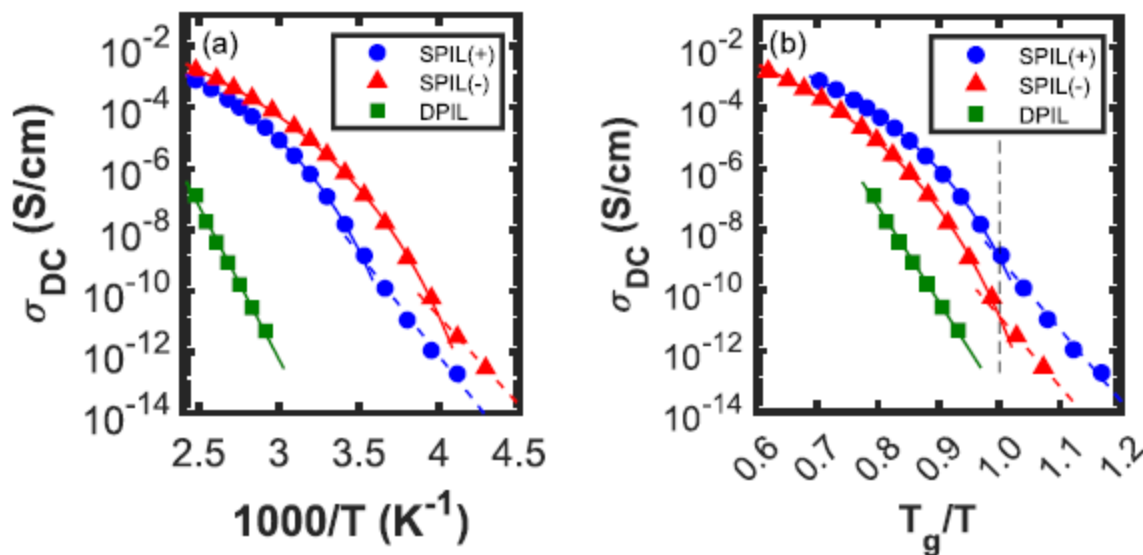


Figure 31 DC conductivity of PILs as a function of (a) $1000/T$ and (b) T_g/T . Solid lines show VFT fits above T_g , while dashed lines show the Arrhenius fits below T_g . T_g values were obtained from analysis of the electrical modulus, as described below.

As shown in the Figure 31, with increasing temperature ionic conductivity increase proportionally. Across the investigated temperature range, SPIL(-) was observed to have a higher conductivity than SPIL(+). Now, if we look at the DPIL, we sort of see a similar plateau, but it is only evident in the highest-temperature samples, and only at very low frequencies. We can't, from this data, determine whether this conduction arises from motion of the polymer chains or from a small amount of un-polymerized monomer that remains in the material; either way, however, this data shows that the conductivity of the DPIL samples is indeed much lower than that of either SPIL and is roughly five orders of magnitude lower than the SPILs, as elaborated in detail, below.

The DC conductivities of the monomeric ionic liquids were also measured at room temperature to compare with the polymerized counterparts. As shown in Table 4, polymerized

ionic liquids had lower DC conductivity at 298 K relative to their corresponding monomeric ionic liquid counterparts.

Table 4 Room-Temperature DC conductivities of monomers and polymers investigated in this work

PILs	σ_{DC} of monomer at 298 K (S/cm)	σ_{DC} of polymer at 298 K (S/cm)
SPIL (+)	7.3×10^{-4}	4.4×10^{-8}
SPIL (-)	3.0×10^{-4}	1.4×10^{-6}
DPIL	2.3×10^{-4}	$< 10^{-12}$

All the three monomeric ionic liquids had similar DC conductivities at room temperature. As expected, after undergoing polymerization, SPILs exhibited a decrease of 2 to 4 orders of magnitude in room temperature DC conductivities whereas for DPIL, 8 orders of magnitude decrease were observed. These results are in reasonable agreement with previous works by Shapalov et. al.³² They have shown that monomeric 1-[2-(Methacryloyloxy)ethyl]-3-methylimidazolium bis(trifluoromethylsulfonyl)imide with T_g of 210 K has σ_{DC} of 7.4×10^{-4} S/cm which is significantly higher than the polymerized counterpart with a T_g of 301 K and σ_{DC} of 2.4×10^{-10} S/cm. Such a low conductivity in polymerized counterparts is likely a consequence of diminution of ions mobility in the polymerized chains.

In the context of understanding the temperature dependence of the investigated PILs, it is useful to study the DC conductivity over the entire temperature range, above and below the T_g . To incorporate this analysis, for the SPILS, Arrhenius model was used to fit the temperature-

dependent DC conductivities below the T_g and to the Vogel-Fulcher-Tammann (VFT) equation was used to fit the DC conductivity above the T_g of the materials.¹²⁷

The Arrhenius equation used to fit the DC conductivity below the T_g is as follows:

$$\sigma_{DC} = \sigma_{\infty} \exp\left(-\frac{E_a}{RT}\right) \quad \text{(Equation 2)}$$

where σ_{∞} (infinite temperature ionic conductivity), where T is temperature, E_a is the activation energy for conducting ions and is a measure of electrostatic attraction between cation and anion, and R is universal gas constant.

The VFT equation used to fit the DC conductivity above the T_g is as follows:

$$\sigma_{DC} = \sigma_{\infty} \exp\left(\frac{-DT_0}{T - T_0}\right) \quad \text{(Equation 3)}$$

where T_0 is the Vogel temperature, σ_{∞} is the ionic conductivity at infinite temperature, D is the strength index describing the strength of temperature dependence of relaxation time.^{128,129} The fitted values of these parameters are summarized in Table 5.

As shown, in Figure 31 a, the conductivity of both SPILs obeys the Arrhenius model below their glass transition temperatures, and above the glass transition temperature, the VFT model is nicely obeyed. The DSC glass transition temperature is approximately 45-70 K above the Vogel temperature T_0 .¹³⁰ This is well in accordance with previously reported works on imidazolium-based methacrylate polymers with mobile BF_4^- and TFSI counterions.⁶

Table 5 Fit parameters for the DC conductivity of polymerized ionic liquids above and below their glass transition temperatures

PIL	$T > T_g$			$T < T_g$	
	σ_∞ (S/cm)	D	T_0 (K)	σ_∞ (S/cm)	E_a (KJ/mol)
SPIL(+) ^{a, b}	1.52	6.52	217	4.13×10^{14}	128
SPIL(-) ^{a, b}	3.16	8.44	189	2.09×10^{12}	111
DPIL ^a	5.08×10^{17}	1.08×10^4	2.11	-	-

^aVFT fit, ^bArrhenius fit

It is expected that below the T_g , a smaller counterion should be able to hop with a greater ease within the glassy polymeric matrix, lowering the energy of activation, E_a for ionic conduction and thus contributing dominantly to T_g -independent ionic conductivity. In the present study, the activation energy of SPIL(-) with EMIM⁺ counterion is 17 KJ/mol lower than SPIL(+) with TFSI counterion. EMIM⁺ with a thermochemical radius of 3.30 Å has an ionic volume of 0.156 ± 0.018 nm³ which is relatively lower than TFSI counterion with a thermochemical radius of 3.81 Å and an ionic volume of 0.232 ± 0.015 nm³. As expected SPIL(-) with a smaller EMIM⁺ counterion has a lower activation energy of conduction than SPIL(+) with TFSI counterion in the Arrhenius regime.^{131,132} Taken together, both the SPILs have similar ion transport mechanisms as demonstrated by the correlation between the conductivity of SPIL(+) and SPIL(-). This is agreement with previously reported works on polymerized ionic liquids with similar chemistries.

In contrast to both SPILs, although the DC conductivity of DPIL could be fit using VFT model, but the resulting fitting parameters, summarized in Table 5, appear unrealistic. Interestingly, the fitted value of the prefactor σ_∞ , and the strength index D, are unphysically large

in contrast to the fitted value of Vogel temperature T_0 , that is unphysically small. This clearly tells that the DC conductivity of the DPIL cannot be well described by the VFT model above T_g . Further these results demonstrate a significant difference in the origin of residual conduction process in DPILs in contrast to SPILs.

Although we cannot say with certainty, however we hypothesize that the DC conductivity of the DPIL may arise from either a small number of unpolymerized monomers, or chains with a net charge produced through the statistical copolymerization of the cationic and the anionic monomers.

Interesting works from Runt's group have shown that the variation of anion molecular volume results in approximately three orders of magnitude difference in the T_g -independent molar conductivity relative to the one decade change from variation in alkyl side chain lengths.^{51,57} Below T_g , the freezing of the segmental dynamics takes place and consequently the ionic conductivity gets the major contribution from hopping of the counterions within the glassy polymeric matrix. Thus, a plot of ionic conductivity as a function of T_g/T , suppresses the differences in T_g of PILs and highlights the differences in conductivity originating from variation in molecular volume/size of counterions. Further comparing the conductivities at the same temperatures relative to T_g is useful, especially for understanding whether the conductivity is coupled to segmental relaxation.

As seen in the Figure 31b, showing the ionic conductivity for all PILs with temperature normalized to T_g -BDS to exclude the influence of shifts in T_g , the DC conductivities of the DPIL are still 2-3 orders of magnitude lower than those of either SPIL, even when compared at the same temperature relative to T_g . Thus, the distance from T_g is not the only factor driving the low DC conductivity of DPIL materials.

3.3.6 Analysis of dielectric T_g

The conductivity relaxation timescales represent an appropriate method for obtaining dielectric glass transition temperatures in these polymerized ionic liquids. The dielectric response is often presented by the use of complex electrical modulus given by $M^*(\omega) = M'(\omega) + iM''(\omega)$. The peak maxima in the imaginary part of dielectric modulus, $M''(\omega)$ is ascribed to ionic motions within the polymer matrix and represents the conductivity relaxation time.¹¹² This peak maximum also lies close to the frequency maxima of the main relaxation peak in ϵ_{der} spectra. Thus, it would be interesting to make a direct comparison between the frequency corresponding to peak maximum in the imaginary part of dielectric modulus, M'' and the relaxation frequency maxima, ω_{max} , obtained from the fits to ϵ_{der} using equation 6 as discussed in section 3.3.7.

As shown in the Figure 32, M'' had a clear distinct peak at each of the obtained relaxation frequencies, $\omega_{M''max}$, for all temperatures.

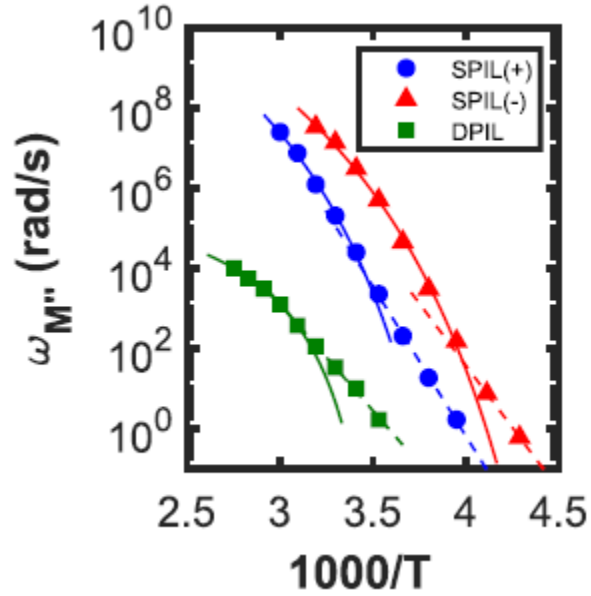


Figure 32 Conductivity relaxation frequencies obtained from M'' . Solid lines show VFT fits above T_g , while dashed lines show the Arrhenius fits below T_g .

As for σ_{DC} , the extracted peak maxima in the imaginary part of electrical modulus representing the conductivity relaxation frequencies were fit to a VFT ($T > T_g$) and Arrhenius ($T < T_g$) dynamics above and below the measured glass transition temperatures, respectively using equation 7 and 8.¹¹² The resulting fits are shown in Figure 32, and the fit parameters are listed in Table 6.

Table 6 Fit Parameters for the Conductivity Relaxation Frequencies of Polymerized Ionic Liquids above and below Their Glass-Transition Temperatures

PIL	$T > T_g$			$T < T_g$	
	ω_∞ (rad/s)	D	T_0 (K)	ω_∞ (rad/s)	E_a (KJ/mol)
SPIL(+)	1.40×10^{13}	7.11	217 ^a	5.01×10^{29}	143
SPIL(-)	2.84×10^{13}	8.89	189 ^a	2.28×10^{26}	118.54
DPIL	9.47×10^5	1.61	268	1.29×10^{19}	102

For the SPIL samples, the value of T_0 was fixed to the same value obtained from the fits to σ_{DC} (Table 5), while for DPIL sample, for which the σ_{DC} data with the VFT dependence above T_g gave unphysically small value of T_0 , the value of T_0 was allowed to vary. The obtained value for the DPIL was somewhat closer to the material's calorimetric T_g than observed in the SPILs, with $T_g - T_0 = 52$ K and are more reasonable than the ones obtained from σ_{DC} . Further the magnitude of activation energy for DPIL was similar to one for SPILs and could be extracted easily due to the presence of a relaxation peak above and below its T_g .

The temperature dependence plot of peak maxima in the imaginary part of electric modulus for polymerized ionic liquids display a crossover from VFT to Arrhenius type of behavior around their glass transition temperature, and this cross over temperature indeed is ascribed to dielectric T_g .¹¹² The dielectric T_g correlates well with the T_g obtained from DSC measurements for each of the investigated polymerized ionic liquid in the present study as shown in Table 3.

The T_g of SPIL(-) extracted from BDS is approximately 14 K higher than that obtained via DSC, while for SPIL(+), there is merely a difference of 2 K between the BDS and DSC T_g . The mismatch is similar for the DPIL, at 28 K, placing the values for all three systems well within the

range observed in other polymerized ionic liquid materials.^{5,133} Considering the fact that glass transition temperature is a kinetic phenomenon, and is highly affected by the cooling rate at which the experiment is conducted, the discrepancies in the dielectric and the calorimetric T_g for SPIL(+) and DPIL is reasonable.¹³⁴

Normally it is expected that the calorimetric T_g should be higher than the dielectric T_g considering the cooling rate in DSC thermal analysis (10 K/min) is way faster than in the BDS experiments (averaging 0.1 K/min) and this is what has been observed for DPIL. Interestingly, SPIL(-) shows a higher dielectric T_g than DSC T_g although somewhat less clear but such discrepancies have been observed in other reported polymerized ionic liquids.¹³³ However, batch-to-batch difference (Figure 29) in T_g of polymerized ionic liquids might be accountable for these observed differences between calorimetric and dielectric T_g .

3.3.7 The Dielectric Function ϵ'

Following the investigation of conductivity in the polymerized ionic liquids, local relaxation of each of the sample was characterized using the dielectric permittivity. These local rearrangements may also be important in determining the function of devices using these materials. Figure 33 elucidates the real part of dielectric permittivity of each investigated polymerized ionic liquid as a function of frequency, and their derivative spectra at different temperatures.

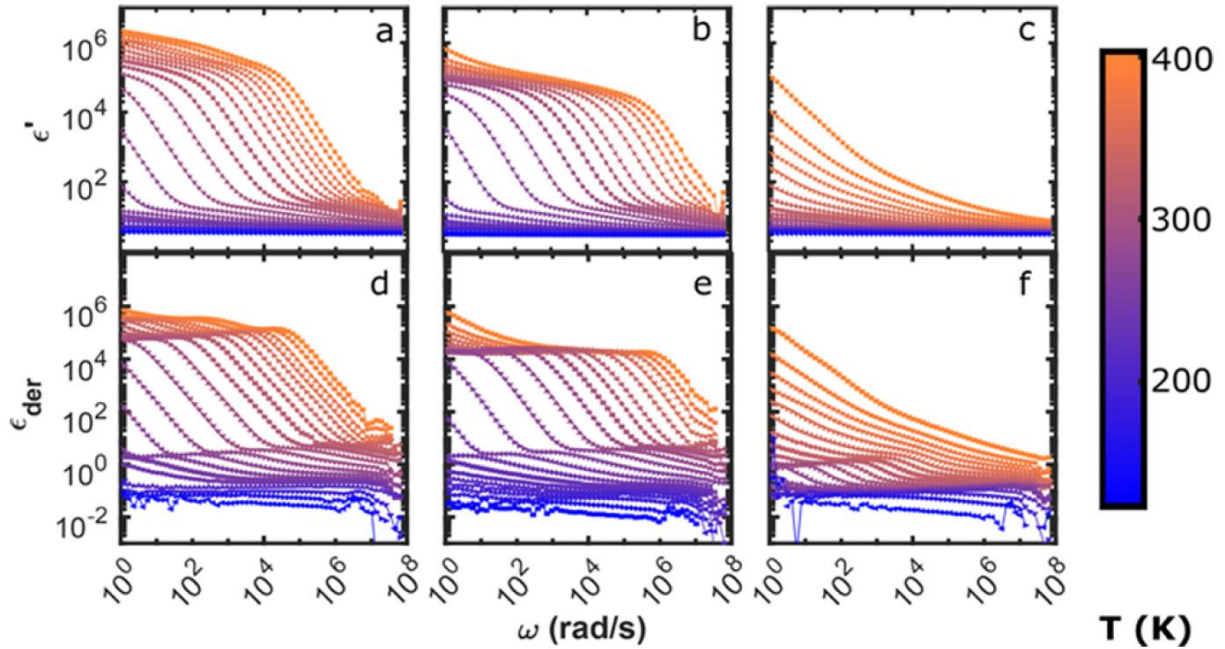


Figure 33 Frequency dependence of (a-c) the dielectric permittivity and (d-f) the dielectric loss derivative function ϵ_{der} for (a, d) SPIL(+), (b, e) SPIL(-), and (c, f) DPIL across the range of temperatures investigated in this work.

Clearly as seen in Figure 33 in panels (a), (b), and (c), with increasing frequency, ϵ' decreases. Additionally, as we can see the dielectric permittivity's of the two SPILs are very similar to each other. The strongly negative-sloped region that predominates in the low frequency regime in the dielectric spectra of SPILs is the electrode polarization phenomenon. On the contrary, in DPIL this response dominates does not contribute significantly to the spectra as observed in the conductivity. In fact, its signatures are displayed only above the material's T_g . As observed in the dielectric spectra of each of the PILs, there exist well-defined signatures of relaxational processes, appearing as steps in the real part of the dielectric response. With increasing temperature, relaxation speed increases and thus these steps shift towards higher frequencies. We

assigned this relaxation process to the reorientation of ion pairs within the PIL in accordance with previous reports on similar polymerized ionic liquids.^{109,110,130}

3.3.8 Dielectric Relaxations

To effectively resolve the relaxations from the PIL samples, the contributions from ionic conductivity were removed by applying the derivative formalism in accordance with previously published works on similar systems.^{33,130,135} This makes that “bump” attributed to ionic rearrangements in the spectra of SPILs much more prominent as observed in Figure 33 in panels d and e. In the spectra of the DPILs, we see similar behavior; one of the interesting qualitative features we notice, though is that as the DPIL is heated through its glass transition temperature, that signature of the ionic rearrangement broadens significantly and ultimately becomes indistinguishable from the rest of the response. Equation 4 was used to calculate the derivative of the real permittivity with respect to frequency and is represented as:^{136,137}

$$\epsilon_{\text{der}} = -\frac{\pi}{2} \frac{\partial \epsilon'(\omega)}{\partial \ln \omega} \quad \text{(Equation 4)}$$

In the derivative spectra, as shown in the Figure 33 (d-f), with increase in temperature the broad steps in ϵ' eventually modify into distinct peaks that become broad and move to higher frequencies. The derivative spectra were fitted with a combination of a power-law electrode polarization response and Havriliak-Negami (HN) relaxation function, which is a useful empirical relaxation function capable of capturing both symmetric and asymmetric broadening of the relaxation around a center frequency and is shown in equation 5.³³ This fit allows us to extract both the characteristic frequency of each mode, which is essentially just the inverse of its relaxation

time, and the relaxation strength, which indicates how strongly the material is able to respond on that timescale.

The dielectric response in previously reported works on similar polymerized ionic liquids has been fully well represented by two HN functions that includes one (α_2) at lower frequency normally assigned to ion pair rearrangement and a second (α) at higher frequency designated to segmental motion of the polymer chains.^{3,5,6} However, in the present analysis the dielectric response was examined using only a single HN function with a constant offset accounting for broad, low amplitude relaxations prevailing at high frequency owing to the broad nature of the higher-frequency α mode that could not be fit accurately.

Equation 5 was used to fit the derivative spectra and is represented as:

$$\epsilon_{\text{der}} = A\omega^{-s} - \frac{\pi}{2} \left[\frac{\partial \epsilon'_{\text{HN}}(\omega)}{\partial \ln \omega} \right] + C \quad \text{(Equation 5)}$$

where s is a constant representing the power-law dependence of the contribution to ϵ_{der} from the electrode polarization, A is the constant amplitude, C is the constant offset included to account for higher-frequency relaxation and was observed to be small and ϵ'_{HN} is a Havriliak-Negami function that is represented by the expression:

$$\epsilon'_{\text{HN}}(\omega) = \text{Re} \left\{ \frac{\Delta\epsilon}{\left[1 + \left(\frac{i\omega}{\omega_{\text{HN}}} \right)^a \right]^b} \right\} \quad \text{(Equation 6)}$$

where $\Delta\epsilon$ is the relaxation strength corresponding to a particular relaxation mode, a and b are the shape parameters, and ω_{HN} is the angular frequency. The frequency of maximal loss ω_{max}

corresponding to a particular relaxation mode can be calculated using the parameters a , b , and ω_{HN} as shown in equation 7.³³

$$\omega_{\text{max}} = \omega_{\text{HN}} \left(\sin \frac{a\pi}{2 + 2b} \right)^{1/a} \left(\sin \frac{ab\pi}{2 + 2b} \right)^{-1/a} \quad (\text{Equation 7})$$

To account for asymmetries in the relaxation spectra, the temperature dependence of the relaxation timescales is evaluated using the frequency of maximal loss instead of ω_{HN} .^{138,139} Figure 34 shows the representative fits of derivative spectra of each polymerized ionic liquid to the functional form given in Equation 5.

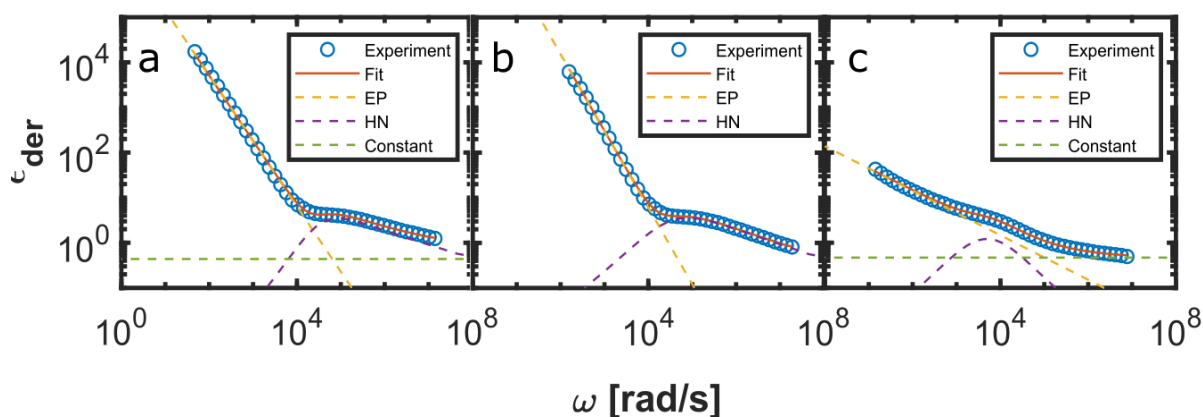


Figure 34 Dielectric loss derivative spectra at T_g fit to the sum of a power law for EP and derivative form of HN function for ion rearrangement of (a) SPIL(+), (b) SPIL(-), and (c) DPIL. The solid curves are three-parameter fits to eq 7 with following values of s , a , and b for (a) SPIL (+): $s = 1.45$, $a = 0.9$, $b = 0.34$ (b) SPIL (-): $s = 1.7$, $a = 0.74$, $b = 0.45$ (c) DPIL: $s = \text{Varied}$, $a = 0.76$, $b = 1.0$

The values of the parameters s , a , and b were fixed to the values given in the caption of Figure 34 to reduce the number of fitting parameters and improve the reproducibility of the fits. The dielectric response was first fitted at the temperature that yielded the most pronounced HN

relaxation. This fitting gave the shape parameters a and b . The same values of the shape parameters a and b in the HN function over the entire temperature range were used considering the same peak shape of α_2 relaxation at different temperatures.¹³³ The value for the contribution from electrode polarization that is the power law exponent s for SPILs was obtained by averaging all the s values over the entire temperature range, a strategy well applied for other similar polymerized ionic liquids.^{3,5,6}

In contrast to SPILs, the parameter s was allowed to vary as fixing the value of s could not describe the electrode polarization phenomenon well. The acquired values of the parameter s were between 0.2 and 0.5 that were relatively lowered when compared to SPILs counterparts. This anomalous frequency scaling of the electrode polarization in the DPIL could arise from compositional variation and/or molecular weight dispersity in the polymer chains. This emphasizes the fact that the behavior of the DPIL system in the low frequency regime cannot be well represented by electrode polarization models that work effectively for ionomers that have free counterions. Further this also highlights a different charge transport mechanism in these materials lacking mobile counterions.

Figures 35 and 36 shows the fitted values of the relaxation peak frequency, ω_{\max} , and the relaxation strength, $\Delta\epsilon$. In the given frequency range studied, we could not capture the dynamics of SPIL(-) as they were too slow. The relaxations for DPIL at higher temperatures owing to their broad shape could not be picked up accurately and therefore could not be fit by HN function.

The variation of relaxation peak frequency ω_{\max} with temperature was fit to Arrhenius model ($T < T_g$) below the glass transition temperature and the VFT model ($T > T_g$) above the glass transition temperature for each (a) SPIL(+), (b) SPIL(-), and (c) DPIL specifically for all data sets for which ω_{\max} could be extracted with greater certainty.⁵

The Arrhenius equation used to fit ω_{\max} below the T_g is as follows:

$$\omega_{\max} = \omega_{\infty} \exp\left(-\frac{E_a}{RT}\right) \text{ for } T < T_g \quad \text{(Equation 8)}$$

The VFT equation used to fit ω_{\max} above the T_g is as follows:

$$\omega_{\max} = \omega_{\infty} \exp\left(-\frac{DT_0}{T - T_0}\right) \text{ for } T > T_g \quad \text{(Equation 9)}$$

Here, ω_{∞} is the unconstrained frequency, D is the strength parameter for the relaxation, T_0 is the Vogel temperature, E_a is the activation energy required for ion pair to rearrange, and R is the universal gas constant. Figure 35 shows the resulting fits and Table 7 summarizes the fit parameters.

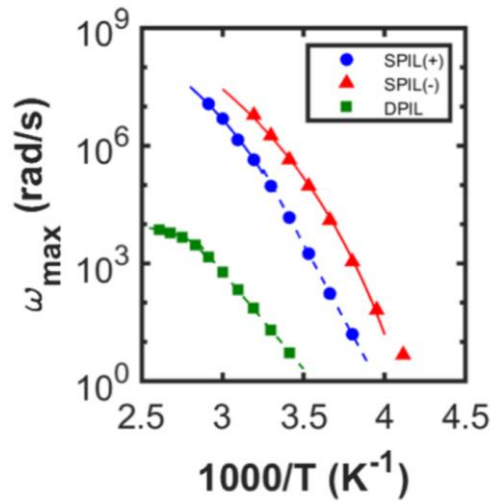


Figure 35 Temperature dependence of relaxation frequency maxima, ω_{\max} , obtained from fits to ϵ_{der} .

Overlaid curves indicate fits to an Arrhenius model (dashed lines) below T_g and a VFT model (solid curves) above T_g .

Table 7 Fitting Parameters for the Arrhenius ($T < T_g$) and VFT ($T > T_g$) temperature dependence of the ion rearrangement frequencies obtained from fits to ϵ_{der} .

PIL	$T > T_g$			$T < T_g$	
	ω_∞ (rad/s)	D	T_0 (K)	ω_∞ (rad/s)	E_a (KJ/mol)
SPIL(+)	3.61×10^{11}	6.01	217 ^a	1.5×10^{30}	146
SPIL(-)	1.11×10^{12}	8.07	189 ^a		
DPIL	1.01×10^5	0.92	281	3.63×10^{18}	100

^a T_0 values for SPIL(+) and SPIL(-) were fixed to the values obtained from fits to σ_{DC}

The Vogel temperature, T_0 was fixed to the values obtained from the fits to DC conductivity (Table 5) for SPIL counterparts. On the contrary, for the DPIL sample T_0 was allowed to vary as the DC conductivity fit of DPIL, did not furnish acceptable value of T_0 . The obtained value of T_0 for DPIL correlates well with the calorimetric T_g ($T_g - T_0 \sim 67$ K).

As seen in previous works on imidazolium-based methacrylate polymers, the peak relaxation frequencies of the α_2 process in SPILs follow similar temperature dependence as their ionic conductivity (Figure 31) and increases with the increase in temperature.^{3,5,6} In contrast to SPILs, the relaxation process was up to 4 orders of magnitude slower in DPIL with both the ionic species immobilized. There is an acceptable agreement between the fit parameters obtained from the temperature dependence of relaxation peak frequency ω_{max} and the one obtained from $\omega_{M''max}$ (frequency corresponding to peak maximum in the imaginary part of dielectric modulus, M'').

Interestingly, for DPIL the activation energy is 35% lower than for SPIL (+). It is unlikely that the lower apparent activation energy for the DPIL is due to mobile content, as the DPIL has a lower total mobile ion content than either of the SPILs (which have free counterions). We speculate that this difference may be due to morphological differences between the materials; if the

polymerization process locks the ions into the positions that are, for example, further apart than they would be if their motion were not restricted, they might exist in a higher-energy configuration to start with and thus have a lower effective activation energy for rearrangement. Further experimental studies would be necessary capable of testing this hypothesis.

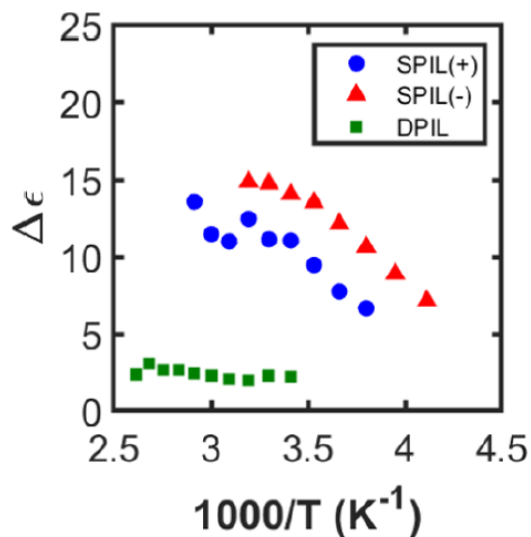


Figure 36 Temperature dependence of relaxation strengths $\Delta\epsilon$ corresponding to ion-rearrangements process for all investigated PILs.

Figure 36 shows the variation of the relaxation strengths ($\Delta\epsilon_{d2}$) for each PIL extracted from the fits of ϵ_{der} . With increase in temperature, the relaxation strength increases for each SPIL counterparts. This trend is well in accordance with the previously published works on imidazolium based polymerized ionic liquids.^{3,5,6} The relaxation strengths increase with increasing temperature, reflecting increased ability of the ions to separate in response to the applied field as the free volume in the material increases.

A larger $\Delta\epsilon_{\alpha 2}$ is observed for SPIL(-) in contrast to SPIL(+). Because SPIL(-) has a longer spacer between the polymer backbone and the charged group than does SPIL(+), it may have more freedom to respond to the applied field, resulting in a larger relaxation strength. In other polymerized systems, the magnitude of the α_2 relaxation strength has been observed in the order of 20-120; which is higher than the one we observed for SPILs in the range of 8-23. The lower $\Delta\epsilon_{\alpha 2}$ value is likely due to ion aggregation that reduces effective ions participating in the ion rearrangement process.^{109,130,135}

On the contrary, DPIL shows a significantly lower value of $\Delta\epsilon_{\alpha 2}$ in the range of 2-3 when compared to SPIL counterparts and is not so much drastically affected by temperature. With both the ionic species immobilized via covalent attachment to the polymer backbone, the ions in each ion pair have significantly fewer degrees of freedom, hindering their response to the applied field and reducing the dielectric relaxation strength. Further in DPIL for ion-pair relaxation to happen must require several rearrangements of the neighboring polymer segments.

3.3.9 Static Dielectric Constant

Another important characteristic of the PILs investigated in this work was the static dielectric constant, ϵ_s . It indicates how easily the molecule can be polarized and in the dielectric response it manifests as a plateau in the low frequency regime in the absence of electrode polarization. However, at low frequency, the static response is destroyed by the electrode polarization in the presence of mobile ions.^{131,140}

Previous works from Sokolov's group have shown that the frequency of maximal loss (ω_{\max}) of a relaxation process in ϵ_{der} plots, reflecting the ion dynamics, lies closely to the frequency

of the plateau region onset in σ' .^{110,112} Thus, it would be appropriate to relate this frequency to the conductivity relaxation time (τ_σ) that represents the start of diffusion of ions. In other word, the conductivity relaxation time can be obtained using the following relationship: $\tau_\sigma = 1/\omega_{\max}$ in which ω_{\max} is the crossover frequency.

ϵ_s for both SPIL samples was estimated using³⁻⁶

$$\tau_\sigma \equiv \frac{\epsilon_s \epsilon_0}{\sigma_{DC}} \quad \text{(Equation 10)}$$

where τ_σ is the conduction timescale and is the inverse of ω_{\max} calculated by equation 10, σ_{DC} is the DC conductivity obtained from the plateau in σ' , and ϵ_0 is permittivity of vacuum.

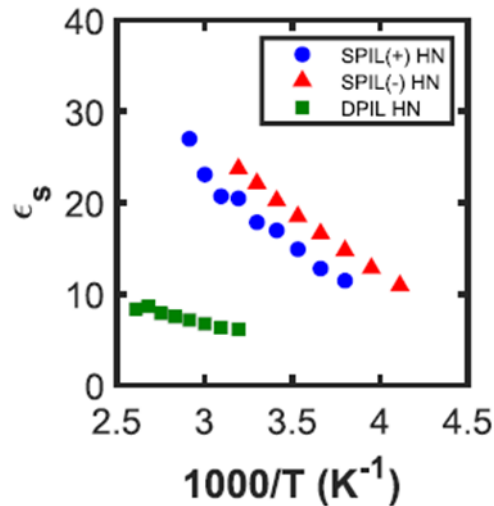


Figure 37 Temperature dependence of static dielectric constant for all PILs in the current study

Figure 37 shows the variation of ϵ_s with temperature. For the SPILs, ϵ_s increases with increasing temperature and has been the case for similar polymerized ionic liquid system. Additionally, SPIL(-) has a higher ϵ_s than SPIL(+) across the entire temperature range. The close proximity of the imidazolium cation to the polymer backbone in polycation restrict their motion

and ability to respond to the field thus lowering ϵ_s .³⁻⁶ Further, SPIL(-) with a lower T_g , responds more readily to the applied field, thereby raising the static dielectric constant in contrast to SPIL(+).

Notably DPIL sample had significantly lower ϵ_s relative to SPILs. We attributed this to the inability of dipoles to respond to the applied electric field due to covalent attachment of the both the ionic species to the polymer backbone and thus lowering configurational entropy. Interestingly in DPIL ϵ_s exhibited a weaker temperature dependence in contrast to SPILs, which is bolstered by the fact that the stronger α_2 relaxation process comprising of ionic rearrangements principally governs the temperature dependence of ϵ_s . The relaxation timescales and relaxation strengths corresponding to rearrangement of ions is much lower for DPIL system, which is directly reflected through a significantly lower value of static dielectric constant of DPIL when compared to SPILs.

3.3.10 Barton-Nakajima-Namikawa (BNN) Function

The final important characteristic of the PILs studied in this work was the investigation of the BNN relation in the context of understanding the connection of ionic conductivity with dielectric loss to further glean information regarding the mechanism of charge transport.

In order to adequately gain physical insight into the basic underlying charge transport mechanism in polymerized ionic liquids, Barton, Nakajima, and Namikawa (BNN) proposed a simple empirical scaling correlation according to which ionic conductivity (σ_{DC}) is proportional to the product of static dielectric constant (ϵ_s) and frequency at the loss maximum of ionic motion ($\omega_{max\alpha_2}$).^{3,133} The BNN relation for DC conductivity can be simply written as:

$$\frac{\sigma_{DC}}{\epsilon_0} = B\epsilon_s\omega_{max} \quad \text{(Equation 11)}$$

where B is a nonuniversal dimensionless constant that corresponds to the number of Debye lengths an ion moves during the rearrangement time and attain values depending on the extent of ion aggregation in the ionomers. This relation suggests that ionic conduction and dielectric relaxation have their inceptions in one diffusion process. Taken together this means that the local ion relaxations and the DC conductivity that originate from the same relaxation process and have the same activation energy will obey the BNN relation.

The mechanism of charge transport for the investigated PILs was studied by BNN relation. DC conductivity rate, σ_{DC}/ϵ_0 , where σ_{DC} obtained from the value of σ' across the plateau was plotted against the product of static dielectric constant, ϵ_s calculated by HN fitting of dielectric loss derivative spectra and the relaxation peak frequency, $\omega_{max\alpha 2}$ of ionic rearrangement process for PILs. The plot was then fitted to BNN relation that yields the slope B.

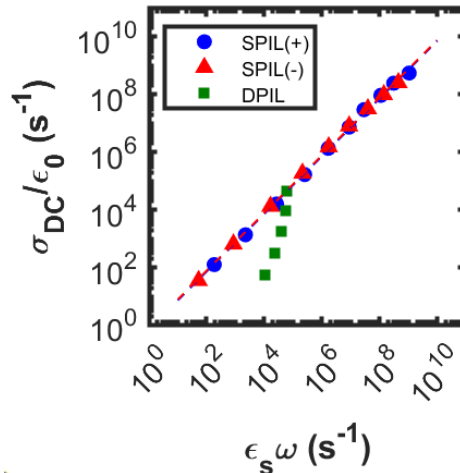


Figure 38 BNN plot for all three polymerized ionic liquids investigated in this work.

As seen in the Figure 38, both SPIL counterparts could be the fit using the BNN relation and ionic conductivity can be successfully scaled in accordance with BNN equation, with the fitting parameters summarized in Table 8.

Table 8 Parameters for BNN fit for investigated PILs

PIL	B (Slope)	Constant
SPIL(+)	0.7256	1.707×10^{-8}
SPIL(-)	0.7679	5.6364×10^{-7}
DPIL	-	-

A value of $B=1$ indicates ions are moving one Debye length in their ion rearrangement process. A value of B less than unity likely indicates ion motions are restricted to hop a distance smaller than the Debye length.^{3,133} A value of $B < 1$ for SPIL(+) (0.7256) and SPIL(-) (0.7679) demonstrates the origin of decoupling between ion conductivity and dielectric loss caused by ion migration.

In contrast to both SPILs, DPIL deviated and could not be fit using BNN relation. Clearly there is a stronger scaling of σ_{DC} with, ω_{max} . The fact that the DC conductivities are not well-described by VFT dynamics indicates that conduction in the DPIL has a substantially different molecular-scale origin than conduction in the SPILs or ion-pair relaxation in the in the SPILs and DPILs. This idea is reinforced by analysis of DC conductivities with the BNN model. In contrast to SPILs, DPILs deviates substantially from the expected linear scaling of σ_{DC} with $\epsilon_s \omega_{max}$, indicating that conduction and ion pair relaxation arise from different molecular-scale processes

in these materials. Further the conduction process in DPIL might be having significantly higher effective activation energy when compared to ion pair relaxation.

3.4 Discussion

Previous works on doubly-polymerized ionic liquids and ionic liquid copolyampholytes have explicitly demonstrated a significant decrease in conductivity relative to singly-polymerized ionic liquid counterparts.^{8,11} Although the non-zero conductivity at high temperatures may indicate that there are small number of mobile charged ions present in the DPIL material, the projected conductivity near T_g is actually comparable to that reported for non-ionic methacrylate like PMMA.¹⁴¹ Thus, even the residual conductivity is rather low in the DPIL irrespective of the high concentration of charged functional groups. However, the molecular scale origin of significant decrease in the bulk ion transport is ambiguous in previous studies encompassing DPILs and copolyampholytes. DPILs, which are amenable to dielectric relaxation measurements should help us to acquire rigorous understanding of the factor responsible for decrease in the bulk ion transport.

Our comprehensive calorimetric and dielectric studies can shed some light if the decreased bulk ion transport is a consequence of strong ionic interactions between the polymer chains as observed in polyampholyte gels or is it due to transformation of small mobile ions to huge immobile polymer chains.¹⁴² As demonstrated in the data above, these studies are more conclusive towards a picture similar in polyampholytes gels suggesting the existence of strong physical crosslinks formed by ion pairs between polymer chains ones the two ionic species are copolymerized and thus obstruct the ion transport in these materials.¹⁴²⁻¹⁴⁴

The physical characteristics of DPIL are highly indicative of the above drawn picture. The higher T_g of DPIL, its insolubility in pretty much all common laboratory solvents, and absence of thermoplastic behavior points towards a presence of highly cross-linked solid rather than non-interacting polymer chains. The glass transition temperature (calorimetric and dielectric) of DPIL is higher than SPILs which is certainly because DPIL lacks the mobile counterions of SPIL instead has fewer mobile species integrated into the polymer chains however ionic interactions between the chains can likely attribute to this observed higher T_g . Notably the well-known Fox equation cannot be used to predict the T_g of DPIL because DPIL cannot be considered as a statistical copolymer of SPIL counterparts as it does not have their mobile counterions. Interesting work by Esako demonstrated a conductivity rise of approximately 85% on addition of 20% vol/vol of [EMIM][BF₄] to poly 1-[10-(methacryloyloxy)decyl]-3-methylimidazolium bromide.¹⁴⁵ Thus, we hypothesize adding [EMIM][TFSI] to DPIL should soften the material and lower its T_g to the value predicted by Fox equation which is roughly 260 K.

Dielectric studies further strengthen the proposition that ionic interactions between the polymer chains dominate the DPIL material. Significantly lower DC conductivity of DPIL in contrast to corresponding SPILs highlight the obstruction of ion transport in DPIL. When DC conductivity is normalized to T_g , still conductivity of DPIL is two orders of magnitude lower than SPILs. This propounds that the strength of decoupling between ionic conductivity and segmental motion is stronger in DPIL than in SPILs. Further the VFT dynamics cannot well explain the variation of DC conductivity with temperature even above the T_g of DPIL. This result again reinforces that bulk ion transport in DPIL is not directly linked to the available free volume and thus multiple ion pairs would have to simultaneously relax to facilitate the ion transport again circles back to the image of DPIL as extensively physically cross-linked material above its T_g .

The dielectric analysis furnishing the relaxation frequencies and relaxation strengths in DPIL further shed light on restriction of local ionic motions in DPIL. DPIL was found to have slower ion pair relaxation rate and smaller relaxation strength in comparison to SPILs. From a molecular perspective, this result actually makes a lot of sense. If we think about what it might take for an ion pair to relax in a SPIL, we see that that process can occur without too much rearrangement of the polymer chain and may proceed via hooping of the free counterions. This is consistent with previous observations that ion pair rearrangement, and ionic conduction, are substantially decoupled from the segmental dynamics of the polymer in most polymerized ionic liquids.^{113,146}

If we think about what it might take for an ion pair to relax in a DPIL, on the other hand, we see that the connectivity of the ions significantly restricts their ability either to separate or to reorient relative to each other. Achieving either of these motions on the same length scales accessible to the SPIL would likely require rearrangement of the polymer backbones. Because of the frequent ionic interactions between the chains, however, this is not a trivial task, and as a result the ability of the ion pairs to respond to the applied electric field is significantly hindered, even if there is substantial free volume above T_g .

Finally, the BNN analysis reveals the decoupling of residual conduction from the local ion pair rearrangement process in DPILs. In contrast to SPIL,^{6,110,133,147} DPIL deviates from the linear scaling σ_{DC} with $\epsilon_s\omega_{max}$. This reflects a stronger temperature dependence by the conduction process in DPIL than the local ion pair rearrangement process reinforcing the simultaneous relaxation of multiple ion pairs for ion transport to happen.

Taken together, these results shed significant light on the mechanisms of ion locking in DPILs. The key is the connectivity of the charged sites in the DPIL. In contrast to SPILs, both

the bulk and local ionic motions in DPILs are significantly restricted by the covalent linkage of both ionic species to the polymer chains. Especially at lower temperatures, ion pairs between the chains likely effectively create frequent ionic crosslinks between the chains. Any ion transport – whether of free ions or large-scale local motions of the polymer chains – likely require significant breakage and re-formation of these inter-chain crosslinks, which is both slow and energetically costly. As a result, from a bulk perspective, the overall ion conductivity is highly suppressed, while from a local perspective, the relaxation strengths of the material are low because the ions don't have the freedom to go very far as shown in Figure 39.

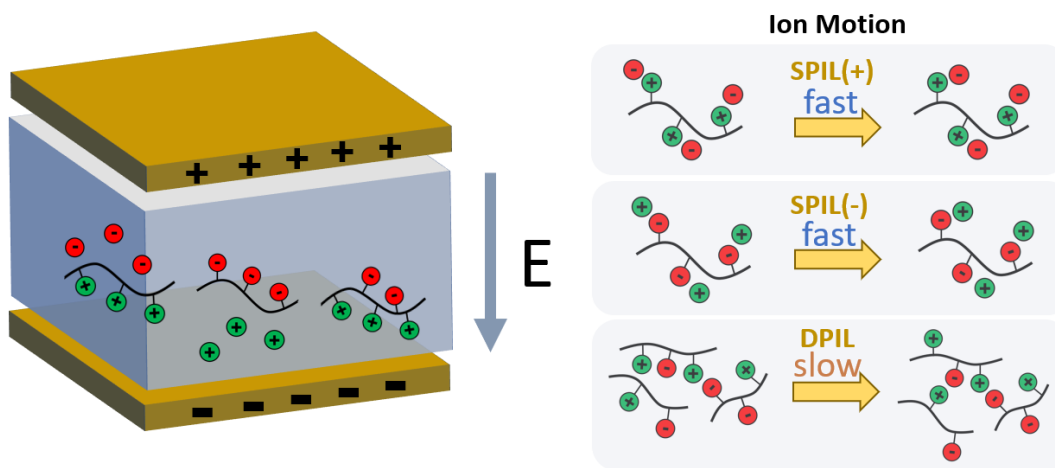


Figure 39 Mechanism of ion transport in SPILs vs. DPIL

Thus, polymerizing both the charged species really slow down the molecular relaxations and have the capability to hold the ions longer in place, catalyzing new classes of organic electronics.

3.5 Conclusion and Future Work

Monomeric dPIL samples were prepared directly from a monomeric substance containing a 1:1 ratio of polymerizable cations to polymerizable anions, with un-polymerizable counterions. Thus, DPIL polymers are, essentially, a 1:1 statistical copolymer of the cationic and anionic monomers lacking mobile counterions. A presence of a single T_g in the DSC data does indeed suggest these are copolymerized relatively random. Doubly-polymerized ionic liquids are interesting material considering on one level, it is just a copolymer, but the ionic interactions create a network. Thus, DPIL materials are effectively an ion-facilitated network, and the terminology reflects and describe how the material is made.

This work highlights the dynamics of ion motion in different types of polymerized ionic liquids. The previously synthesized SPIL and DPIL typed ionic liquid polymers are characterized using broadband dielectric spectroscopy to understand how crosslinking of PIL gels will influence the ion pair relaxation rates and strengths. The findings in this work emphasizes that the mobile counterions are needed to achieve high ion transport and conductivity.

The primary outcomes of our work are as follows:

- (a) We showed for the first time that the dynamics of both conduction and local relaxations slow down by at least 4 orders of magnitude when the cation and anionic species of an ionic liquid are copolymerized in the absence of other free ions.
- (b) We also showed for the first time that the relaxation strength of the DPIL materials is 2-3 times lower than in the corresponding SPILs.
- (c) We showed that the conduction process in DPILs appear to be decoupled from the local ionic relaxations, as seen in the BNN analysis. This behavior strongly contrasts that seen

in conventional polymerized ionic liquid systems, including both the SPILs reported in our work and related systems reported by other groups.

The DPILs were designed to have as low a conductivity as possible, which is critical for ion locking applications in flexible electronics, where they are emerging as a viable way to introduce persistent doping in two-dimensional semiconductors.¹³ Our goals in this study were to understand the mechanism of this ion locking process, and characterize the remaining timescales for rearrangement, which will dictate the timescales over which the devices relying on ion locking will function.

Although our goal in this study was solely to understand the timescales for ionic motion that are relevant for electronic devices, we believe these materials can display great mechanical properties because of their highly crosslinked state due to strong ionic interactions.

Looking forward, there are a lot of interesting open questions about these materials. To begin with how would the directly-polymerized DPIL, in which both monomers are polymerized in a single step as in the present study, compare with systems containing a mixture of anionic and cationic homopolymers. Although in both the scenarios there will be lack of mobile counterions but we expect them to behave differently as the arrangement of monomers, the net charge on the overall polymer, and consequently their response to the electric field will be different.

Further it would also be interesting to see if there is a significant difference between these polyampholyte (doubly polymerized ionic liquid) and their blends. Although blends of SPIL(+) and SPIL(-) homopolymers would not be comparable to the DPIL because they would contain additional mobile counterions, it might be possible to prepare “homopolymer blend” with no mobile counterions by, for example, polymerizing, SPIL(+), exchanging the anionic counterions

with their polymerizable analogues, and then polymerizing a second time to form the anionic chains.

We expect different molecular factors ranging from copolymer ratio, presence of free or unpolymerized ions, molecular weight of the polymers, charge distribution within the chains might mediate ion transport and local relaxations in these systems. This counteracts to our desired goal of specifically characterizing the 1:1 copolymer ratio with no mobile counterions for ion-locking applications. Moving forward, it would be informative to study the influence of systematically varying the copolymer ratio on EDL relaxation process considering EDL retention times should be strongly correlated to the free ion content and the mobility of the DPIL material.

As chemists, we would be really interested in learning more about the structure-function relationships in these materials to understand how changes to the chemical structures of the polymerizable monomers affects both the bulk ion transport and the local ionic relaxations. For example, increasing the length of the linkers between the polymer backbones and the ionic groups could increase the flexibility of the polymers, facilitating faster ionic relaxations. On the other hand, incorporating long alkyl linkers could promote microphase segregation, which might restrict ion transport over larger length scales and promote EDL retention in DPIL materials. This can be well understood by physical characterization techniques like small- and wide-angle X-ray scattering (SAXS and WAXS), which have been extensively used in singly-polymerized ionic liquids to decipher the variation of the spacing between chains and the aggregation of nonpolar pendant groups with changes in molecular structure.^{64,148,149}

To develop a deeper insight into the EDL relaxation mechanism, doubly-polymerized ionic liquids can be combined with the difunctional crosslinker, such as ethylene glycol dimethacrylate that should not affect the timescales of local ion rearrangement, but should inhibit segmental and

chain relaxation.¹⁵⁰ From a more physical perspective, we think it would also be fascinating to try to distinguish the bulk dynamics of these materials with their interfacial dynamics, since interfacial processes are critical for the function of electric double-layer-based devices like the ones we described in this study.

We hope to continue working in developing DPIL materials in which the EDL retention times can be tailored to meet the application-specific needs and to push the envelope of what we can do with these ion-locked materials.

Appendix A NMR Characterization for synthetic intermediates in Chapter 2 and 3

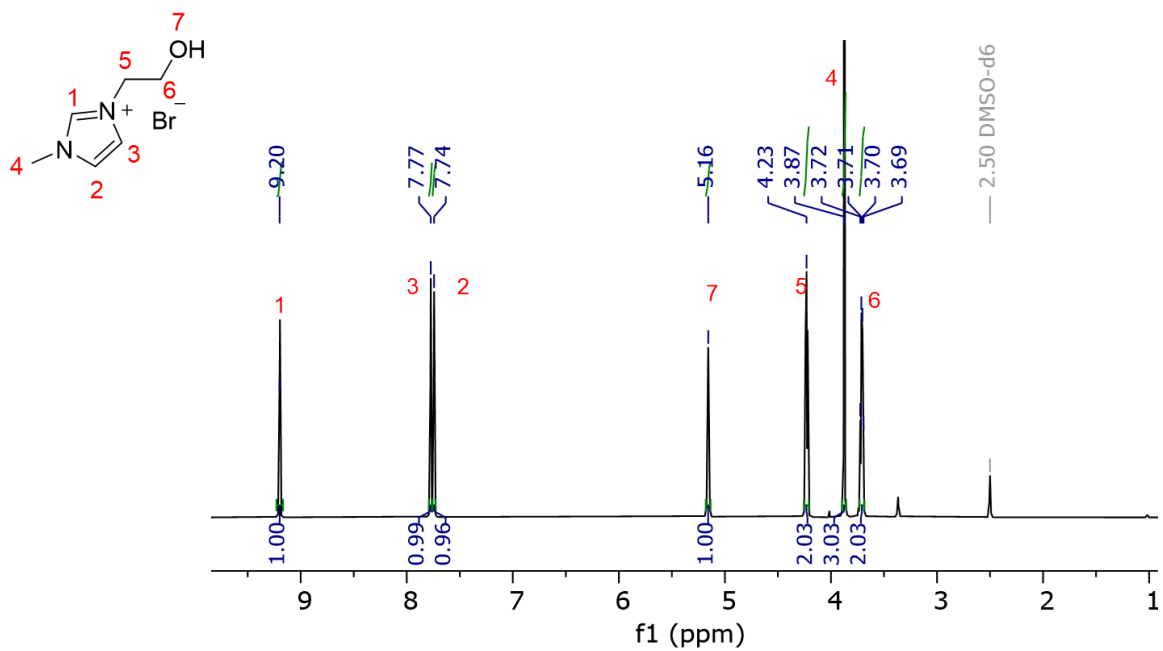


Figure 40 ¹H-NMR for synthetic intermediate 7 in Figure 12

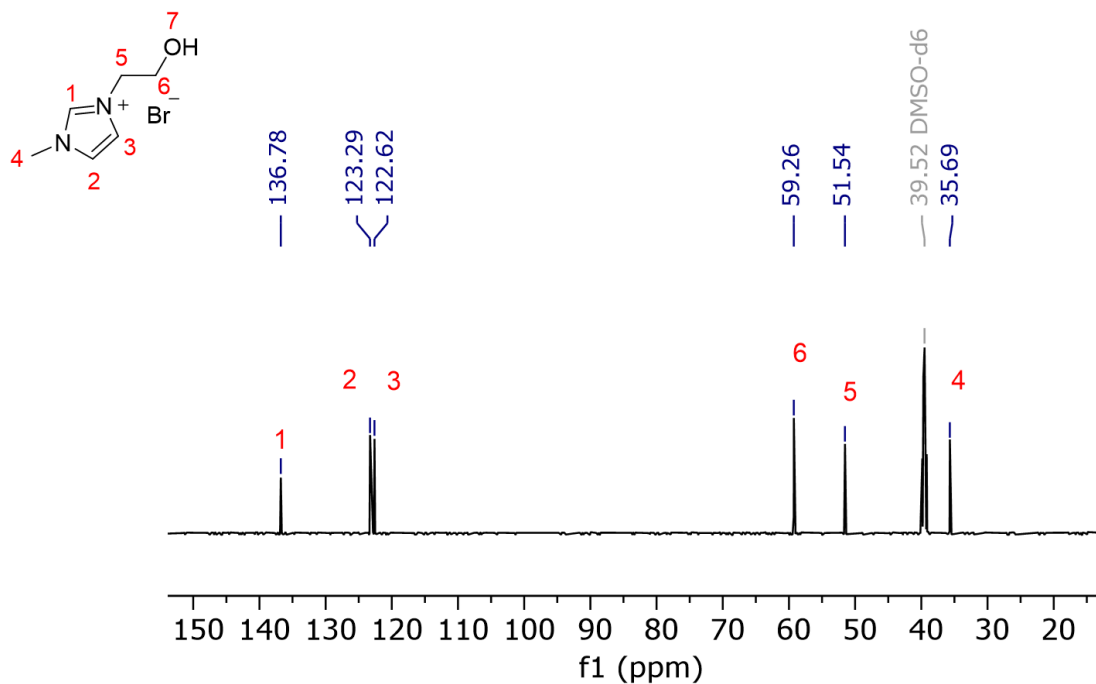


Figure 41 $^{13}\text{C-NMR}$ for synthetic intermediate 7 in Figure 12

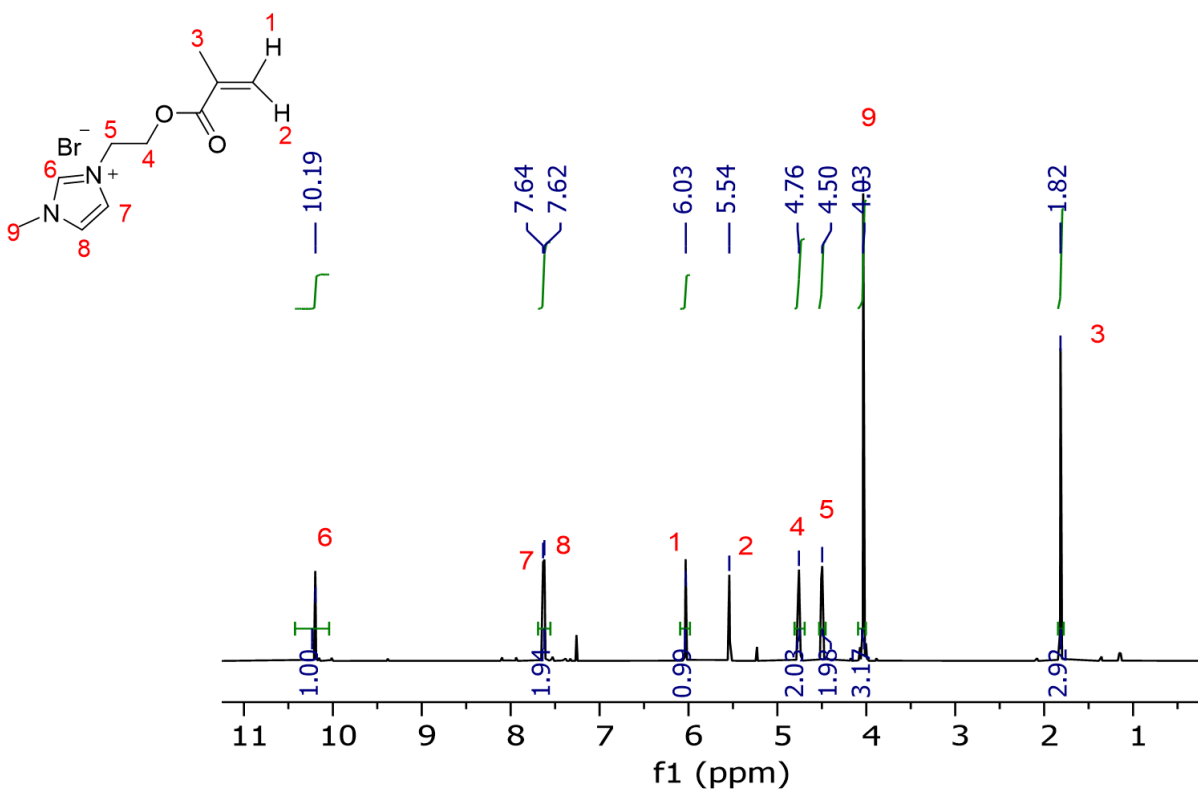


Figure 42 $^1\text{H-NMR}$ for synthetic intermediate 8 in Figure 12

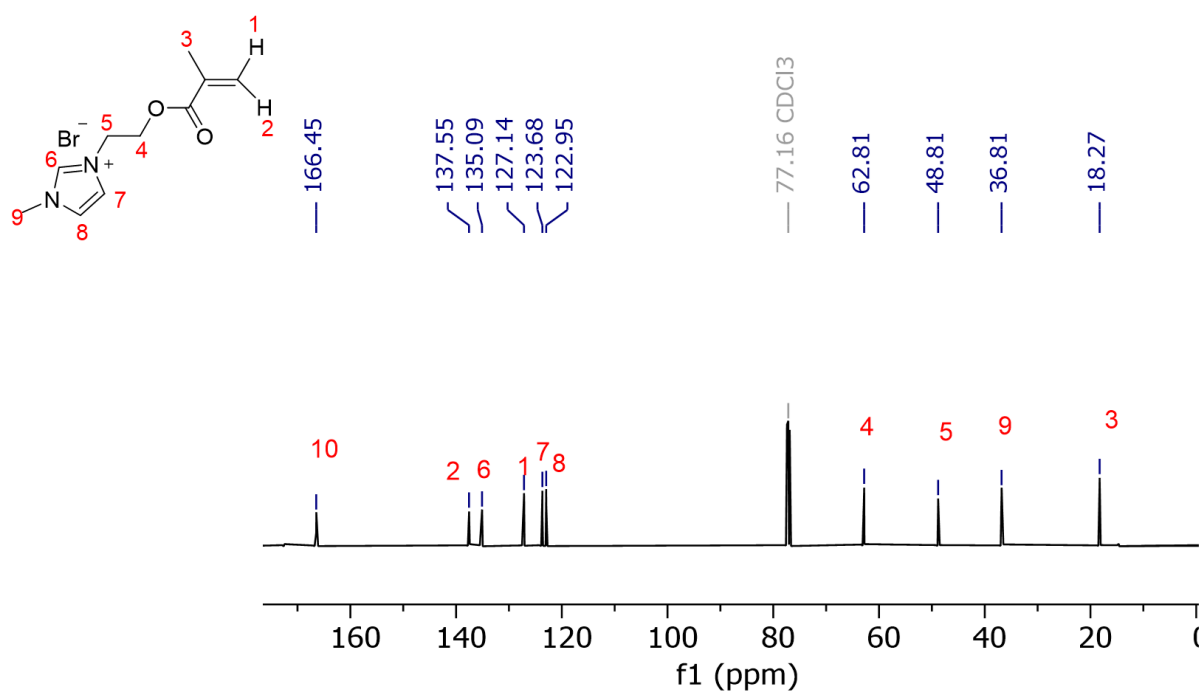


Figure 43 ¹³C-NMR for synthetic intermediate 8 in Figure 12

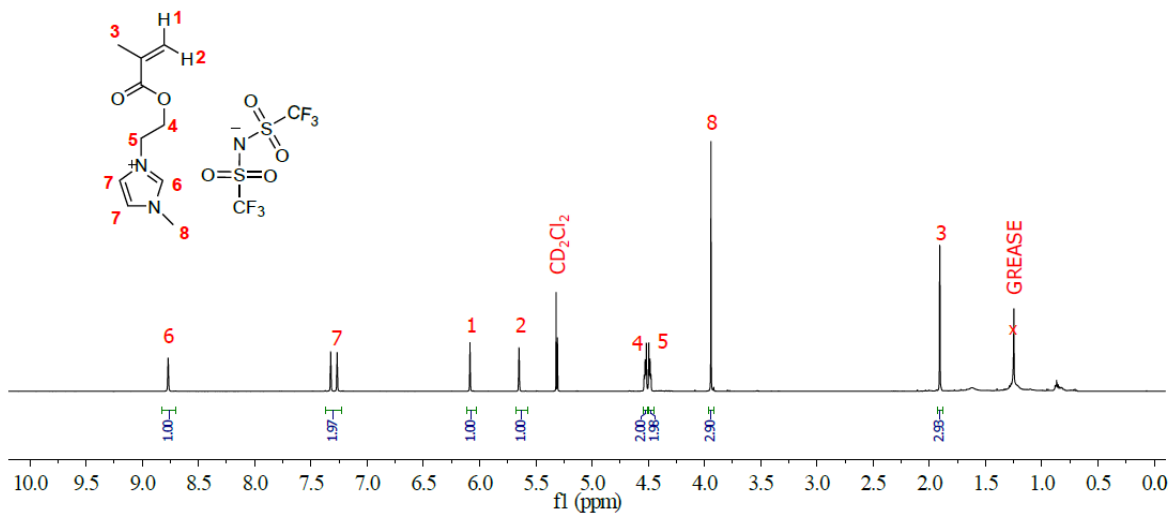


Figure 44 ¹H-NMR for synthetic intermediate 9 in Figure 12

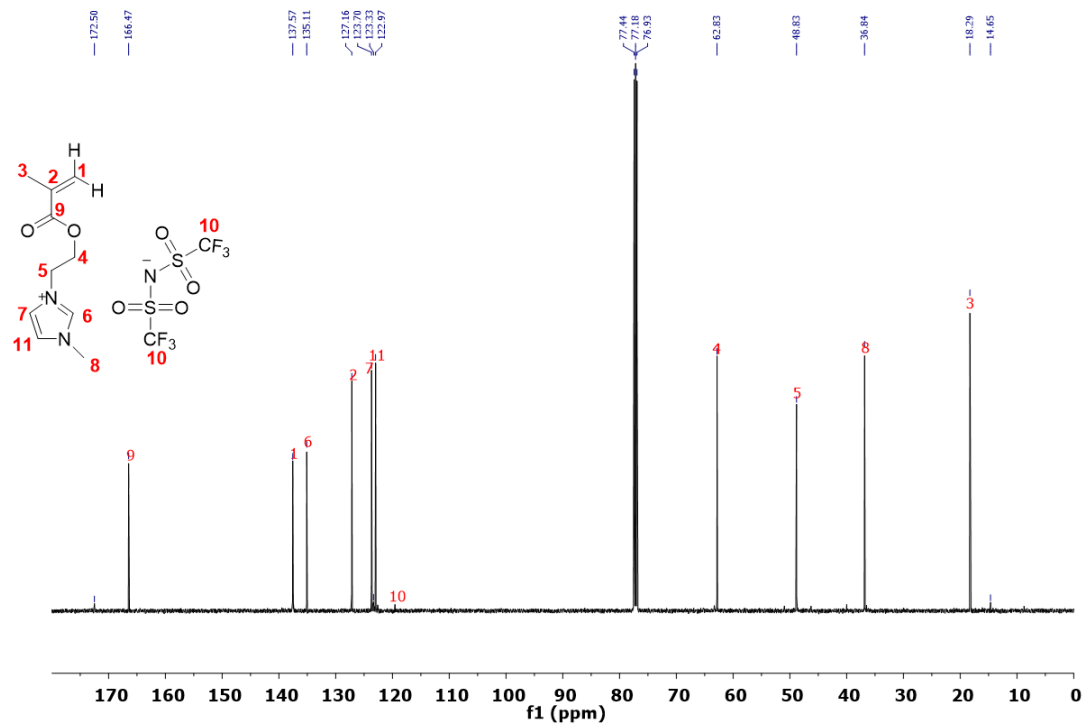


Figure 45 ¹³C-NMR for synthetic intermediate 9 in Figure 12

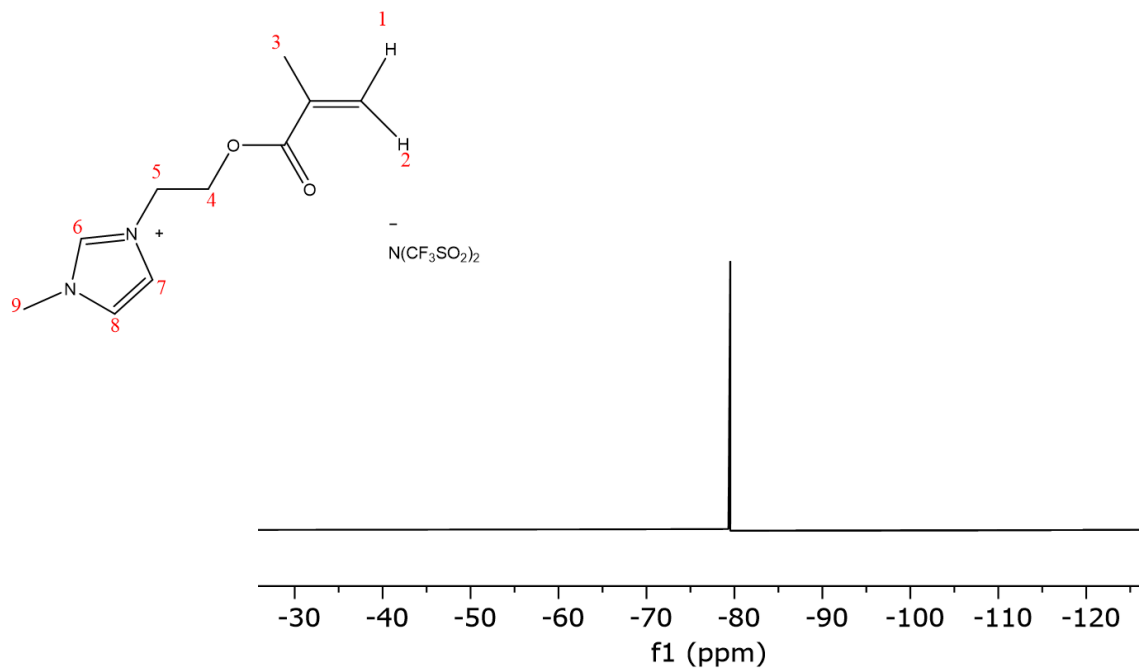


Figure 46 ^{19}F -NMR for synthetic intermediate 9 in Figure 12

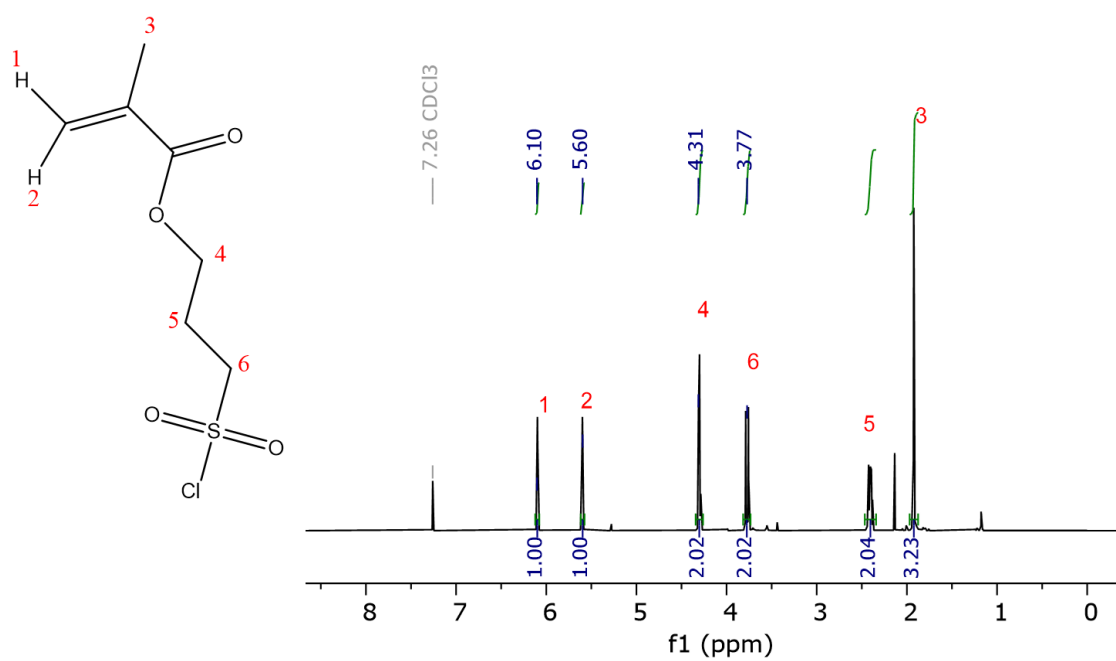


Figure 47 ^1H -NMR for synthetic intermediate 11 in Figure 13

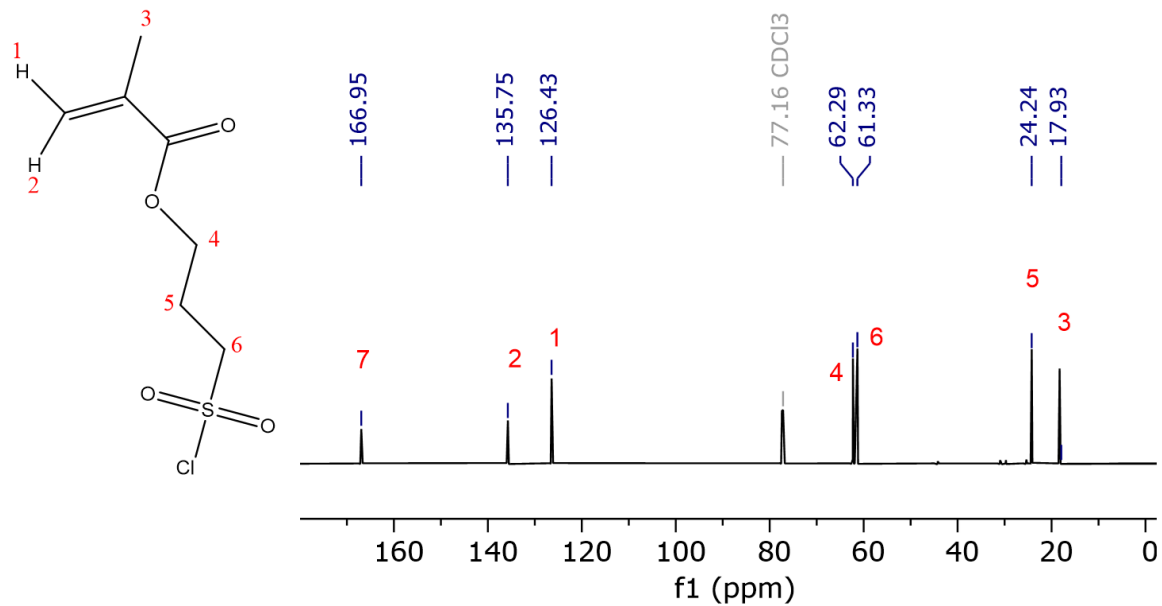


Figure 48 ¹³C-NMR for synthetic intermediate 11 in Figure 13

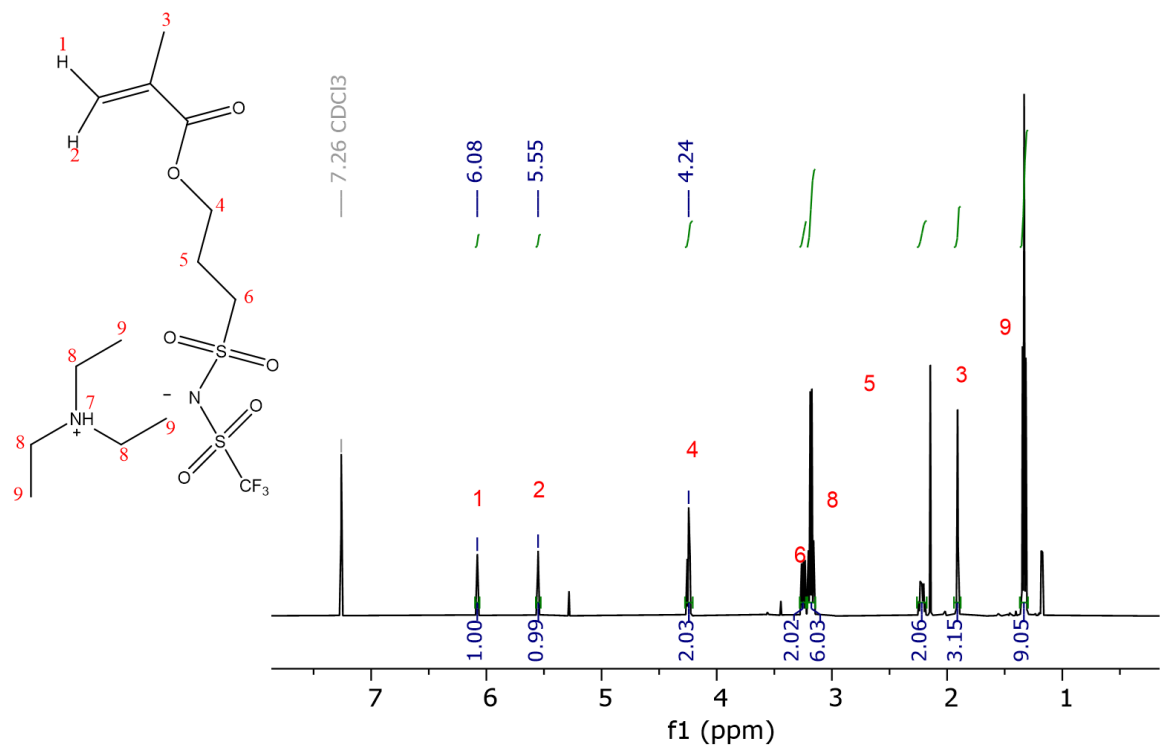


Figure 49 ¹H-NMR for synthetic intermediate 12 in Figure 13

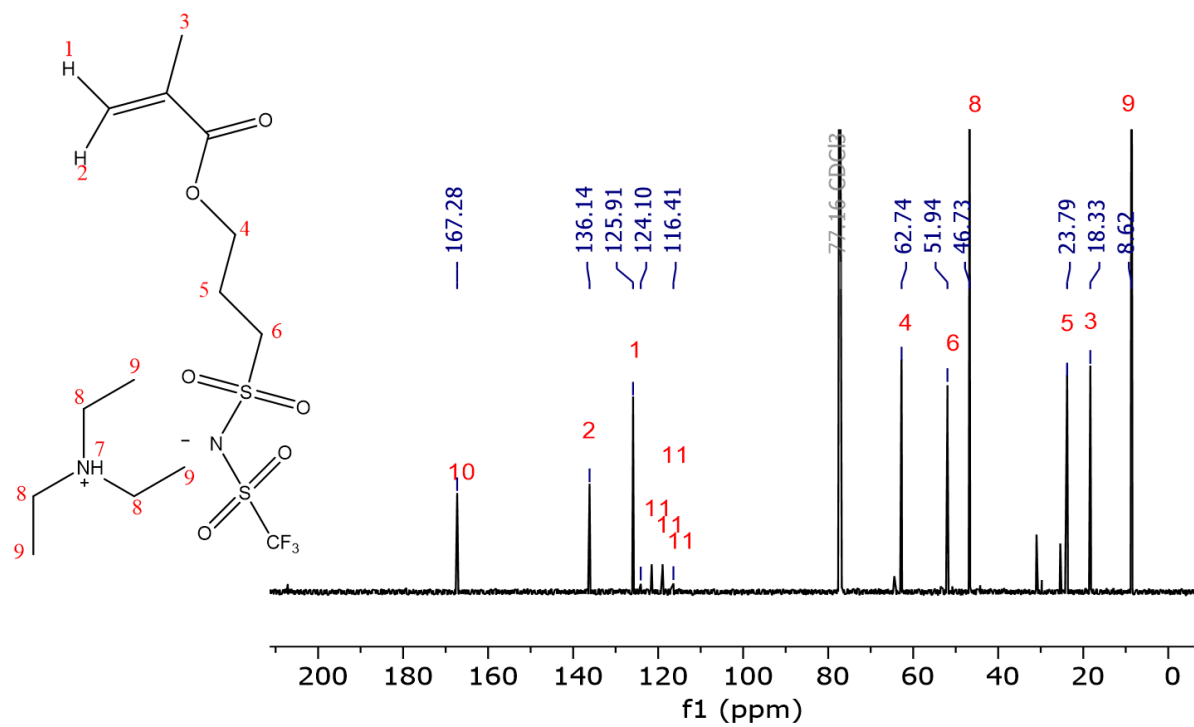


Figure 50 ^{13}C -NMR for synthetic intermediate 12 in Figure 13

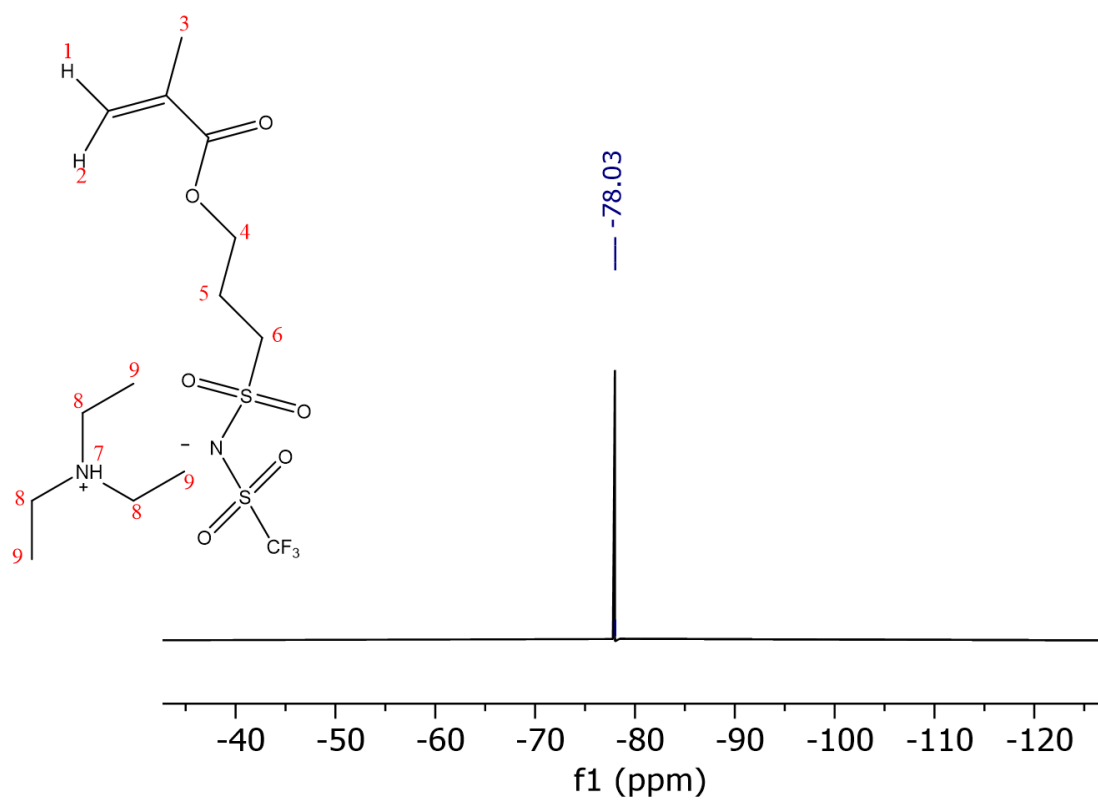


Figure 51 ^{19}F -NMR for synthetic intermediate 12 in Figure 13

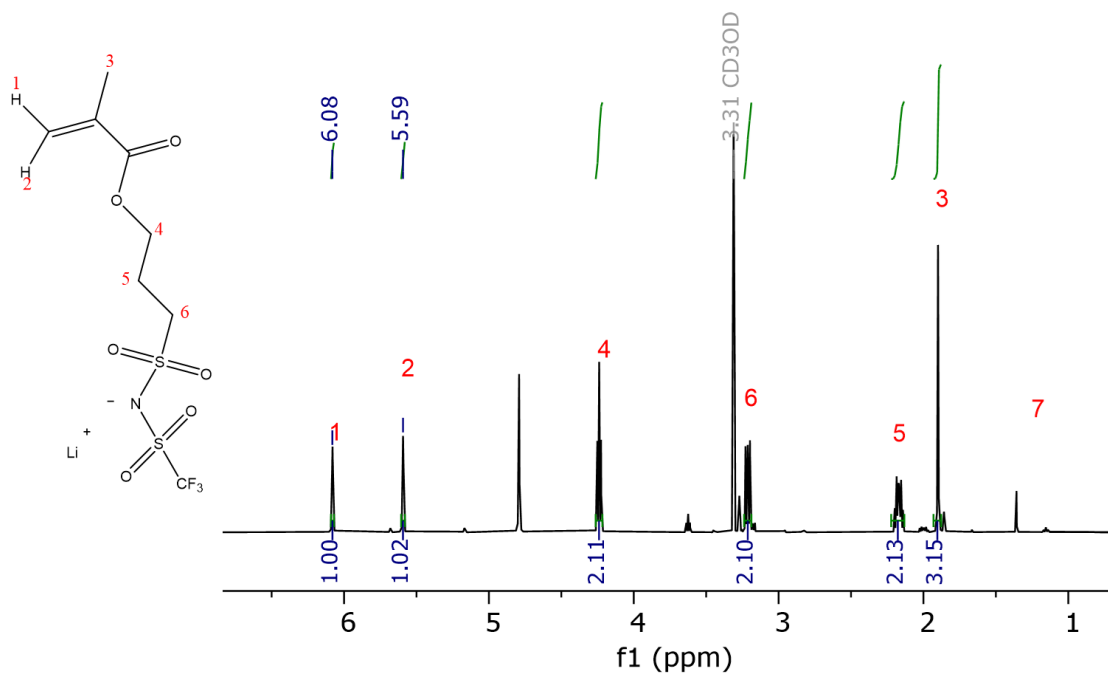


Figure 52 $^1\text{H-NMR}$ for synthetic intermediate 13 in Figure 13

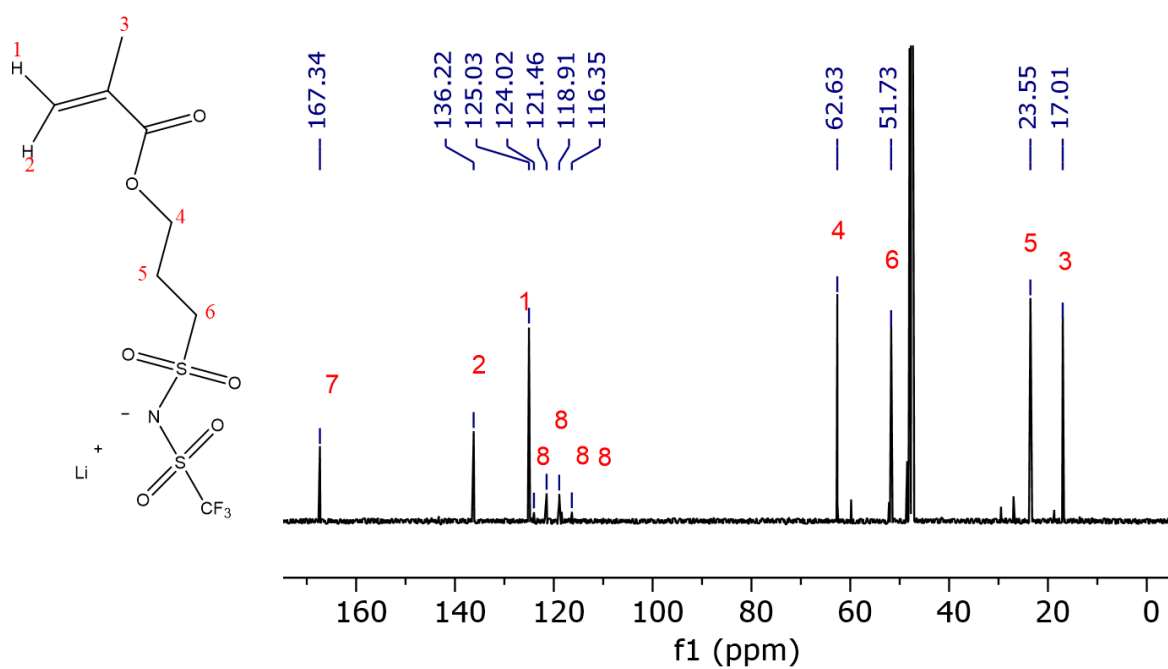


Figure 53 $^{13}\text{C-NMR}$ for synthetic intermediate 13 in Figure 13

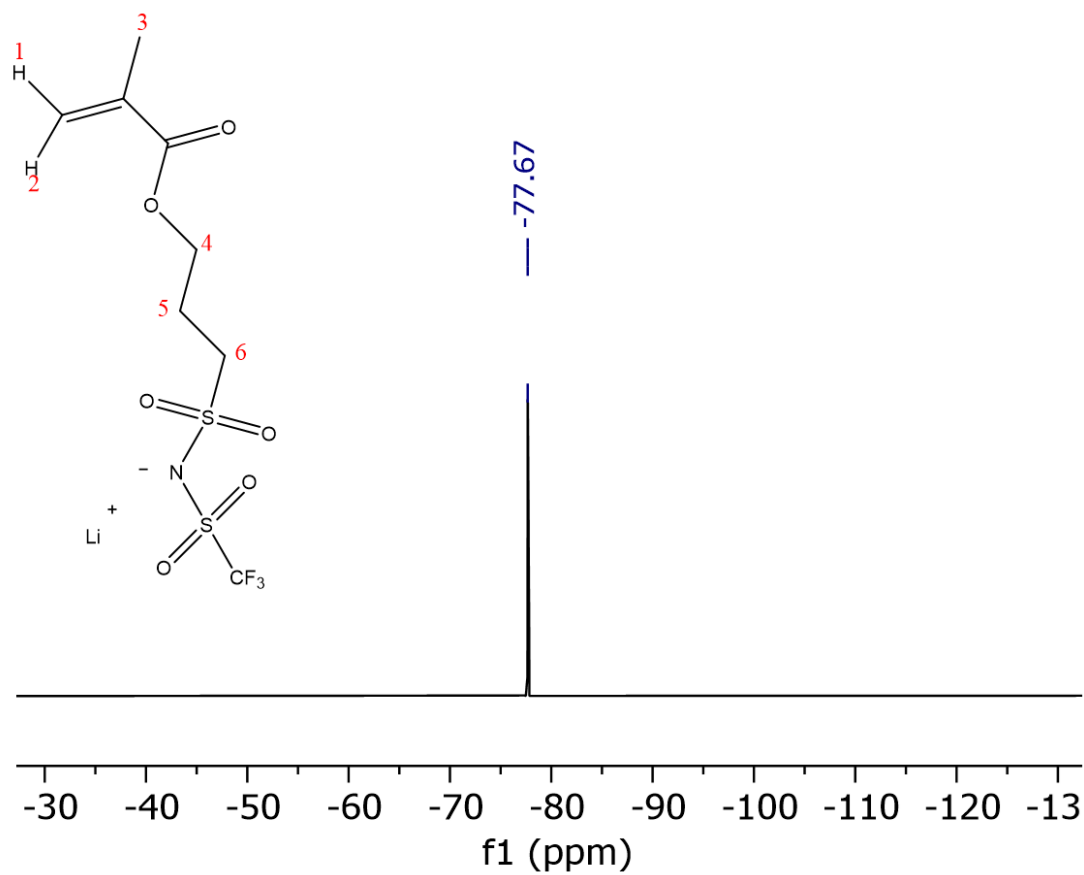


Figure 54 ^{19}F -NMR for synthetic intermediate 13 in Figure 13

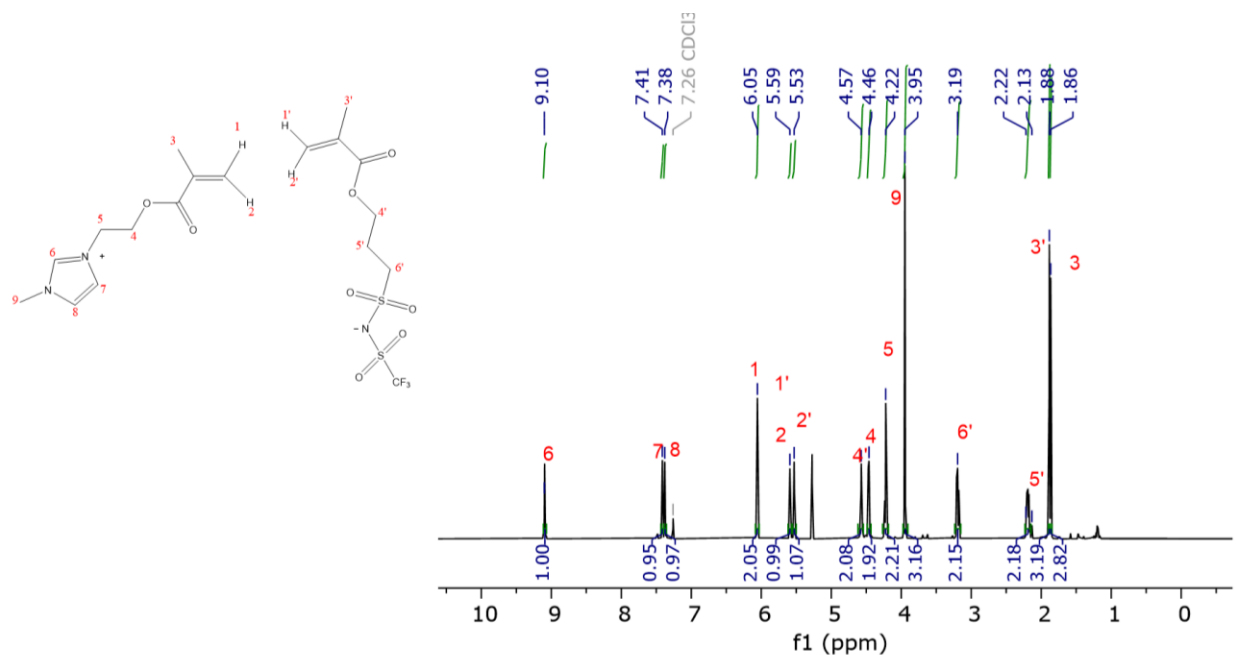


Figure 55 $^1\text{H-NMR}$ for synthetic intermediate 14 in Figure 13

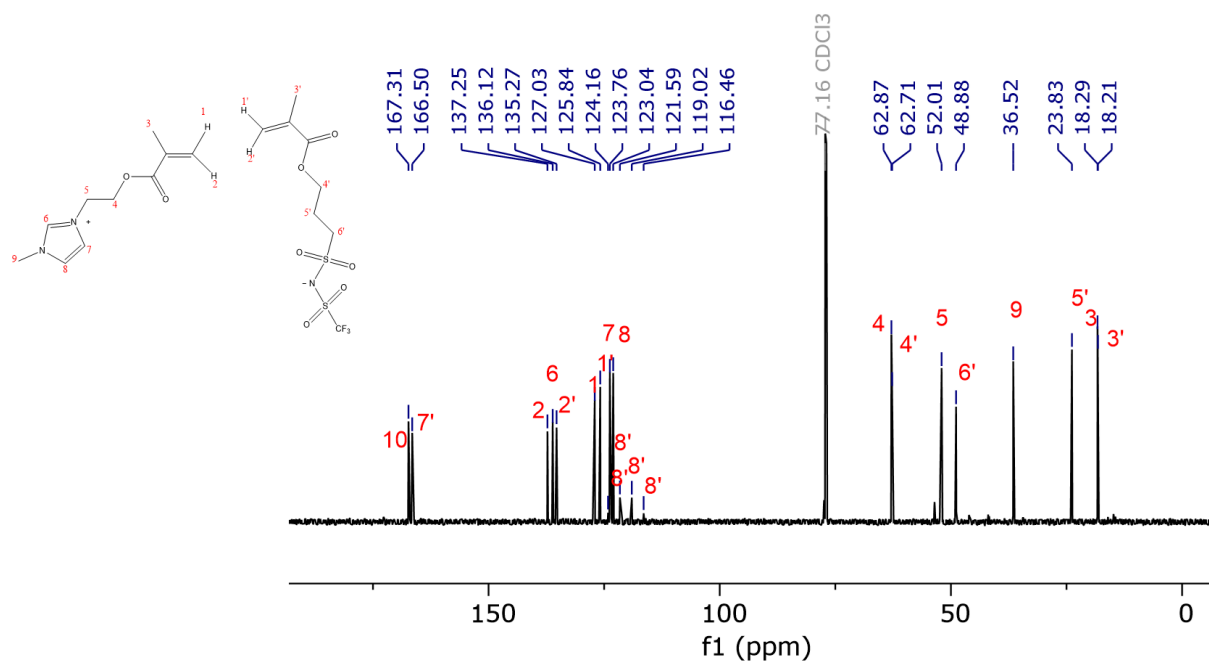


Figure 56 $^{13}\text{C-NMR}$ for synthetic intermediate 14 in Figure 13

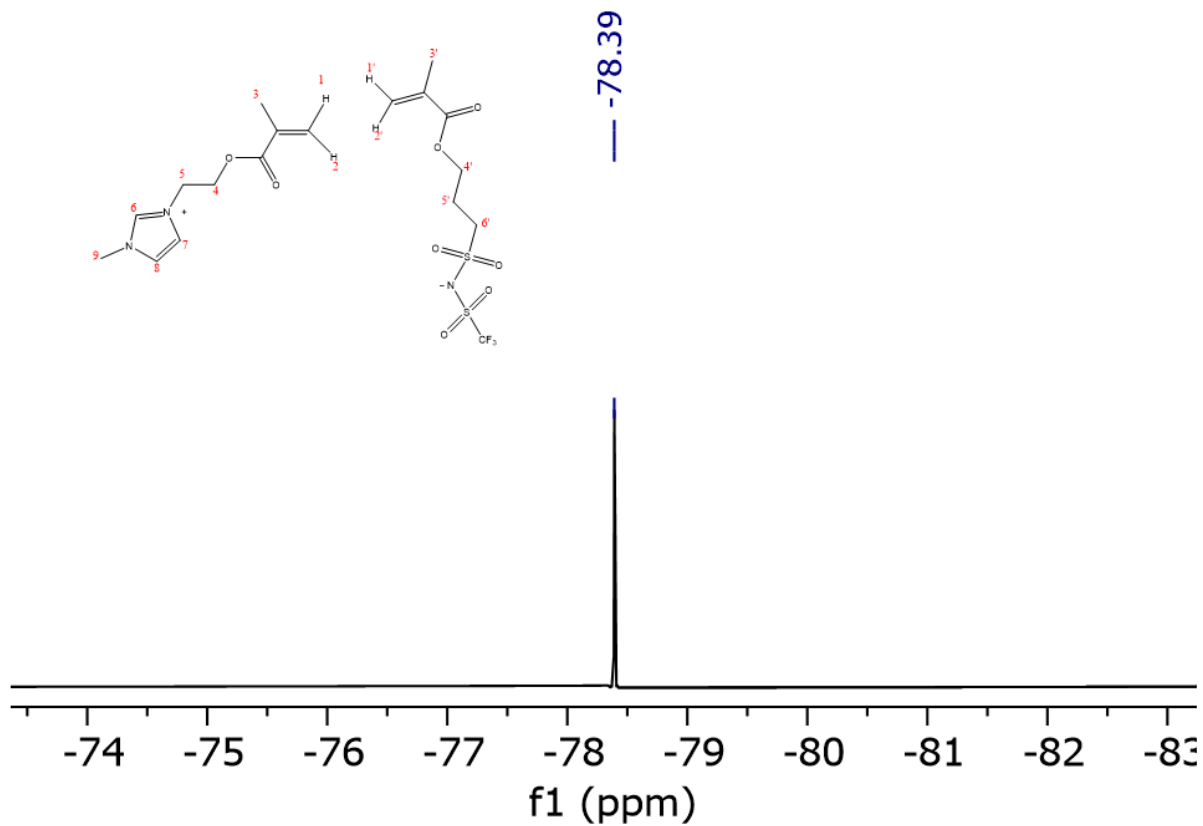


Figure 57 ^{19}F -NMR for synthetic intermediate 14 in Figure 13

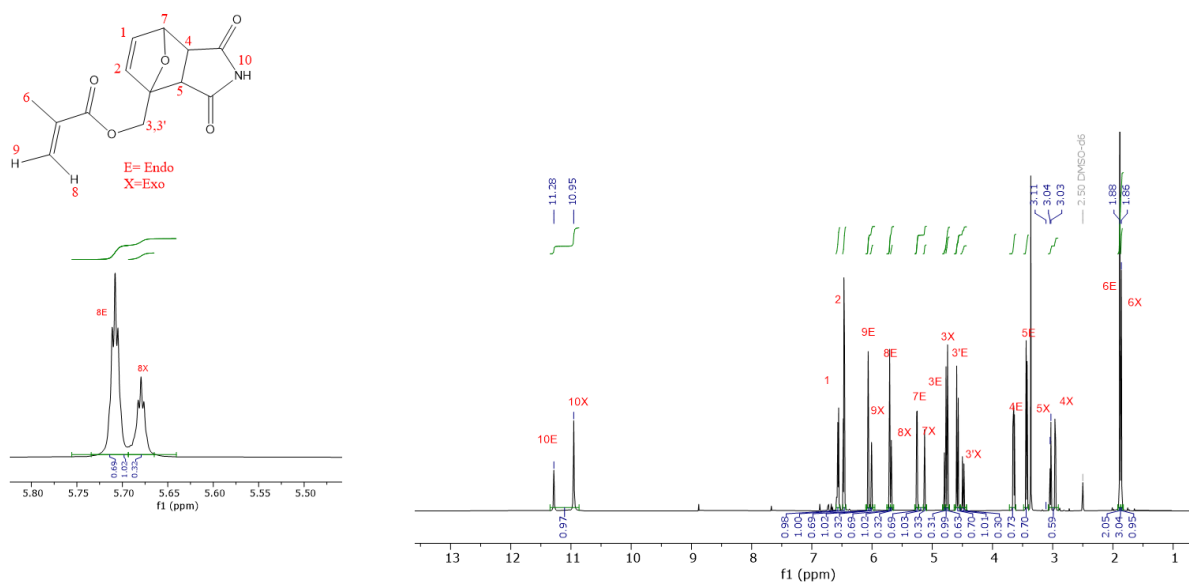


Figure 58 ^1H -NMR for synthetic intermediate 2 in Figure 11

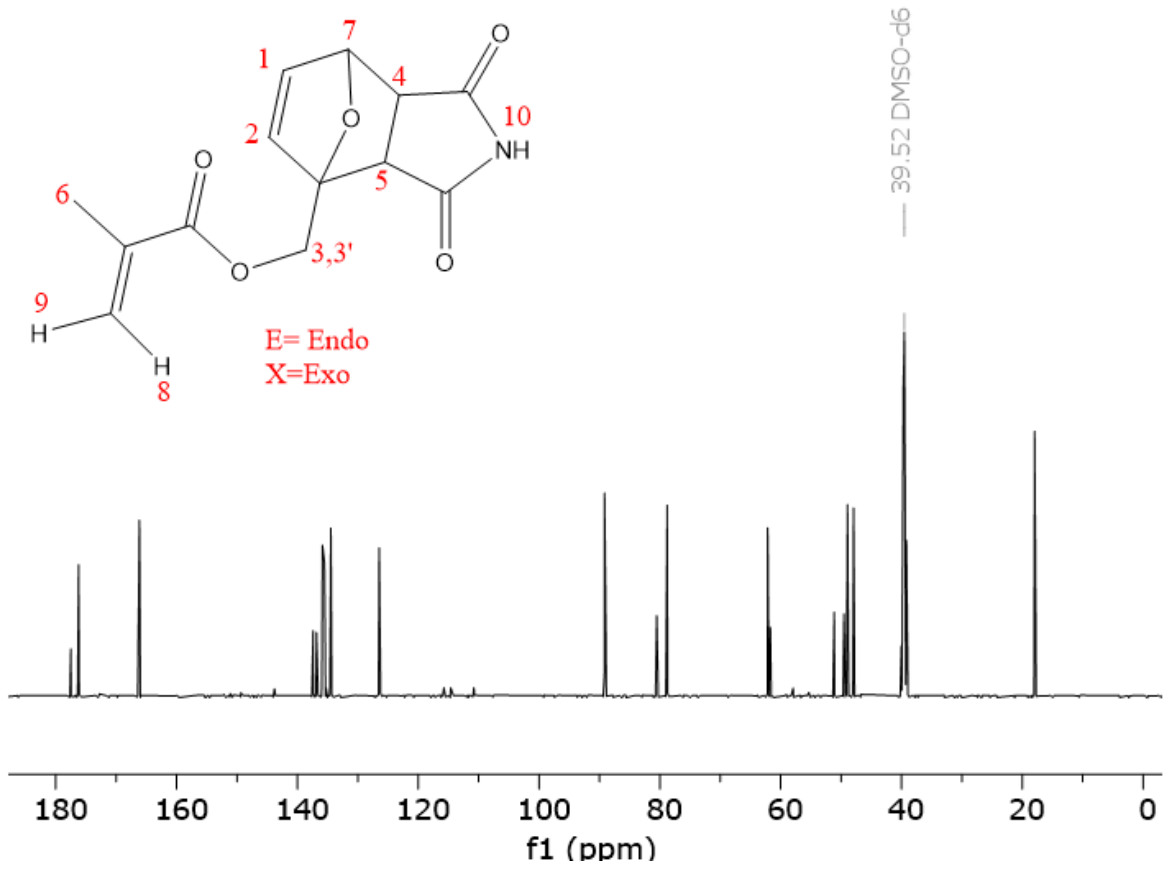


Figure 59 $^{13}\text{C-NMR}$ for synthetic intermediate 2 in Figure 11

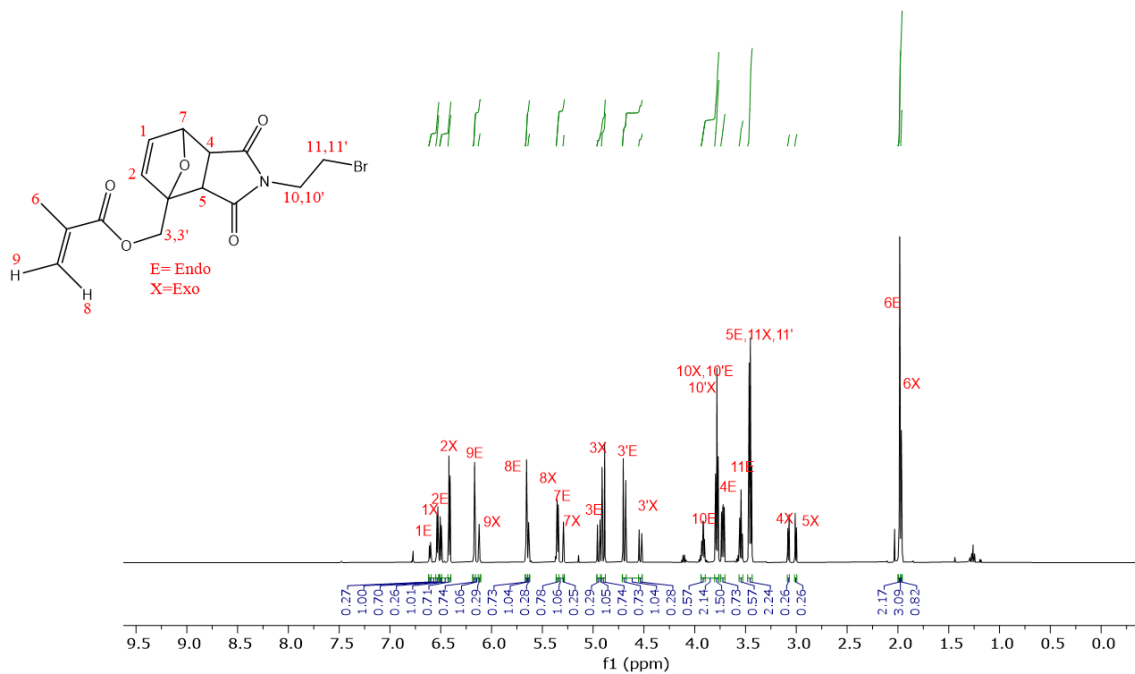


Figure 60 $^1\text{H-NMR}$ for synthetic intermediate 3 in Figure 11

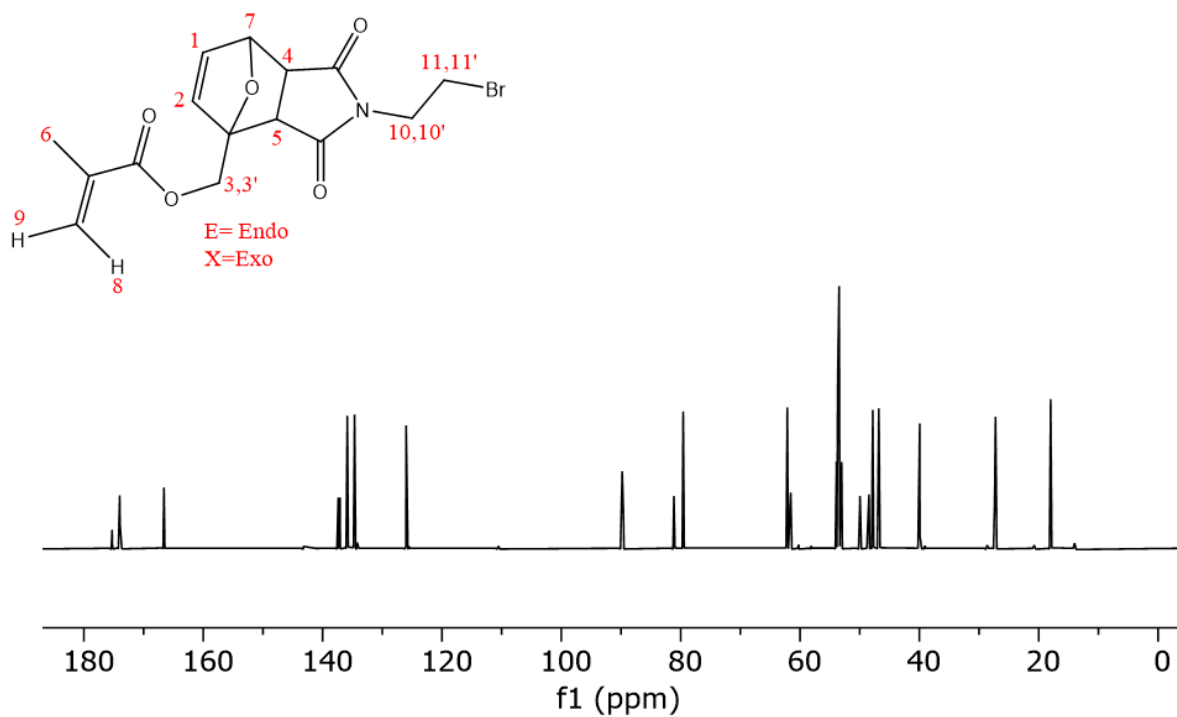


Figure 61 ^{13}C -NMR for synthetic intermediate 3 in Figure 11

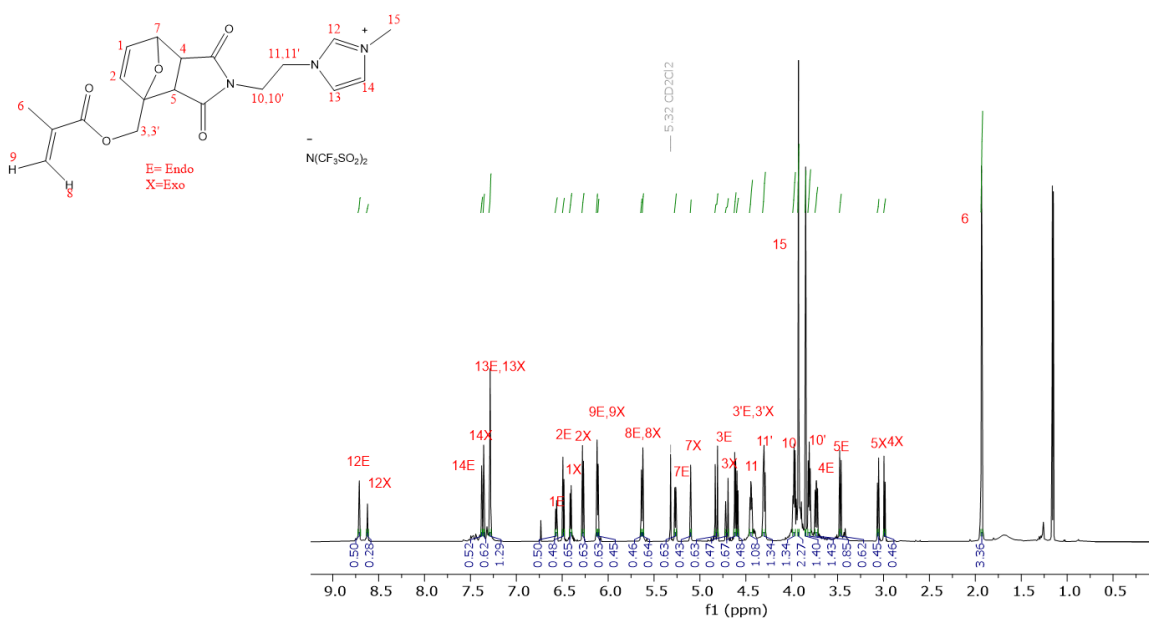


Figure 62 ^1H -NMR for synthetic intermediate 5 in Figure 11

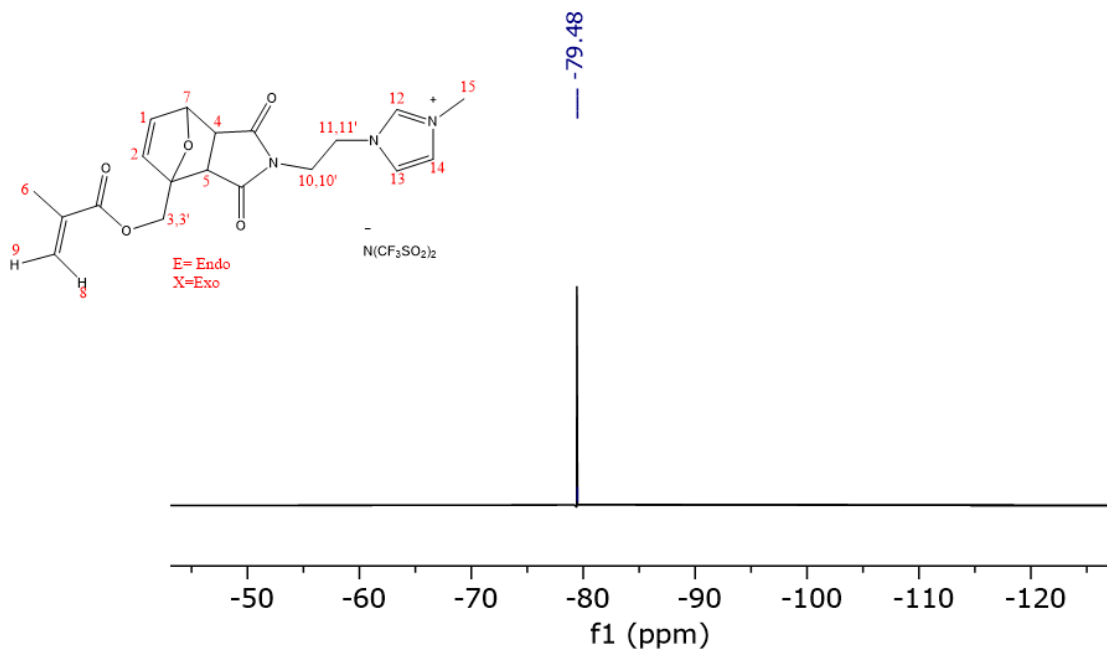


Figure 63 ^{19}F -NMR for synthetic intermediate 5 in Figure 11

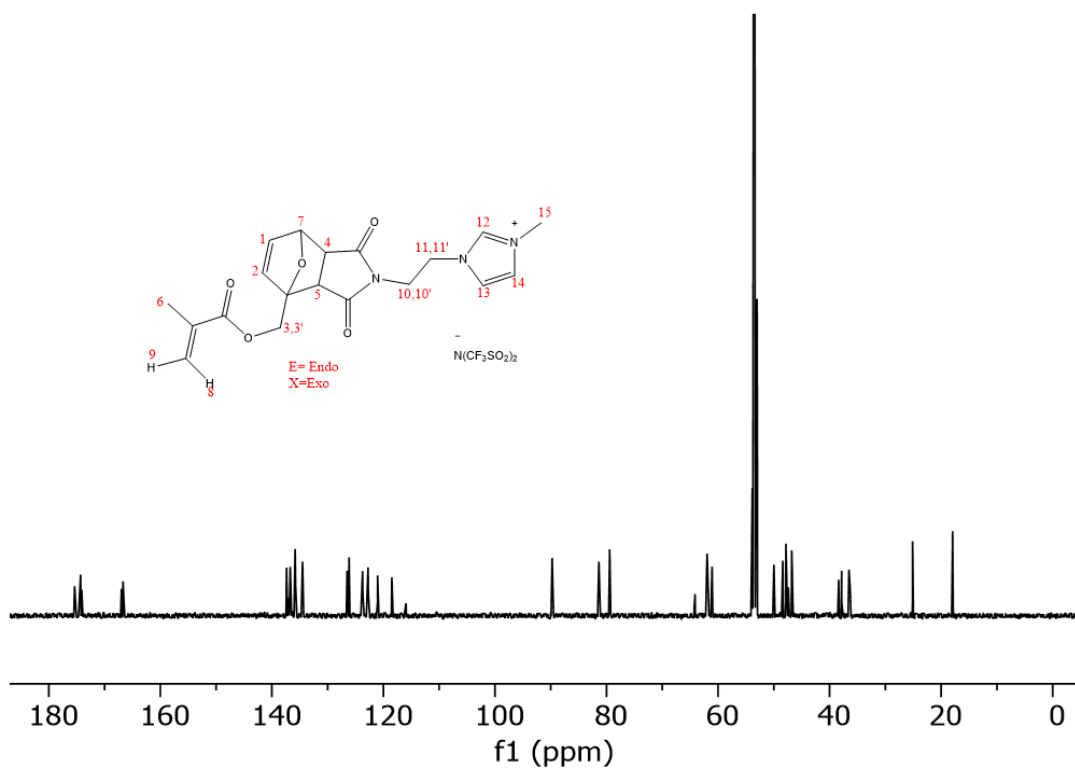


Figure 64 ^{13}C -NMR for synthetic intermediate 5 in Figure 11

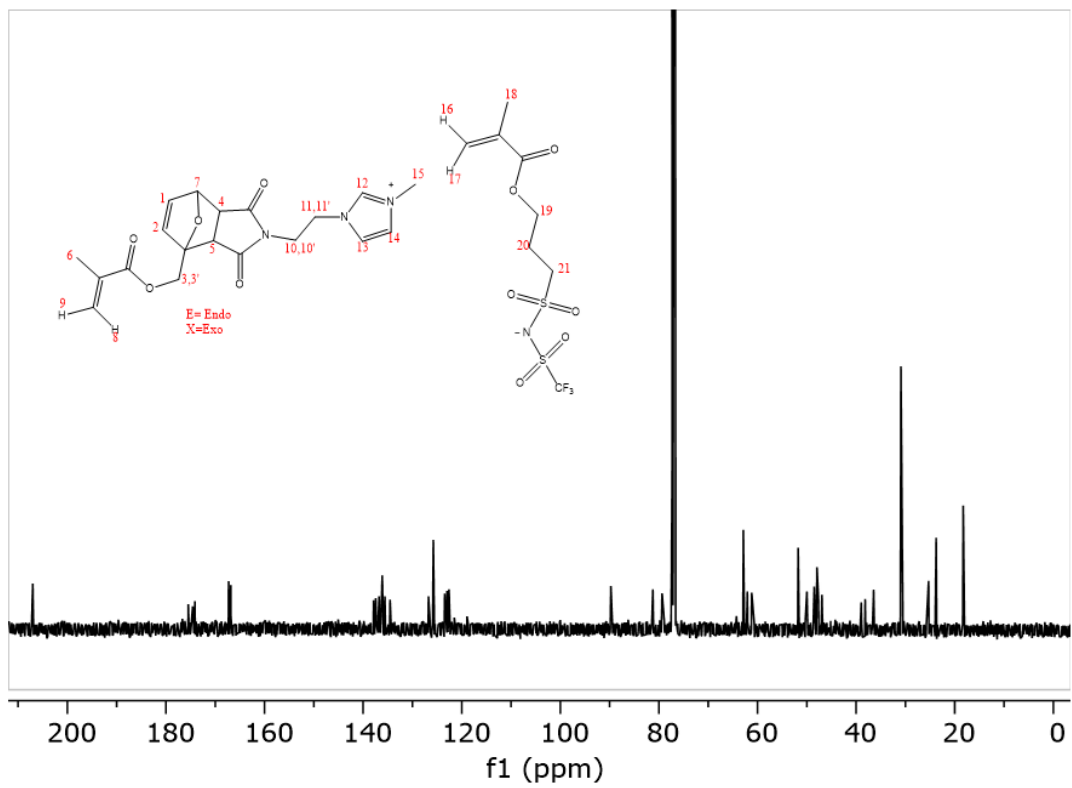


Figure 67 ^{13}C -NMR for synthetic intermediate 15 in Figure 14

Appendix B Supporting Data for Chapter 3

Appendix B.1 Conductivity of SPIL and DPIL samples

Individual plots of σ' for all three samples are shown in Figures 68-70. These plots contain the same data as Figure 30 in section 3.3.5 in Chapter 3, but are broken out to allow explicit labeling of the individual traces in each plot.

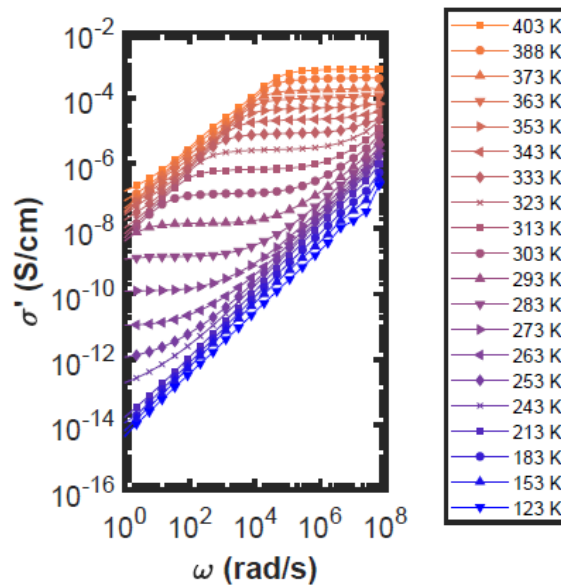


Figure 68 Real part of the conductivity (σ') for SPIL(+) as a function of angular frequency across the range of temperatures investigated in this work.

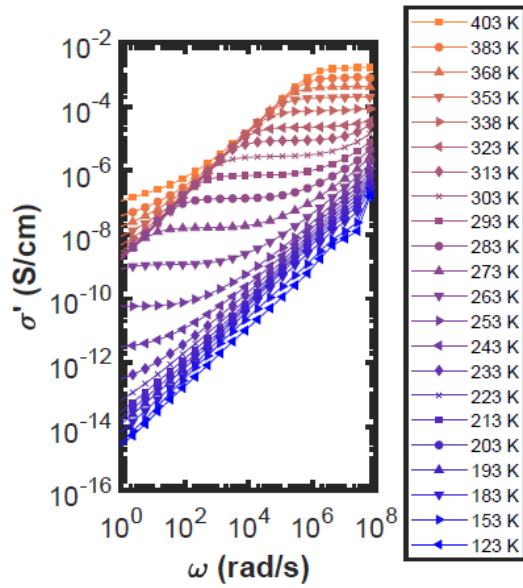


Figure 69 Real part of the conductivity (σ') for SPIL(-) as a function of angular frequency across the range of temperatures investigated in this work.

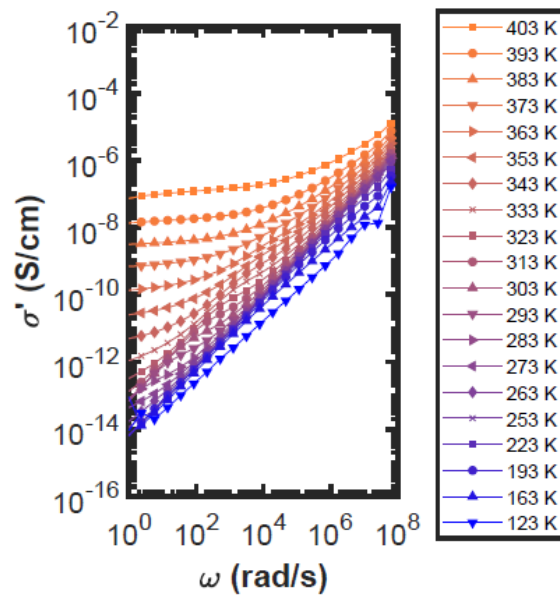


Figure 70 Real part of the conductivity (σ') for DPIL as a function of angular frequency across the range of temperatures investigated in this work.

Appendix B.2 Electrical Modulus of SPIL and DPIL samples

Individual plots of M'' for all three samples are shown in Figures 71-73. The frequency at which M'' was maximized in each trace was used to obtain the values of $\omega_{M''_{max}}$ plotted in Figure 32 in section 3.3.6 in Chapter 3.

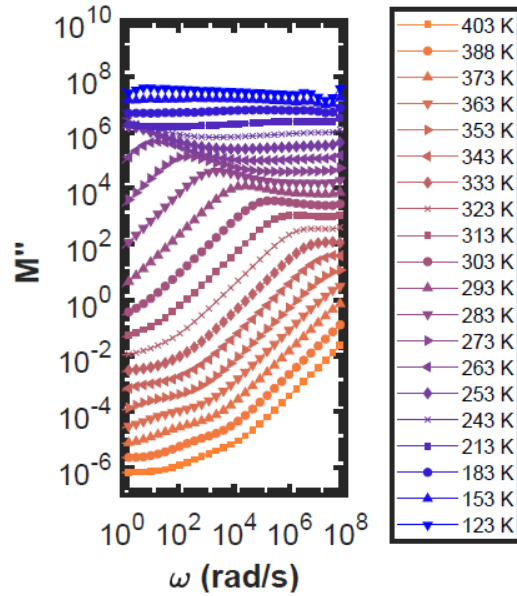


Figure 71 Imaginary part of the electrical modulus (M'') for SPIL(+) as a function of angular frequency across the range of temperatures investigated in this work. Each trace is offset by a factor of $(10)^{1/2}$ from the preceding trace to minimize overlap and make it easier to see the peaks in each plot.

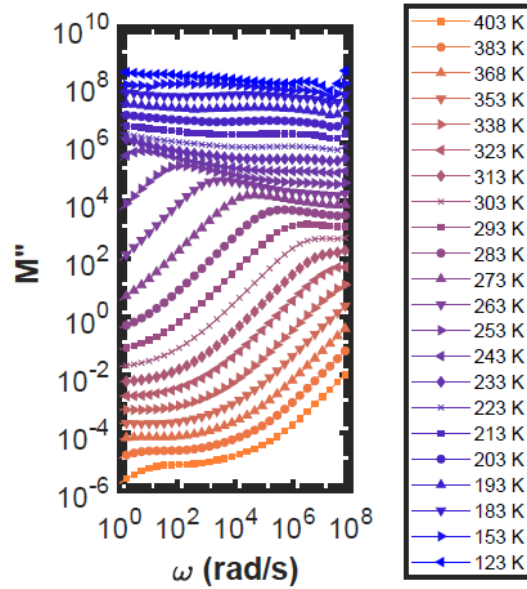


Figure 72 Imaginary part of the electrical modulus (M'') for SPIL(-) as a function of angular frequency across the range of temperatures investigated in this work. Each trace is offset by a factor of $(10)^{1/2}$ from the preceding trace to minimize overlap and make it easier to see the peaks in each plot.

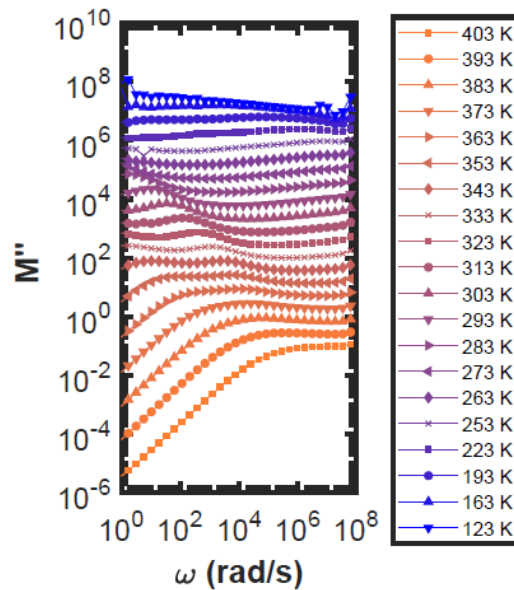


Figure 73 Imaginary part of the electrical modulus (M'') for DPIL as a function of angular frequency across the range of temperatures investigated in this work. Each trace is offset by a factor of $(10)^{1/2}$ from the preceding trace to minimize overlap and make it easier to see the peaks in each plot.

Appendix B.3 Permittivity of SPIL and DPIL samples

Individual plots of ϵ' and ϵ_{der} for all three samples are shown in Figures 74-76. These plots contain the same data as Figure 33 and 34 in section 3.3.7 and 3.3.8 in Chapter 3, but are broken out to allow explicit labeling of the individual traces in each plot.

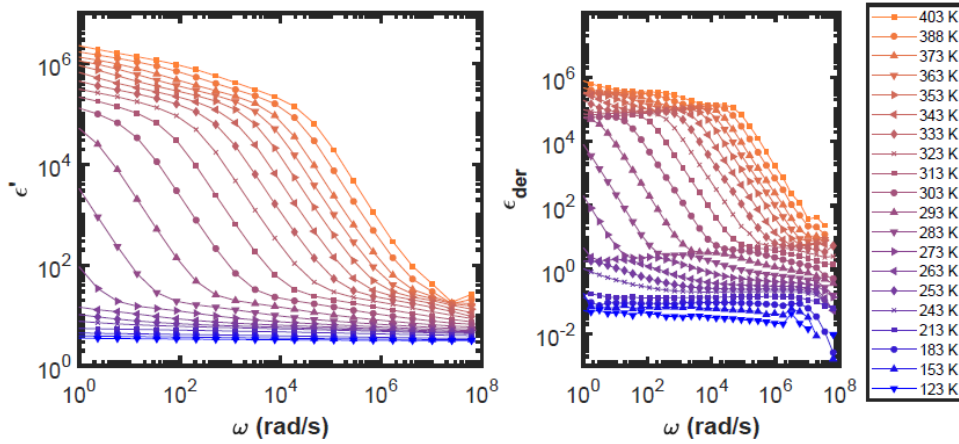


Figure 74 Real part of the permittivity (ϵ') and its derivative spectrum (ϵ_{der}) for SPIL(+) as a function of angular frequency across the range of temperatures investigated in this work.

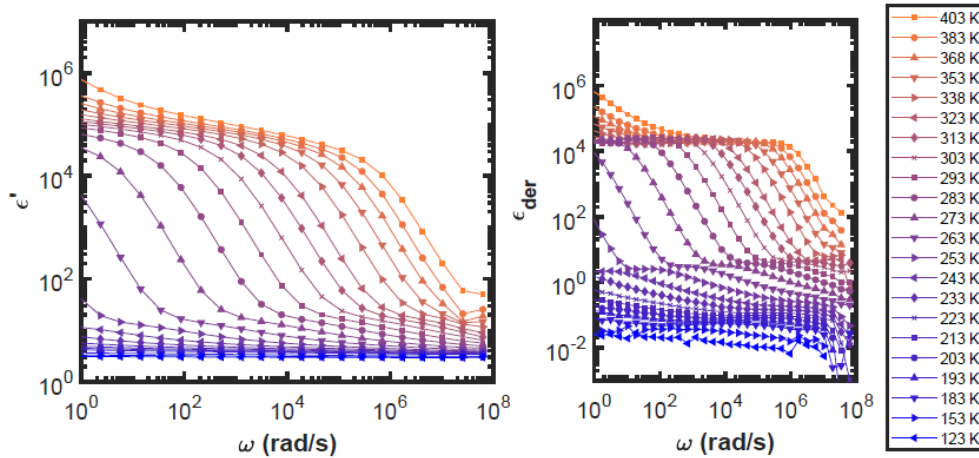


Figure 75 Real part of the permittivity (ϵ') and its derivative spectrum (ϵ_{der}) for SPIL(-) as a function of angular frequency across the range of temperatures investigated in this work.

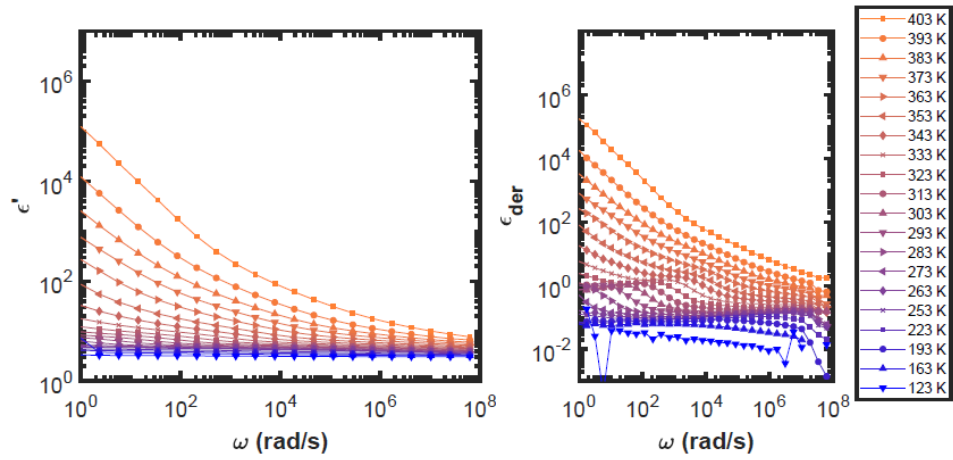


Figure 76 Real part of the permittivity (ϵ') and its derivative spectrum (ϵ'_{der}) for DPIL as a function of angular frequency across the range of temperatures investigated in this work.

Bibliography

- 1) R. A. Weiss, W. J. MacKnight, R. D. Lundberg, K. A. Mauritz, C. Thies, D. A. Brant, Structure and Applications of Ion-Containing Polymers in *ACS Symposium Series*, American Chemical Society, **1986**, 302, 2–19.
- 2) Bisri, S.Z.; Shimizu, S.; Nakano, M.; Iwasa, Y. Endeavor of Iontronics: From Fundamentals to Applications of Ion-Controlled Electronics. *Adv. Mater.* **2017**, 29, 1607054 -1607102.
- 3) Choi, U. H.; Mittal, A.; Price, T. L.; Gibson, H. W.; Runt, J.; Colby, R. H. Polymerized Ionic Liquids with Enhanced Static Dielectric Constants. *Macromolecules* **2013**, 46, 1175–1186.
- 4) Lee, M.; Choi, U. H.; Colby, R. H.; Gibson, H. W. Ion Conduction in Imidazolium Acrylate Ionic Liquids and their Polymers. *Chem. Mater.* **2010**, 22, 5814–5822.
- 5) Choi, U. H.; Lee, M.; Wang, S.; Liu, W.; Winey, K. I.; Gibson, H. W.; Colby, R. H. Ionic Conduction and Dielectric Response of Poly(imidazolium acrylate) Ionomers. *Macromolecules* **2012**, 45, 3974–3985.
- 6) Choi, U. H.; Ye, Y.; de la Cruz, D. S.; Liu, W.; Winey, K. I.; Elabd, Y. A.; Runt, J.; Colby, R. H. Dielectric and Viscoelastic Responses of Imidazolium-Based Ionomers with Different Counter- ions and Side Chain Lengths. *Macromolecules* **2014**, 47, 777–790.
- 7) Evans, C. M.; Bridges, C. R.; Sanoja, G. E.; Bartels, J.; Segalman, R. A. Role of Tethered Ion Placement on Polymerized Ionic Liquid Structure and Conductivity: Pendant versus Backbone Charge Placement. *ACS Macro Lett.* **2016**, 5, 925–930.
- 8) Yoshizawa, M.; Ogihara, W.; Ohno, H. Novel polymer electrolytes prepared by copolymerization of ionic liquid monomers. *Polym. Adv. Technol.* **2002**, 13, 589–594.
- 9) Shaplov, A. S.; Vlasov, P. S.; Lozinskaya, E. I.; Ponkratov, D. O.; Malyshkina, I. A.; Vidal, F.; Okatova, O. V.; Pavlov, G. M.; Wandrey, C.; Bhide, A.; Schönhoff, M.; Vygodskii, Y. S. Polymeric Ionic Liquids: Comparison of Polycations and Polyanions. *Macromolecules* **2011**, 44, 9792–9803.
- 10) Gu, H.; Yan, F.; Texter, J. Polymerized Paired Ions as Polymeric Ionic Liquid-Proton Conductivity. *Macromol. Rapid Commun.* **2016**, 37, 1218–1225.
- 11) Fouillet, C. C. J.; Greaves, T. L.; Quinn, J. F.; Davis, T. P.; Adamcik, J.; Sani, M.-A.; Separovic, F.; Drummond, C. J.; Mezzenga, R. Copolyampholytes Produced from RAFT Polymerization of Protic Ionic Liquids. *Macromolecules* **2017**, 50, 8965–8978.

- 12) Arora, S.; Liang, J.; Fullerton-Shirey, S. K.; Laaser, J. E. Triggerable Ion Release in Polymerized Ionic Liquids Containing Thermally Labile Diels–Alder Linkages. *ACS Mater. Lett.* **2020**, 2, 331–335.
- 13) Liang, J.; Xu, K.; Arora, S.; Laaser, J. E.; Fullerton-Shirey, S. K. Ion-Locking in Solid Polymer Electrolytes for Reconfigurable Gateless Lateral Graphene p-n Junctions. *Materials* **2020**, 13, No. 1089.
- 14) Frontier Economics estimating the global economic and social impacts of counterfeiting and piracy. **2011**;
http://www.inta.org/communications/documents/2017_frontier_report.pdf.
- 15) Hallett, J. P.; Welton, T. Room-Temperature Ionic Liquids: Solvents for Synthesis and Catalysis. *Chemical Reviews* **2011**, 111, 3508–3576.
- 16) Brooke, R.; Fabretto, M.; Krasowska, M.; Talemi, P.; Pering, S.; Murphy, P. J.; Evans, D. Organic energy devices from ionic liquids and conducting polymers. *Journal of Materials Chemistry C* **2016**, 4, 1550–1556.
- 17) Moon, H. C.; Kim, C.-H.; Lodge, T. P.; Frisbie, C. D. Multicolored, Low-Power, Flexible Electrochromic Devices Based on Ion Gels. *ACS Applied Materials & Interfaces* **2016**, 8, 6252–6260.
- 18) Watanabe, M.; Thomas, M. L.; Zhang, S.; Ueno, K.; Yasuda, T.; Dokko, K. Application of Ionic Liquids to Energy Storage and Conversion Materials and Devices. *Chemical Reviews* **2017**, 117, 7190–7239.
- 19) Seo, D. G.; Moon, H. C. Mechanically Robust, Highly Ionic Conductive Gels Based on Random Copolymers for Bending Durable Electrochemical Devices. *Advanced Functional Materials* **2018**, 28, 1706948.
- 20) Misra, R.; McCarthy, M.; Hebard, A. F. Electric field gating with ionic liquids. *Applied Physics Letters* **2007**, 90, 052905.
- 21) Fujimoto, T.; Awaga, K. Electric-double-layer field-effect transistors with ionic liquids. *Physical Chemistry Chemical Physics* **2013**, 15, 8983.
- 22) Hoarfrost, M. L.; Segalman, R. A. Ionic Conductivity of Nanostructured Block Copolymer/Ionic Liquid Membranes. *Macromolecules* **2011**, 44, 5281–5288.
- 23) Mogurampelly, S.; Borodin, O.; Ganesan, V. Computer Simulations of Ion Transport in Polymer Electrolyte Membranes. *Annual Review of Chemical and Biomolecular Engineering* **2016**, 7, 349–371.
- 24) Yuan, J.; Mecerreyes, D.; Antonietti, M. Poly(ionic liquid)s: An update. *Prog. Polym. Sci.* **2013**, 38, 1009–1036.

- 25) Shaplov, A. S.; Ponkratov, D. O.; Vygodskii, Y. S. Poly(ionic liquid)s: Synthesis, properties, and application. *Polym. Sci., Ser. B* **2016**, *58*, 73–142.
- 26) Qian, W.; Texter, J.; Yan, F. Frontiers in poly(ionic liquid)s: syntheses and applications. *Chem. Soc. Rev.* **2017**, *46*, 1124–1159.
- 27) O’Mahony, A. M.; Silvester, D. S.; Aldous, L.; Hardacre, C.; Compton, R. G. Effect of Water on the Electrochemical Window and Potential Limits of Room-Temperature Ionic Liquids. *Journal of Chemical & Engineering Data* **2008**, *53*, 2884–2891.
- 28) Yan, B.; Yang, P.; Zhao, Y.; Zhang, J.; An, M. Electrocodeposition of lithium and copper from room temperature ionic liquid 1-ethyl-3-methylimidazolium bis(trifluoromethylsulfonyl)imide. *RSC Advances* **2012**, *2*, 12926.
- 29) Nakajima, H.; Ohno, H. Preparation of thermally stable polymer electrolytes from imidazolium-type ionic liquid derivatives. *Polymer* **2005**, *46*, 11499–11504.
- 30) Ogihara, W.; Washiro, S.; Nakajima, H.; Ohno, H. Effect of cation structure on the electrochemical and thermal properties of ion conductive polymers obtained from polymerizable ionic liquids. *Electrochimica Acta* **2006**, *51*, 2614–2619.
- 31) Green, M. D.; Long, T. E. Designing Imidazole-Based Ionic Liquids and Ionic Liquid Monomers for Emerging Technologies. *Polymer Reviews* **2009**, *49*, 291–314.
- 32) Shaplov, A. S.; Lozinskaya, E. I.; Ponkratov, D. O.; Malyskina, I. A.; Vidal, F.; Aubert, P.-H.; Okatova, O. V.; Pavlov, G. M.; Komarova, L. I.; Wandrey, C.; Vygodskii, Y. S. Bis(trifluoromethylsulfonyl)amide based “polymeric ionic liquids”: Synthesis, purification and peculiarities of structure–properties relationships. *Electrochimica Acta* **2011**, *57*, 74–90.
- 33) Broadband Dielectric Spectroscopy, Kremer, F., Schönhals, A., Eds.; *Springer Berlin Heidelberg*, **2003**.
- 34) a) Z. Xue, D. He, X. Xie, J. Mater. Chem. A **2015**, *3*(38), 19218–19253; b) H. Xu, S. Fathipour, E. W. Kinder, A. C. Seabaugh, S. K. Fullerton-Shirey, ACS Nano **2015**, *9*(5), 4900–4910; c) G. Jo, H. Jeon, M. J. Park, *ACS Macro Lett.* **2015**, *4*(2), 225–230.
- 35) Kong, H.; Dawidczyk, T. J.; Ozgun, R.; Andreou, A. G.; Katz, H. E. In Autonomous Sensor Networks: Collective Sensing Strategies for Analytical Purposes; Filippini, D., Ed.; *Springer Berlin Heidelberg: Berlin, Heidelberg*, **2013**; pp 191–216.
- 36) Lochner, C. M.; Khan, Y.; Pierre, A.; Arias, A. C. All-organic optoelectronic sensor for pulse oximetry. *Nature Communications* **2014**, *5*, 1-7.
- 37) Mazzio, K. A.; Luscombe, C. K. The future of organic photovoltaics. *Chemical Society Reviews* **2015**, *44*, 78–90.

- 38) Muench, S.; Wild, A.; Friebe, C.; Haupler, B.; Janoschka, T.; Schubert, U. S. Polymer-Based Organic Batteries. *Chemical Reviews* **2016**, 116, 9438–9484.
- 39) Luo, G.; Ren, X.; Zhang, S.; Wu, H.; Choy, W. C. H.; He, Z.; Cao, Y. Recent Advances in Organic Photovoltaics: Device Structure and Optical Engineering Optimization on the Nanoscale. *Small* **2016**, 12, 1547–1571.
- 40) Moeller, S.; Perlov, C.; Jackson, W.; Taussig, C.; Forrest, S. R. A polymer/semiconductor write-once read-many-times memory. *Nature* **2003**, 426, 166–169
- 41) Lai, Y.-C.; Huang, Y.-C.; Lin, T.-Y.; Wang, Y.-X.; Chang, C.-Y.; Li, Y.; Lin, T.-Y.; Ye, B.-W.; Hsieh, Y.-P.; Su, W.-F.; Yang, Y.-J.; Chen, Y.-F. Stretchable organic memory: toward learn-able and digitized stretchable electronic applications. *NPG Asia Materials* **2014**, 6, e87, 1-7.
- 42) Zhang, B.; Chen, Y.; Neoh, K.-G.; Kang, E.-T. *Polymer Chemistry Series; Royal Society of Chemistry*, **2016**; pp 1–53.
- 43) Zhou, L.; Mao, J.; Ren, Y.; Han, S.-T.; Roy, V. A. L.; Zhou, Y. Recent Advances of Flexible Data Storage Devices Based on Organic Nanoscaled Materials. *Small* **2018**, 14, 1703126.
- 44) Hwang, S.-W. et al. A Physically Transient Form of Silicon Electronics. *Science* **2012**, 337, 1640–1644.
- 45) Fu, K. K.; Wang, Z.; Dai, J.; Carter, M.; Hu, L. Transient Electronics: Materials and Devices. *Chemistry of Materials* **2016**, 28, 3527–3539.
- 46) Gao, Y.; Zhang, Y.; Wang, X.; Sim, K.; Liu, J.; Chen, J.; Feng, X.; Xu, H.; Yu, C. Moisture-triggered physically transient electronics. *Science Advances* **2017**, 3, e1701222.
- 47) Li, R.; Wang, L.; Kong, D.; Yin, L. Recent progress on biodegradable materials and transient electronics. *Bioactive Materials* **2018**, 3, 322–333.
- 48) Hernandez, H. L.; Kang, S.-K.; Lee, O. P.; Hwang, S.-W.; Kaitz, J. A.; Inci, B.; Park, C. W.; Chung, S.; Sottos, N. R.; Moore, J. S.; Rogers, J. A.; White, S. R. Triggered Transience of Metastable Poly(phthalaldehyde) for Transient Electronics. *Advanced Materials* **2014**, 26, 7637–7642.
- 49) Park, C. W.; Kang, S.-K.; Hernandez, H. L.; Kaitz, J. A.; Wie, D. S.; Shin, J.; Lee, O. P.; Sottos, N. R.; Moore, J. S.; Rogers, J. A.; White, S. R. Thermally Triggered Degradation of Transient Electronic Devices. *Advanced Materials* **2015**, 27, 3783–3788.
- 50) Kim, B. H. et al. Dry Transient Electronic Systems by Use of Materials that Sublime. *Advanced Functional Materials* **2017**, 27, 1606008.

- 51) Zhang, Y. J.; Ye, J. T.; Yomogida, Y.; Takenobu, T.; Iwasa, Y. Formation of a Stable p-n Junction in a Liquid-Gated MoS₂ Ambipolar Transistor. *Nano Letters* **2013**, 13, 3023–3028.
- 52) Xu, H.; Fathipour, S.; Kinder, E. W.; Seabaugh, A. C.; Fullerton-Shirey, S. K. Reconfigurable Ion Gating of 2H-MoS₂ Field-Effect Transistors Using Poly(ethylene oxide)-CsClO₄ Solid Polymer Electrolyte. *ACS Nano* **2015**, 9, 4900–4910.
- 53) Li, H.-M.; Xu, K.; Bourdon, B.; Lu, H.; Lin, Y.-C.; Robinson, J. A.; Seabaugh, A. C.; Fullerton-Shirey, S. K. Electric Double Layer Dynamics in Poly(ethylene oxide) LiClO₄ on Graphene Transistors. *The Journal of Physical Chemistry C* **2017**, 121, 16996–17004.
- 54) Rosenblatt, S.; Yaish, Y.; Park, J.; Gore, J.; Sazonova, V.; McEuen, P. L. High Performance Electrolyte Gated Carbon Nanotube Transistors. *Nano Letters* **2002**, 2, 869–872.
- 55) Lu, C.; Fu, Q.; Huang, S.; Liu, J. Polymer Electrolyte-Gated Carbon Nanotube Field-Effect Transistor. *Nano Letters* **2004**, 4, 623–627.
- 56) Efetov, D. K.; Kim, P. Controlling Electron-Phonon Interactions in Graphene at Ultrahigh Carrier Densities. *Physical Review Letters* **2010**, 105, 256805-256810.
- 57) Lin, M.-W.; Liu, L.; Lan, Q.; Tan, X.; Dhindsa, K. S.; Zeng, P.; Naik, V. M.; Cheng, M. M.-C.; Zhou, Z. Mobility enhancement and highly efficient gating of monolayer MoS₂ transistors with polymer electrolyte. *Journal of Physics D: Applied Physics* **2012**, 45, 345102.
- 58) Allain, A.; Kis, A. Electron and Hole Mobilities in Single-Layer WSe₂. *ACS Nano* **2014**, 8, 7180–7185.
- 59) Kinder, E. W.; Fuller, A.; Lin, Y.-C.; Robinson, J. A.; Fullerton-Shirey, S. K. Increasing the Room-Temperature Electric Double Layer Retention Time in Two-Dimensional Crystal FETs. *ACS Applied Materials & Interfaces* **2017**, 9, 25006–25013.
- 60) Lundberg, R. D.; Bailey, F. E.; Callard, R. W. Interactions of inorganic salts with poly(ethylene oxide). *Journal of Polymer Science Part A-1: Polymer Chemistry* **1966**, 4, 1563–1577.
- 61) Ohno, H.; Wang, P. Solubility of Inorganic Salts in Poly(ethylene oxide) and Effects of Poly(ethylene oxide) Molecular Weight and Salt Species on the Ionic Conductivity. *NIPPON KAGAKU KAISHI* **1991**, 1588–1593.
- 62) Xue, Z.; Qin, L.; Jiang, J.; Mu, T.; Gao, G. Thermal, Electrochemical and Radiolytic Stabilities of Ionic Liquids. *Phys. Chem. Chem. Phys.* **2018**, 20 (13), 8382–8402.
- 63) Shaplov, A. S.; Vlasov, P. S.; Armand, M.; Lozinskaya, E. I.; Ponkratov, D. O.; Malysheva, I. A.; Vidal, F.; Okatova, O. V.; Pavlov, G. M.; Wandrey, C.; et al. Design

- and Synthesis of New Anionic “Polymeric Ionic Liquids” with High Charge Delocalization. *Polym. Chem.* **2011**, 2 (11), 2609.
- 64) Jacob, C.; Matsumoto, A.; Brennan, M.; Liu, H.; Paddison, S. J.; Urakawa, O.; Inoue, T.; Sangoro, J.; Runt, J. Polymerized Ionic Liquids: Correlation of Ionic Conductivity with Nanoscale Morphology and Counterion Volume. *ACS Macro Lett.* **2017**, 6 (9), 941–946.
 - 65) Wang, A.; Xu, H.; Liu, X.; Gao, R.; Wang, S.; Zhou, Q.; Chen, J.; Liu, X.; Zhang, L. The Synthesis of a Hyperbranched Star Polymeric Ionic Liquid and Its Application in a Polymer Electrolyte. *Polym. Chem.* **2017**, 8 (20), 3177–3185.
 - 66) Ohno, H.; Yoshizawa, M.; Ogihara, W. Development of New Class of Ion Conductive Polymers Based on Ionic Liquids. *Electrochimica Acta* **2004**, 50 (2–3), 255–261.
 - 67) Yoshizawa, M.; Ohno, H. Synthesis of Molten Salt-Type Polymer Brush and Effect of Brush Structure on the Ionic Conductivity. *Electrochimica Acta* **2001**, 46 (10–11), 1723–1728.
 - 68) Froidevaux, V.; Borne, M.; Laborbe, E.; Auvergne, R.; wata, A.; Boutevin, B. Study of the Diels–Alder and Retro-Diels–Alder Reaction between Furan Derivatives and Maleimide for the Creation of New Materials. *RSC Adv.* **2015**, 5 (47), 37742–37754.
 - 69) Fan, M.; Liu, J.; Li, X.; Zhang, J.; Cheng, J. Recyclable Diels–Alder Furan/Maleimide Polymer Networks with Shape Memory Effect. *Ind. Eng. Chem. Res.* **2014**, 53 (42), 16156–16163.
 - 70) Liu, Y.-L.; Chuo, T.-W. Self-Healing Polymers Based on Thermally Reversible Diels–Alder Chemistry. *Polym. Chem.* **2013**, 4 (7), 2194.
 - 71) Padhan, A. K.; Mandal, D. Thermo-Reversible Self-Healing in a Fluorous Crosslinked Copolymer. *Polym. Chem.* **2018**, 9 (23), 3248–3261.
 - 72) M. Mihailov, H. Boudevska, A. A. Berlin, *Dokl. Bolg. Akad. Nauk* **1966**, 19, 909–912.
 - 73) A. S. Shaplov, E. I. Lozinskaya, D. O. Ponkratov, I. A. Malyshkina, F. Vidal, P.-H. Aubert, O. V. Okatova, G. M. Pavlov, L. I. Komarova, C. Wandrey, Y. S. Vygodskii *Electrochim. Acta* **2011**, 57, 74–90.
 - 74) K. P. ohako Esko, T. Taaber, K. Saal, R. L. ohmus, I. Kink, U. Mäeorg, *Synth. Commun.* **2013**, 43(21), 2846–2852.
 - 75) H. Kokubo, R. Sano, K. Murai, S. Ishii, M. Watanabe, *Eur. Polym. J.* **2018**, 106, 266–272.
 - 76) V. Mucci, C. Vallo, *J. Appl. Polym. Sci.* **2011**, 123(1), 418–425.
 - 77) K. Matsumoto, B. Talukdar, T. Endo. Methacrylate-based ionic liquid: Radical polymerization/copolymerization with methyl methacrylate and evaluation of molecular weight of the obtained homopolymers. *Polymer Bulletin* **2010**, 66, 199–210.

- 78) A. S. Shaplov, D. O. Ponkratov, P. S. Vlasov, E. I. Lozinskaya, L. I. Komarova, I. A. Malyshkina, F. Vidal, G. T. M. Nguyen, M. Armand, C. Wandrey, Y. S. Vygodskii, *Polym. Sci. Ser. B* **2013**, 55(3-4), 122–138.
- 79) N. DeVos, C. Maton, C. V. Stevens, *ChemElectroChem* **2014**, 1(8), 1258–1270.
- 80) C. Villagran, C. E. Banks, C. Hardacre, R. G. Compton, *Anal. Chem.* **2004**, 76(7), 1998–2003.
- 81) S. R. Waldvogel, B. Janza, *Angew. Chem. Int. Ed.* **2014**, 53(28), 7122–7123.
- 82) Gandini, A.; Silvestre, A. J. D.; Coelho, D. Reversible Click Chemistry at the Service of Macromolecular Materials. 2. Thermoreversible Polymers Based on the Diels-Alder Reaction of an A-B Furan/Maleimide Monomer. *J. Polym. Sci. A Polym. Chem.* **2010**, 48 (9), 2053–2056.
- 83) Watanabe, M.; Yoshie, N. Synthesis and Properties of Readily Recyclable Polymers from Bisfuranic Terminated Poly(Ethylene Adipate) and Multi-Maleimide Linkers. *Polymer* **2006**, 47 (14), 4946–4952.
- 84) Ye, Y.; Elabd, Y. A. Anion Exchanged Polymerized Ionic Liquids: High Free Volume Single Ion Conductors. *Polymer* **2011**, 52 (5), 1309–1317.
- 85) Handy, S. T.; Grieco, P. A.; Mineur, C.; Ghosez, L. *Synlett* **1995**, 1995, 565-567.
- 86) Dispinar, T.; Sanyal, R.; Sanyal, A. A Diels-Alder/Retro Diels-Alder Strategy to Synthesize Polymers Bearing Maleimide Side Chains. *J. Polym. Sci. A Polym. Chem.* **2007**, 45 (20), 4545–4551.
- 87) Jegat, C.; Mignard, N. Effect of the Polymer Matrix on the Thermal Behaviour of a Furan-Maleimide Type Adduct in the Molten State. *Polym. Bull.* **2008**, 60 (6), 799–808.
- 88) Gousse, C.; Gandini, A. Diels-Alder Polymerization of Difurans with Bismaleimides. *Polymer International* **1999**, 48, 723-731.
- 89) Kadoma, Y.; Fujisawa, S. Kinetic Evaluation of Reactivity of Bisphenol A Derivatives as Radical Scavengers for Methacrylate Polymerization. *Biomaterials* **2000**, 21 (21), 2125–2130.
- 90) Boutelle, R. C.; Northrop, B. H. Substituent Effects on the Reversibility of Furan–Maleimide Cycloadditions. *J. Org. Chem.* **2011**, 76 (19), 7994–8002.
- 91) Uygun, M.; Tasdelen, M.H.; Yagci, Y. Influence of Type of Initiation on Thiol-Ene “Click” Chemistry. *Macromol. Chem.Phys.* **2010**, 211, 103-110.
- 92) Canadell, J.; Fischer, H.; De With, G.; van Benthem, R. A. T. M. Stereoisomeric Effects in Thermo-Remendable Polymer Networks Based on Diels-Alder Crosslink Reactions. *J. Polym. Sci. A Polym. Chem.* **2010**, 48 (15), 3456–3467.

- 93) Chen, M.; Zhong, M.; Johnson, J. A. Light-Controlled Radical Polymerization: Mechanisms, Methods, and Applications. *Chem. Rev.* **2016**, 116 (17), 10167–10211.
- 94) Mucci, V.; Vallo, C. Efficiency of 2,2-Dimethoxy-2-Phenylacetophenone for the Photopolymerization of Methacrylate Monomers in Thick Sections. *J. Appl. Polym. Sci.* **2012**, 123 (1), 418–425.
- 95) Li, Q.; Jiang, J.; Li, G.; Zhao, W.; Zhao, X.; Mu, T. The Electrochemical Stability of Ionic Liquids and Deep Eutectic Solvents. *Sci. China Chem.* **2016**, 59 (5), 571–577.
- 96) Elgrishi, N.; Rountree, K. J.; McCarthy, B. D.; Rountree, E. S.; Eisenhart, T. T.; Dempsey, J. L. A Practical Beginner's Guide to Cyclic Voltammetry. *J. Chem. Educ.* **2018**, 95 (2), 197–206.
- 97) Tian, Y.-H.; Goff, G. S.; Runde, W. H.; Batista, E. R. Exploring Electrochemical Windows of Room-Temperature Ionic Liquids: A Computational Study. *J. Phys. Chem. B* **2012**, 116 (39), 11943–11952.
- 98) Noack, K.; Schulz, P. S.; Paape, N.; Kiefer, J.; Wasserscheid, P.; Leipertz, A. The Role of the C2 Position in Interionic Interactions of Imidazolium Based Ionic Liquids: A Vibrational and NMR Spectroscopic Study. *Phys. Chem. Chem. Phys.* **2010**, 12, 14153–14161.
- 99) De Vos, N.; Maton, C.; Stevens, C. V. Electrochemical Stability of Ionic Liquids: General Influences and Degradation Mechanisms. *ChemElectroChem* **2014**, 1, 1258–1270.
- 100) Murugesan, S.; Quintero, O. A.; Chou, B. P.; Xiao, P.; Park, K.; Hall, J. W.; Jones, R. A.; Henkelman, G.; Goodenough, J. B.; Stevenson, K. J. Wide Electrochemical Window Ionic Salt for Use in Electropositive Metal Electrodeposition and Solid-State Li-Ion Batteries. *J. Mater. Chem. A* **2014**, 2, 2194–2201.
- 101) Cao, Y.; Chen, Y.; Sun, X.; Zhang, Z.; Mu, T. Water Sorption in Ionic Liquids: Kinetics, Mechanisms and Hydrophilicity. *Phys. Chem. Chem. Phys.* **2012**, 14 (35), 12252.
- 102) Hwang, H. J.; Chi, W. S.; Kwon, O.; Lee, J. G.; Kim, J. H.; Shul, Y.-G. Selective Ion Transporting Polymerized Ionic Liquid Membrane Separator for Enhancing Cycle Stability and Durability in Secondary Zinc–Air Battery Systems. *ACS Appl. Mater. Interfaces* **2016**, 8, 26298–26308.
- 103) Nykaza, J. R.; Savage, A. M.; Pan, Q.; Wang, S.; Beyer, F. L.; Tang, M. H.; Li, C. Y.; Elabd, Y. A. Polymerized ionic liquid diblock copolymer as solid-state electrolyte and separator in lithium-ion battery. *Polymer* **2016**, 101, 311–318.
- 104) Ohno, H.; Ito, K. Room-Temperature Molten Salt Polymers as a Matrix for Fast Ion Conduction. *Chem. Lett.* **1998**, 27, 751–752.

- 105) Washiro, S.; Yoshizawa, M.; Nakajima, H.; Ohno, H. Highly ion conductive flexible films composed of network polymers based on polymerizable ionic liquids. *Polymer* **2004**, *45*, 1577–1582.
- 106) Peters, E. C.; Lee, E. J. H.; Burghard, M.; Kern, K. Gate dependent photocurrents at a graphene p–n junction. *Appl. Phys. Lett.* **2010**, *97*, No. 193102.
- 107) Frisenda, R.; Molina-Mendoza, A. J.; Mueller, T.; Castellanos-Gomez, A.; Van Der Zant, H. S. J. Atomically Thin P-n Junctions Based on Two-Dimensional Materials. *Chem. Soc. Rev.* **2018**, *47* (9), 3339–3358.
- 108) Wang, G.; Zhang, M.; Chen, D.; Guo, Q.; Feng, X.; Niu, T.; Liu, X.; Li, A.; Lai, J.; Sun, D.; et al. Seamless Lateral Graphene p–n Junctions Formed by Selective in Situ Doping for High-Performance Photodetectors. *Nat. Commun.* **2018**, *9* (1), 1–9.
- 109) Nakamura, K.; Saiwaki, T.; Fukao, K. Dielectric Relaxation Behaviour of Polymerized Ionic Liquid. *Macromolecules* **2010**, *43*, 6092–6098.
- 110) Sangoro, J. R.; Iacob, C.; Agapov, A. L.; Wang, Y.; Berdzinski, S.; Rexhausen, H.; Strehmel, V.; Friedrich, C.; Sokolov, A. P.; Kremer, F. Decoupling of ionic conductivity from structural dynamics in polymerized ionic liquids. *Soft Matter* **2014**, *10*, 3536–3540.
- 111) Rivera, A.; Brodin, A.; Pugachev, A.; Rössler, E. A. Orientational and translational dynamics in room temperature ionic liquids. *J. Chem. Phys.* **2007**, *126*, No. 114503.
- 112) Fan, F.; Wang, Y.; Hong, T.; Heres, M. F.; Saito, T.; Sokolov, A. P. Ion Conduction in Polymerized Ionic Liquids with Different Pendant Groups. *Macromolecules* **2015**, *48*, 4461–4470.
- 113) Frenzel, F.; Folikumah, M. Y.; Schulz, M.; Anton, A. M.; Binder, W. H.; Kremer, F. Molecular Dynamics and Charge Transport in Polymeric Polyisobutylene-Based Ionic Liquids. *Macromolecules* **2016**, *49*, 2868–2875.
- 114) Cosby, T.; Vicars, Z.; Wang, Y.; Sangoro, J. Dynamic- Mechanical and Dielectric Evidence of Long-Lived Mesoscale Organization in Ionic Liquids. *J. Phys. Chem. Lett.* **2017**, *8*, 3544–3548.
- 115) Frenzel, F.; Borchert, P.; Anton, A. M.; Strehmel, V.; Kremer, F. Charge transport and glassy dynamics in polymeric ionic liquids as reflected by their inter- and intramolecular interactions. *Soft Matter* **2019**, *15*, 1605–1618.
- 116) Sangoro, J. R.; Serghei, A.; Naumov, S.; Galvosas, P.; Kärger, J.; Wespe, C.; Bordusa, F.; Kremer, F. Charge transport and mass transport in imidazolium-based ionic liquids. *Phys. Rev. E* **2008**, *77*, No. 051202.
- 117) Iacob, C.; Sangoro, J. R.; Serghei, A.; Naumov, S.; Korth, Y.; Kärger, J.; Friedrich, C.; Kremer, F. Charge transport and glassy dynamics in imidazole-based liquids. *J. Chem. Phys.* **2008**, *129*, No. 234511.

- 118) Sangoro, J.; Iacob, C.; Serghei, A.; Naumov, S.; Galvosas, P.; Kärger, J.; Wespe, C.; Bordusa, F.; Stoppa, A.; Hunger, J.; Buchner, R.; Kremer, F. Electrical conductivity and translational diffusion in the 1-butyl-3-methylimidazolium tetrafluoroborate ionic liquid. *J. Chem. Phys.* **2008**, 128, No. 214509.
- 119) Pöhako-Esko, K.; Taaber, T.; Saal, K.; Lõhmus, R.; Kink, I.; Mäeorg, U. New Method for Synthesis of Methacrylate-Type Polymerizable Ionic Liquids. *Synth. Commun.* **2013**, 43, 2846–2852.
- 120) Kammakakam, I.; Bara, J. E.; Jackson, E. M.; Lertxundi, J.; Mecerreyes, D.; Tomé, L. C. Tailored CO₂-Philic Anionic Poly(ionic liquid) Composite Membranes: Synthesis, Characterization, and Gas Transport Properties. *ACS Sustainable Chem. Eng.* **2020**, 8, 5954–5965.
- 121) Gordon, J. M.; Rouse, G. B.; Gibbs, J. H.; Risen, W. M. The composition dependence of glass transition properties. *J. Chem. Phys.* **1977**, 66, 4971–4976.
- 122) Loshaek, S. Crosslinked polymers. II. Glass temperatures of copolymers of methyl methacrylate and glycol dimethacrylates. *J. Polym. Sci.* **1955**, 15, 391–404.
- 123) Stutz, H.; Illers, K.-H.; Mertes, J. A generalized theory for the glass transition temperature of crosslinked and uncrosslinked polymers. *J. Polym. Sci., Part B: Polym. Phys.* **1990**, 28, 1483–1498.
- 124) Klein, R. J.; Zhang, S.; Dou, S.; Jones, B. H.; Colby, R. H.; Runt, J. Modeling electrode polarization in dielectric spectroscopy: Ion mobility and mobile ion concentration of single-ion polymer electrolytes. *J. Chem. Phys.* **2006**, 124, No. 144903.
- 125) Serghei, A.; Tress, M.; Sangoro, J. R.; Kremer, F. Electrode polarization and charge transport at solid interfaces. *Phys. Rev. B: Condens. Matter Mater. Phys.* **2009**, 80, No. 184301.
- 126) Jain, H. Composition dependence of frequency power law of ionic conductivity of glasses. *Solid State Ionics* **1998**, 105, 129–137.
- 127) Watanabe, M.; Sanui, K.; Ogata, N.; Kobayashi, T.; Ohtaki, Z. Ionic conductivity and mobility in network polymers from poly-(propylene oxide) containing lithium perchlorate. *J. Appl. Phys.* **1985**, 57, 123–128.
- 128) Böhmer, R.; Ngai, K. L.; Angell, C. A.; Plazek, D. J. Nonexponential relaxations in strong and fragile glass formers. *J. Chem. Phys.* **1993**, 99, 4201–4209.
- 129) Angell, C.; Borick, S. Specific heats C_p , C_v , C_{conf} and energy landscapes of glass forming liquids. *J. Non-Cryst. Solids* **2002**, 307, 393–406.
- 130) Fragiadakis, D.; Dou, S.; Colby, R. H.; Runt, J. Molecular mobility and Li⁺ conduction in polyester copolymer ionomers based on poly(ethylene oxide). *J. Chem. Phys.* **2009**, 130, 064907-064913.

- 131) Daguinet, C.; Dyson, P. J.; Krossing, I.; Oleinikova, A.; Slattery, J.; Wakai, C.; Weingärtner, H. Dielectric Response of Imidazolium- Based Room-Temperature Ionic Liquids. *J. Phys. Chem. B* **2006**, 110, 12682–12688.
- 132) Slattery, J. M.; Daguinet, C.; Dyson, P. J.; Schubert, T. J. S.; Krossing, I. How to Predict the Physical Properties of Ionic Liquids: A Volume-Based Approach. *Angew. Chem., Int. Ed.* **2007**, 46, 5384–5388.
- 133) Wang, J.-H. H.; Yang, C. H.-C.; Masser, H.; Shiau, H.-S.; O'Reilly, M. V.; Winey, K. I.; Runt, J.; Painter, P. C.; Colby, R. H. Ion States and Transport in Styrenesulfonate Methacrylic PEO₉ Random Copolymer Ionomers. *Macromolecules* **2015**, 48, 7273–7285.
- 134) Hiemenz, P. C.; Lodge, T. P. *Polymer Chemistry*; CRC Press, **2007**.
- 135) Fragiadakis, D.; Dou, S.; Colby, R. H.; Runt, J. Molecular Mobility, Ion Mobility, and Mobile Ion Concentration in Poly- (ethylene oxide)-Based Polyurethane Ionomers. *Macromolecules* **2008**, 41, 5723–5728.
- 136) van Turnhout, J.; Wübberhorst, M. Analysis of complex dielectric spectra. II: Evaluation of the activation energy landscape by differential sampling. *J. Non-Cryst. Solids* **2002**, 305, 50–58.
- 137) Wübberhorst, M.; van Turnhout, J. Analysis of complex dielectric spectra. I. One-dimensional derivative techniques and three- dimensional modelling. *J. Non-Cryst. Solids* **2002**, 305, 40–49.
- 138) Díaz-Calleja, R. Comment on the Maximum in the Loss Permittivity for the Havriliak–Negami Equation. *Macromolecules* **2000**, 33, 8924.
- 139) Boersma, A.; van Turnhout, J.; Wübberhorst, M. Dielectric Characterization of a Thermotropic Liquid Crystalline Copolyester- amide: 1. Relaxation Peak Assignment. *Macromolecules* **1998**, 31, 7453–7460.
- 140) Wakai, C.; Oleinikova, A.; Ott, M.; Weingartner, H. How Polar Are Ionic Liquids? Determination of the Static Dielectric Constant of an Imidazolium-based Ionic Liquid by Microwave Dielectric Spectroscopy. *J. Phys. Chem. B* **2005**, 109, 17028.
- 141) Ou, R.; Gupta, S.; Parker, C. A.; Gerhardt, R. A. Fabrication and Electrical Conductivity of Poly(methyl methacrylate) (PMMA)/ Carbon Black (CB) Composites: Comparison between an Ordered Carbon Black Nanowire-Like Segregated Structure and a Randomly Dispersed Carbon Black Nanostructure. *J. Phys. Chem. B* **2006**, 110, 22365–22373.
- 142) Sun, T. L.; Kurokawa, T.; Kuroda, S.; Ihsan, A. B.; Akasaki, T.; Sato, K.; Haque, M. A.; Nakajima, T.; Gong, J. P. Physical hydrogels composed of polyampholytes demonstrate high toughness and viscoelasticity. *Nat. Mater.* **2013**, 12, 932–937.
- 143) Loshaek, S. Crosslinked polymers. II. Glass temperatures of copolymers of methyl methacrylate and glycol dimethacrylates. *J. Polym. Sci.* **1955**, 15, 391–404.

- 144) Stutz, H.; Illers, K.-H.; Mertes, J. A generalized theory for the glass transition temperature of crosslinked and uncrosslinked polymers. *J. Polym. Sci., Part B: Polym. Phys.* **1990**, *28*, 1483–1498.
- 145) Põhako-Esko, K., Timusk, M., Saal, K. et al. Increased conductivity of polymerized ionic liquids through the use of a nonpolymerizable ionic liquid additive. *Journal of Materials Research* *28*, 3086–3093 (**2013**).
- 146) Mogurampelly, S.; Keith, J. R.; Ganesan, V. Mechanisms Underlying Ion Transport in Polymerized Ionic Liquids. *J. Am. Chem. Soc.* **2017**, *139*, 9511–9514.
- 147) Frenzel, F.; Guterman, R.; Anton, A. M.; Yuan, J.; Kremer, F. Molecular Dynamics and Charge Transport in Highly Conductive Polymeric Ionic Liquids. *Macromolecules* **2017**, *50*, 4022–4029.
- 148) Chu, B.; Hsiao, B. S. Small-Angle X-ray Scattering of Polymers. *Chemical Reviews* **2001**, *101*, 1727–1762.
- 149) Ge, Q.; Lou, D.; Zeng, J.; Pan, C.; Wang, S.; Zhang, W.; Zhang, L.; Wang, X. Structural evolution of imidazolium-based poly (ionic liquid) assemblies during solvent evaporation. *Express Polymer Letters* **2017**, *11*, 84–95.
- 150) Kramarenko, V. Y.; Ezquerra, T. A.; Sics, I.; Balta´-Calleja, F. J.; Privalko, V. P. Influence of cross-linking on the segmental dynamics in model polymer networks. *The Journal of Chemical Physics* **2000**, *113*, 447–452.